Functional characterization of local feedback excitation onto different types of GABAergic inhibitory cells in the basal amygdala

Ph.D. thesis

Tibor Andrási

Semmelweis University
János Szentágothai Doctoral School of Neurosciences

Supervisor: Norbert Hájos, Ph.D., D.Sc.

Official Reviewers: Tibor Zelles, Ph.D.
Gábor Molnár, Ph.D.

Chair of the Final Examination Board: Anita Kamondi, Ph.D., D.Sc.
Members of the Final Examination Board: Lucia Wittner, Ph.D.
Alán Alpár, Ph.D., D.Sc.

Budapest

2018

TABLE OF CONTENTS

LIST OF ABBREVIATIONS

AAC	Axo-axonic cell
AAV	Adeno-associated virus
ABC	Avidin-biotin complex
ACSF	Artificial cerebrospinal fluid
AHP	Afterhyperpolarization
AIS	Axon initial segment
AMPA	α-amino-3-hydroxy-5-methyl-4-isoxazolepropionic acid
AP	Action potential
BA	Basal amygdala
BAC	Bacterial artificial chromosome
BC	Basket cell
BLA	Basolateral amygdala
BMA	Basomedial amygdala
CA1/CA3	Cornu ammonis 1/3
Calb	Calbindin
CaMKII	Calcium/calmodulin-dependent protein kinase 2
CB1	Type 1 cannabinoid receptor
CCK	Cholecystokinin
CCKBC	Cholecystokinin expressing basket cell
CeA	Central amygdala
CeL/CEl	Centrolateral amygdala
CeM/CEm	Centromedial amygdala
ChR2	Channelrhodopsin-2
CR	Calretinin
CS	Conditioned stimulus
Ctx	Cortex
CV	Coefficient of variation
DAB	Diaminobenzidine
DG	Dentate gyrus

DIC	Differential interference contrast microscopy
DMD	Digital mirror device
DSI	Depolarization-induced suppression of inhibition
eGFP	Enhanced green fluorescent protein
EM	Electron microscope
Ent/EC	Entorhinal cortex
eYFP	Enhanced yellow fluorescent protein
fMRI	Functional magnetic resonance imaging
GABA	Gamma-amino butyric acid
GAD	Glutamic acid decarboxylase
Hip(p)	Hippocampus
IL	Infralimbic cortex
IN	Interneuron
ISI	Interneuron-selective interneuron
ITC	Intercalated cells
LA	Lateral amygdala
LP	Localization point
LTP/LTD	Long-term potentiation/long-term depression
LV	Lateral ventricle
MSN	Medium spiny neuron
NAcc	Nucleus accumbens
NDS	Normal donkey serum
NMDA	N-methyl-D-aspartate
NPY	Neuropeptide Y
PB	Phosphate buffer
PFA	Paraformaldehyde
PFC	Prefrontal cortex
Pir ctx	Piriform cortex
PL	Prelimbic cortex
PN	Principal neuron
PTI	Perisomatic region-targeting interneuron
PV/Pvalb	Parvalbumin

PVBC	Parvalbumin-expressing basket cell
ROI	Region of interest
S	Subiculum
SOM	Somatostatin
STORM	Stochastic optical reconstruction microscopy
TTX	Tetrodotoxin
uEPSC/P	unitary excitatory postsynaptic current/potential
uIPSC/P	unitary inhibitory postsynaptic current/potential
US	Unconditioned stimulus
VAChT	Vesicular acethylcholine transporter
VGAT	Vesicular GABA transporter
VGLUT1	Type 1 vesicular glutamate transporter
VGLUT3	Type 3 vesicular glutamate transporter
VIP	Vasoactive intestinal polypeptide

1. INTRODUCTION

1.1 Overview

Computations performed by neural networks depend on the connectivity among excitatory and inhibitory neurons. Gamma-amino butyric acid (GABA) releasing basket and axo-axonic cells (AACs) targeting the perisomatic region of cortical principal neurons (PNs) are in a key position to effectively control the firing of their postsynaptic partners (Cobb et al., 1995; Miles et al., 1996). Consequently, perisomatic region-targeting inhibitory neurons (PTIs) are essential for neural computations and thus cognitive processes like learning & memory, perception, and motor control (Hu et al., 2014; Kepecs and Fishell, 2014). The critical role that these inhibitory interneurons (INs) play in circuit operation is reflected in the wide variety of neurological and psychiatric diseases that have been implicated in their malfunction, including epilepsy, schizophrenia and autism (Lewis et al., 2012; Marin, 2012; Prager et al., 2016). In cortical structures two distinct types of basket cells (BCs) expressing either parvalbumin (PV, PVBCs) or cholecystokinin and type 1 cannabinoid receptor (CCK/CB1, CCKBCs) give rise to the main inhibitory input onto the soma and proximal dendrites of excitatory PNs, while their axon initial segment (AIS) is innervated by PV-expressing AACs (Freund and Katona, 2007; Klausberger and Somogyi, 2008; Somogyi et al., 1998). The two BC types are markedly dissimilar in many single-cell features and are thought to generate postsynaptic inhibition with different properties (Glickfeld and Scanziani, 2006; Hefft and Jonas, 2005; Klausberger et al., 2005; Kohus et al., 2016; Szabo et al., 2010), suggesting distinct functions in cortical computation (Freund and Katona, 2007), presumably also supported by their different connectivity with local excitatory and inhibitory cells. However, the wiring motifs of cortical INs responsible for perisomatic inhibition are largely unknown.

The basolateral complex of the amygdala (composed of the lateral (LA), basal (BA) (or basolateral (BLA)) and accessory basal (or basomedial (BMA)) nuclei is a cortical structure known to be a site of plastic changes during fear learning (LeDoux, 2000; Pape and Pare, 2010; Tovote et al., 2015). PNs in this region are glutamatergic excitatory neurons that give rise to local collaterals and project to remote areas,

including cortical (e.g. prefrontal cortex (PFC), hippocampus) and subcortical (e.g. nucleus accumbens (NAcc)) structures (Sah et al., 2003). In contrast, the vast majority of GABAergic cells, which provide less than 20% of the total neuronal population, have only local axon arbor, often forming a dense axonal meshwork (Ehrlich et al., 2009; Spampanato et al., 2011). The three previously described types of perisomatic inhibitory cells have also been recognized in amygdalar networks (Bienvenu et al., 2012; Vereczki et al., 2016). However, as in other cortical regions, the synaptic organizing principles between these GABAergic cell types and PNs, a key knowledge for understanding microcircuit operation, are ill-defined.

To uncover the principles of connectivity within the amygdala circuitry formed by PNs and PTIs, we combined electrophysiological and neuroanatomical techniques with optogenetics. Investigations were performed in the basal nucleus of the amygdala. Our results uncovered a surprising cell-type specific connectivity matrix in this microcircuitry, which may be a general circuit organization motif in cortical regions, contributing critically to local information processing.

1.2 Cytoarchitecture of cortical structures

In cortical regions, the most abundant cell type is the excitatory glutamatergic pyramidal or principal neurons. They compose of the 70-90 percent of the neurons, while the GABA releasing inhibitory neuron population gives the remaining fraction (Fishell and Rudy, 2011; Harris and Shepherd, 2015; Hendry et al., 1987; Sahara et al., 2012). The PN somata are often ordered to layer-like structures building up functional groups within a cortical region. In the neocortex conventionally six layers are distinguished, but layer 1contains typically only GABAergic cell types. In contrast in the hippocampus, one of the most investigated cortical structure, only one pyramidal cell layer can be noticed, although recent studies have proposed that this layer can be divided both functionally and morphologically at least into two sublayers in the CA1 region (Mizuseki et al., 2011). By contrast, the BLA nuclei do not have an apparent layered structure, but rather a mass of neurons without obvious orientation and/or polarization, even though the main cell types are similar to those found in the neocortex

and hippocampus (Faber et al., 2001; McDonald, 1992; Pitkanen et al., 2000; Sah et al., 2003; Washburn and Moises, 1992).

1.2.1 Glutamate releasing excitatory cells in cortical structures

In cortical regions, the PN morphology is highly specialized to its functions. Typically, they have one or two thick apical dendrites emanating from the soma and spanning through across different layers having oblique dendritic branches on their trunk and ending with rich arborization called dendritic tuft. Additionally, on the counter pole of the soma, thinner, more uniform basal dendrites are emitted. The apical and basal dendrites together are recipient of synaptic inputs originating from different afferents. In the BLA complex, however, large portions of PNs show stellate like appearance lacking any apparent apical dendrite. Even those that have a clear apical dendrite do not show any orientation, forming no layered structure in contrast to other cortical areas. The perisomatic region of the PNs -consisting of the soma, proximal dendrites and AIS- receives only GABAergic synapses originated mostly from the local PTIs (Halasy et al., 1996; Megias et al., 2001; Somogyi et al., 1983; Vereczki et al., 2016; Veres et al., 2017). The AIS is a specialized part of the axon, which is dedicated to translate the processed and summed information coming from the dendrites and soma to an "all or none" output (Kole and Stuart, 2012; Palay et al., 1968; Peters et al., 1968; Rasband, 2010; Somogyi, 1977). This part of the axon is covered by synapses of the AACs (chandelier cells)(Fairen and Valverde, 1980; Somogyi, 1977; Veres et al., 2014). The soma itself and the proximal part of the PN dendrites are targeted by two different BC types, the PV- and the CCK/CB1-expressing BCs (Bartos and Elgueta, 2012; Freund and Katona, 2007; Hu et al., 2014; Kubota et al., 2015; Pelkey et al., 2017; Vereczki et al., 2016; Veres et al., 2017). Together with the AIS, the soma and the proximal dendrites are key sites where the neural spiking, i.e. the output can be the most effectively controlled by PTIs (Daw et al., 2009; Doischer et al., 2008; Hefft and Jonas, 2005; Hu et al., 2014; Veres et al., 2017; Veres et al., 2014). In cortical structures one of the most characteristic morphological features of the PNs is that their dendrites are densely covered by spines (Citri and Malenka, 2008), which is a specialized

computational domain receiving excitatory glutamatergic inputs, while the inhibitory GABAergic synapses mostly target the dendritic shafts (Chen et al., 2012; Megias et al., 2001; Mullner et al., 2015). It is also characteristic to the PN dendrites that different voltage gated and ligand gated channels are present, supporting the active cable properties of the dendrites. For instance, voltage gated sodium channels help conducting back-propagating action potentials (APs) toward distal ends of the dendrites, thereby giving a basis for induction of long-term plastic changes (long-term potentiation, LTP; long-term depression, LTD), processes which are elemental requirements of learning and memory at the cellular level. Moreover, non-specific cation conductances, e.g. I_h, voltage gated calcium channels (like L-type Ca^{2+} channels) and ligand gated extrasynaptic receptors (e.g. N-methyl-D-aspartate (NMDA) type of ionotropic glutamate receptors) serve as active participants on dendrites to integrate, modify and conduct received information toward the soma (Citri and Malenka, 2008; Magee, 2000; Magee and Johnston, 1995; Malenka and Bear, 2004; Stuart and Sakmann, 1994). In neuronal networks, PNs receive, compute and forward information. The processed information is transformed to output signal at the AIS that propagate to the axon terminals as an „all or none" signal. Cortical PNs have only a single axon typically originating from the soma or the proximal part of the dendrites and send axon collaterals locally as well as to remote cortical and subcortical regions (Thome et al., 2014). In the central nervous system, cortical glutamatergic cells possess small excitatory terminals, which target other PNs as well as GABAergic cell types typically with 1-2 boutons per cell in the hippocampus and with multiple boutons per cell in the neocortex (Gulyas et al., 1993; Guzman et al., 2016; Molnar et al., 2016). Electrophysiological recordings in many cortical areas revealed the properties of the local PN connectivity and characteristics of their inputs to different cell types (Geiger et al., 1995; Harris and Shepherd, 2015; Holmgren et al., 2003; Jiang et al., 2015; Jonas et al., 1994; Kisvarday et al., 1986; Levy and Reyes, 2012; Miles and Wong, 1986; Pala and Petersen, 2015; Perin et al., 2011). Most of the data comes from the hippocampus and neocortex, as these regions are in the focus of neuroscientific interest.

In spite of the facts that PNs in cortical structures have numerous similar properties, several region specific differences can be found from the synaptic level to the network organization. As aforementioned, not in all cortical regions, PNs are

organized to well defined layers, and not all of the PNs possess well-distinguished apical dendrites or orientation. Moreover, information processing in cortical structures requires local interconnectivity among PNs, which is typically present in most of the cortical regions, including the hippocampal CA3 area and the BLA, but such interconnectivity among PNs is lacking e.g. in the dentate gyrus (DG) (Harris and Shepherd, 2015; Holmgren et al., 2003; Kisvarday et al., 1986; Miles and Wong, 1986; Perin et al., 2011). For a long time it was the prevailing view that PNs in a given cortical region form a more or less homogenous population, but this theory has been challenged by findings that PNs may significantly differ and/or can be involved in completely different functions even though they are the closest neighbours within a region (Krook-Magnuson et al., 2012). Strong evidence supports the idea that PNs in a given region are often specialized to different functions like grid cells, head direction cells, border cells etc. in the entorhinal cortex, subiculum or CA1 (Hafting et al., 2005; Krook-Magnuson et al., 2012; Mizuseki et al., 2011; Solstad et al., 2008; Taube et al., 1990; Varga et al., 2010). Similarly, the BA PNs may belong to e.g. fear engram cells, fear extinction cells or reward cells (Kim et al., 2016; Ramirez et al., 2013; Ramirez et al., 2015). This heterogenity sheds light on the fact that to understand network operation it is necessary to investigate the wiring principles of PNs in details. Besides the local interconnectivity among PNs, they also target different GABAergic cell types thereby giving rise to feedback and lateral inhibition within the networks (Glickfeld and Scanziani, 2006; Pouille et al., 2009; Pouille and Scanziani, 2001; Willadt et al., 2013). These circuit motifs increase computational power of networks.

1.2.2 Unravelling the GABAergic neuron diversity in cortical networks

In cortical networks information processing is critically depended on the accurate spatio-temporal control of PN activity. Although the excitatory PN population represents the vast majority of the neurons, they work in a tight co-operation with the significantly smaller number of GABA releasing inhibitory cells in order to fulfill their function. GABAergic INs represent the 10-20 percent of the neuron population, but in spite of this, they show incredible heterogenity in their anatomical, electrophysiological

and molecular properties (Buzsaki and Chrobak, 1995; Cobb et al., 1995; Fishell and Rudy, 2011; Freund and Buzsaki, 1996; Kepecs and Fishell, 2014; Markram et al., 2004; Miles et al., 1996; Paulsen and Moser, 1998; Pelkey et al., 2017). In the CA1 region of the rodent hippocampus more than 21 different types of GABAergic cells have been distinguished so far, while in the neocortex additional types may exist (**Fig. 1**)(DeFelipe et al., 2013; Jiang et al., 2015; Klausberger and Somogyi, 2008; Pelkey et al., 2017). As similar cell types are present in all cortical regions, there should be some general principles along which the PNs and INs are organized. Unfortunately, the literature is not sufficiently consistent in the terminology of the different GABAergic cell types, yet there is a clear demand to resolve this issue (Ascoli et al., 2008; DeFelipe et al., 2013; Freund and Buzsaki, 1996; Jiang et al., 2015; Klausberger and Somogyi, 2008; Markram et al., 2004; Pelkey et al., 2017; Spampanato et al., 2011). The most important step is to standardize the criteria, which guide researchers classifying GABAergic cell types. These criteria should be strict enough and valid in every cortical structure (Ascoli et al., 2008).

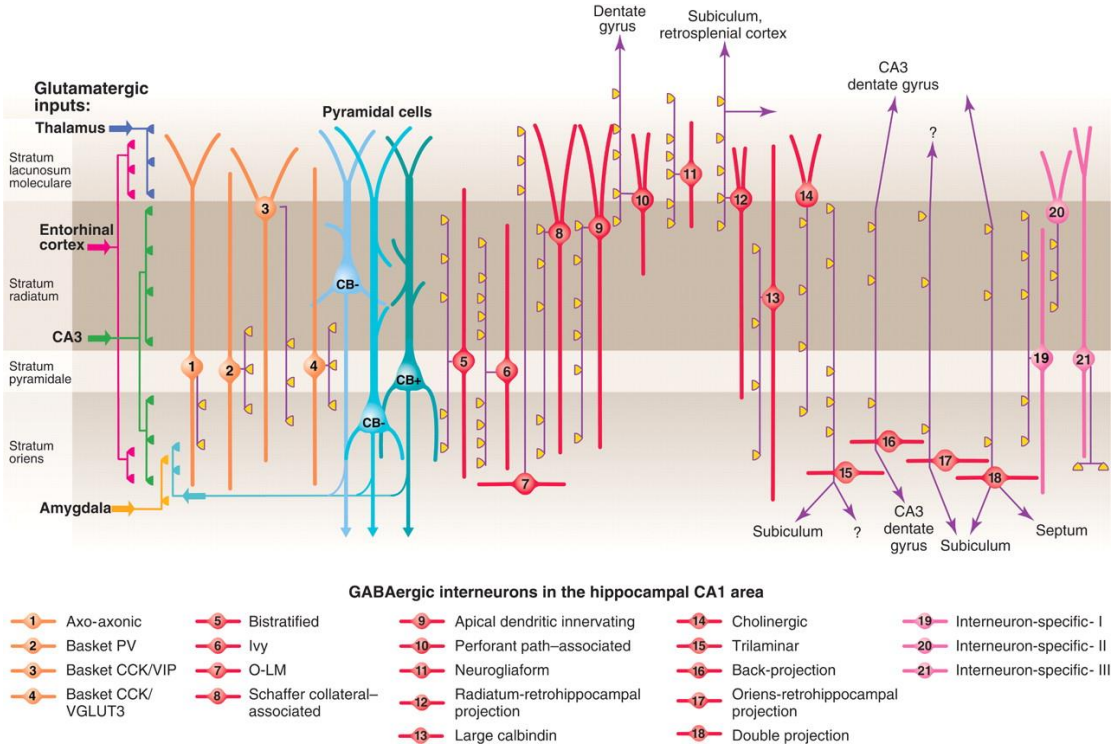

Figure 1. ***Interneuron diversity in the hippocampus****. Three types of pyramidal cells are accompanied by at least 21 classes of interneurons in the hippocampal CA1 area. The main termination of the five glutamatergic inputs are indicated on the left. The somata and dendrites of interneurons innervating pyramidal cells (blue) are orange and red, while those innervating mainly other interneurons are pink. Axons are purple; the main synaptic termination fields are shown in yellow. Note the association of the output synapses of different interneuron types with the perisomatic region (left) and either the Schaffer collateral/commissural or the entorhinal pathway termination zones (right), respectively. VIP, vasoactive intestinal polypeptide; VGLUT, vesicular glutamate transporter; O-LM, oriens lacunosum moleculare. (Figure adapted from (Klausberger and Somogyi, 2008))*

Considering this approach, classically there are three main groups of features, which can serve as a basis for classification, namely the morphological, electrophysiological and molecular properties of GABAergic cells. Morphological analysis of the GABAergic cells divides them into different groups based on the shape, size and location of the soma, the extent of dendritic and axonal arbor that substantially

determine the cell's afferent inputs and their possible targets, respectively. The simplest and widely used classification is to divide cortical inhibitory INs into three different groups based on their targeted cell types and the target domain preference. Potent inhibition of different computational domains of PNs provides a powerful tool for the network to finely control PN activity. In cortical regions there are GABAergic cell types dedicated to target the dendrites of PNs or their perisomatic region. Dendrite-targeting inhibitory cells are often further specialized to innervate certain segments of the dendritic tree, thereby differentially regulating the spatially segregated afferent inputs (e.g. OLM cells vs. bistratified cells in the hippocampus (Buhl and Dann, 1991; Buhl et al., 1994a; Klausberger et al., 2004; Maccaferri et al., 2000; McBain et al., 1994)). This type of INs is in the position to precisely control the early phase of the information processing and enhance the computational power of dendrites (Chen et al., 2012; Cobb et al., 1995; Gidon and Segev, 2012). The PTIs inhibit the proximal dendrites, the soma and the AIS of the PNs, domains which are the place of summation and transformation of the processed information to an output signal (Buhl et al., 1994a; Buhl et al., 1994b; Cobb et al., 1995; Kubota et al., 2015; Maccaferri et al., 2000; Vereczki et al., 2016; Veres et al., 2017). In contrast to these two types of INs, there are GABAergic cells that exclusively target other inhibitory cell types, therefore they are called interneuron-selective interneurons (ISI) (Acsady et al., 1996; David et al., 2007; Gulyas et al., 1996; Gulyas et al., 2003; Pfeffer et al., 2013; Pi et al., 2013). In addition to the classical three inhibitory IN types, there are GABAergic cells that beside their local axon collaterals project to other distant areas (Cossart, 2014; Gulyas et al., 1996; Gulyas et al., 2003; Jinno et al., 2007; McDonald and Zaric, 2015; Melzer et al., 2012; Sik et al., 1995). These inhibitory neurons form a fourth category, the GABAergic projection neurons. The term "interneuron" originally referred to cortical neurons with locally restricted axon arbor, but discovery of GABAergic projection cell types in cortical regions extended the inhibitory neuron classes (**Fig. 1**).

The comparison of the electrophysiological properties of GABAergic cell types gives another tool to make a distinction among different inhibitory neurons based on their intrinsic membrane properties and firing characteristics. The firing pattern of the different cell types can be characteristic for certain cell types, like the well-known fast spiking INs (Doischer et al., 2008; Kohus et al., 2016; Rudy and McBain, 2001). In

addition, their intrinsic electrophysiological properties such as input resistance, membrane capacitance and the presence or lack of a certain channels in their membrane are characteristic for different INs. The molecular features also help in the classification using the comparison of neurochemical marker content (neuropeptides as CCK, somatostatin (SOM), vasoactive intestinal polypeptide (VIP) and neuropeptide Y (NPY) or calcium binding proteins such as PV, calbindin (CB) and calretinin (CR)) and the presence or lack of certain receptors, receptor subunits and transcription factors (Ascoli et al., 2008; Cea-del Rio et al., 2011; Glickfeld and Scanziani, 2006; Jiang et al., 2015; Pelkey et al., 2017; Woodruff and Sah, 2007b).

One clear example for successful classification is the division of PTIs in the neocortex, hippocampus and basal nucleus of the amygdala. PTIs mostly target the soma and proximal dendrites (BCs) or the AIS of PNs (AACs or chandelier cells). In the neocortex and hippocampus, it is relatively easy to distinguish the BCs from other INs, since their axonal arbor is largely confined to that area or layer, where the somata of PNs are ordered (Freund and Buzsaki, 1996; Jiang et al., 2015; Klausberger and Somogyi, 2008; Maccaferri et al., 2000). By contrast, the BA has no layered structure, the appearance of the axon cloud of BCs and dendrite-targeting INs therefore has a similar appearance. To distinguish these functionally distinct INs, a detailed morphological analysis should be performed that is not necessary for those GABAergic cells located in layered cortical structures (Vereczki et al., 2016; Veres et al., 2017; Veres et al., 2014). Based on morphological properties, it is impossible to further subdivide the BC populations, but they can be separated by the expression of PV or CCK/CB1 (Freund and Buzsaki, 1996; Katona et al., 1999; Kawaguchi and Kondo, 2002; Keimpema et al., 2012; Kohus et al., 2016; Marsicano and Lutz, 1999; Mascagni and McDonald, 2003; Pawelzik et al., 2002; Tsou et al., 1999). In addition, the single-cell membrane characteristics of the PTIs are also helpful in distinguishing the PV-expressing BCs and AACs from CCK/CB1-expressing BCs. For instance, the PV-expressing INs are capable to fire APs at much higher frequencies than CCK/CB1-expressing BCs (Cea-del Rio et al., 2010; Glickfeld and Scanziani, 2006; Kohus et al., 2016; Pawelzik et al., 2002; Rudy and McBain, 2001). However, the two PV-expressing PTI types are hard to distinguish based on only their electrophysiological properties (Kohus et al., 2016; Papp et al., 2013; Povysheva et al., 2013; Taniguchi et

al., 2011). In light of these examples, in this study the three different types of PTIs were unequivocally identified using combined morphological, neurochemical and electrophysiological features.

1.2.3 PTIs in cortical structures

The perisomatic region of the PNs consists of the soma, the proximal dendrites - typically less than 100 μm from the soma- and the AIS. The BCs, expressing either PV or CCK/CB1, provide synaptic inhibition onto this membrane domain via their terminals (**Fig. 3**) (Maccaferri et al., 2000; Megias et al., 2001; Vereczki et al., 2016; Veres et al., 2017). The AIS is exclusively targeted by the PV containing AACs (**Fig. 3**)(Buhl et al., 1994b; Fairen and Valverde, 1980; Somogyi, 1977; Veres et al., 2014). However, there are region specific differences in the definition what is considered as a BC, at least regarding the ratio of their terminals on the perisomatic region and dendrites. In the hippocampus, this ratio is relatively high, since BC terminals are largely restricted to the pyramidal cell layer, 70-80 percent of them covering the soma and proximal dendrites. In the neocortex only 25-30 percent of the BC terminals target unequivocally the perisomatic region, the remaining portion innervate more distal dendrites of PNs (Freund and Katona, 2007; Maccaferri et al., 2000; Vereczki et al., 2016; Veres et al., 2017). In contrast, within the BA PVBCs show much more variability in the ratio of their terminals targeting the perisomatic region or dendrites of the PNs, thereby it turns the definition of a BC in this region is not straightforward (Veres et al., 2017). Identification of the third type of the PTI, the AACs or chandelier cells seems to be easier, because they exclusively target the AIS of the nearby PNs as aforementioned. In addition, it is also characteristic to the BCs that they innervate the perisomatic region via several boutons that contributes to their inhibitory efficacy (Halasy et al., 1996; Kubota et al., 2015; Maccaferri et al., 2000; Vereczki et al., 2016; Veres et al., 2017). The AACs are also capable to effectively regulate a PN output via inhibiting that part of the axon where the APs are initiated (Veres et al., 2014). Surprisingly, in the rat neocortex and mouse BA it has been shown AACs in certain circumstances are able to monosynaptically excite PNs, but the mechanism underlying

this excitatory effect has not been fully clarified yet (Glickfeld et al., 2009; Khirug et al., 2008; Szabadics et al., 2006; Woodruff et al., 2011).

1.2.4 CCK/CB1-expressing BCs

Inhibitory cells expressing CCK and CB1 were divided into two main classes in the hippocampus, one of them targets the perisomatic region of the PNs and the other type targets the dendrites (Cope et al., 2002; Lasztoczi et al., 2011; Papp et al., 2013; Pawelzik et al., 2002; Szabo et al., 2010). CCK is a gastrointestinal peptide, which is also expressed in many neuron types within the central nervous system, e.g. a large proportion of the cortical PNs also express CCK and CB1 (Marsicano and Lutz, 1999; Mascagni and McDonald, 2003; McDonald and Mascagni, 2001b). Although the release mechanism of CCK is currently unknown, its effects on network operation has been found to be substantial (Foldy et al., 2007; Lee and Soltesz, 2011; Lee et al., 2011; Petkova-Kirova et al., 2012). For instance, PVBCs express CCK2 receptors and respond with depolarization and increased activity upon CCK administration in vitro (Foldy et al., 2007; Lee and Soltesz, 2011; Lee et al., 2011). By contrast, the administration of CCK reduce the CCKBC activity possibly in an indirect way. CCKBCs have typically a large soma and multiple smooth dendrites. One axon emanates from the soma, which densely arborizes and forms synapses via several release sites on the postsynaptic targets (Biro et al., 2006; Freund and Buzsaki, 1996; Vereczki et al., 2016; Veres et al., 2017). Besides of the characteristic CCK and CB1 expression, these BCs can express VIP, Vglut3 (type 3 vesicular glutamate transporter) or CB which suggest heterogenity and possible existence of further subtypes within CCKBC category (Bezaire and Soltesz, 2013; Freund and Buzsaki, 1996; Mascagni and McDonald, 2003; Rovira-Esteban et al., 2017). The soma and dendritic shafts of these INs receive both excitatory and inhibitory terminals, and interestingly it was shown in the hippocampus that the number of excitatory contacts is only one third/one fifth of that covering the PVBC membrane surface (Matyas et al., 2004). The firing pattern typically displays a regular spiking profile with accommodation (Cea-del Rio et al., 2010; Cope et al., 2002; Evstratova et al., 2011; Papp et al., 2013; Szabo et al.,

2010). So far, only a few studies have investigated the in vivo firing properties of the CCKBCs. These showed that CCKBCs tend to discharge in the ascending phase of the theta rhythm, a synchronous network activity that dominates the hippocampal EEG during exploration. Furthermore, these studies found that CCKBCs display rare activity during gamma or higher frequency oscillations in anesthetized mice without any phase preference (Klausberger et al., 2005; Lasztoczi et al., 2011). The membrane properties of CCKBCs can be characterized by slow membrane time constant, which provides a wide time window for event summation making them suitable for an efficient integration of afferent information (Basu et al., 2013; Evstratova et al., 2011; Glickfeld and Scanziani, 2006; Hefft and Jonas, 2005). Supporting this idea, it was demonstrated in the hippocampal CA1 region that CCKBCs may participate in the Schaffer collateral-mediated feedforward inhibition, thereby shaping the input in CA1 pyramidal cells in a time dependent manner (Basu et al., 2013; Glickfeld and Scanziani, 2006). In addition, the output of CCKBCs is regulated not only by the afferent excitatory inputs but also via the retrograde neurotransmitter endocannabinoids. The membrane of CCKBC terminals is enriched with CB1s, which are targeted by the endocannabinoids deliberated from the postsynaptic PNs (Freund et al., 2003; Katona et al., 1999; Neu et al., 2007; Wilson and Nicoll, 2001). Several known signaling pathways that are commonly related to the depolarization/activity of the postsynaptic cell can initiate the synthesis of endocannabinoids on the postsynaptic site. Once the endocannabinoids are bound to the presynaptic CB1 receptors, a G-protein coupled signalling cascade leads to the reduction in the availability of the N-type voltage sensitive calcium channels that are necessary for the transmitter release, thereby effectively decreases or inhibits the release probability from the terminals (Szabo et al., 2014). This process is called depolarization-induced suppression of inhibition (DSI) (Freund et al., 2003; Kano et al., 2009; Wilson and Nicoll, 2001, 2002). This type of control of GABA release from the axon terminals of CCKBCs is supposed to have a role in place cell coding in the CA1: the most active PNs can escape from CCKBC-mediated synaptic inhibition and participate in coding, while the less active PNs receive strong inhibition, keeping them below firing threshold (Freund, 2003; Freund and Katona, 2007; Losonczy et al., 2010). In addition to the supposed integratory role of CCKBCs, there is another theory about the CCKBC function in the brain. It is

hypothesized that they show sensitivity to neuromodulatory control arriving from subcortical nuclei and this view is strongly supported by the expression of the different neuromodulatory receptors by this BC type, such as serotonin receptors (5HT), muscarinic (M1/3) and ionotropic (α4 and α7) acethylcholine receptors, and oestrogen receptors (Cea-del Rio et al., 2010; Freund, 2003; Freund and Katona, 2007; Hart et al., 2007; Keimpema et al., 2012; Morales et al., 2008). The sensitivity of CCKBCs to neuromodulators inspired their other common name, the so-called „mood cell" (Freund, 2003; Freund and Katona, 2007). CCKBCs contact local PNs via several boutons, providing synaptic inhibition, which can be characterized by variable release probability and apparent asynchronous release (Biro et al., 2006; Daw et al., 2009; Glickfeld and Scanziani, 2006; Hefft and Jonas, 2005; Maccaferri et al., 2000; Szabo et al., 2010). An explanation of the variable release properties can be that the N-type voltage gated calcium channels in the membrane of the terminals are randomly distributed in or near the active zone and only loosely coupled to the calcium sensor of the release machinery. This microdomain coupling gives uncertainty to the release: the calcium influx into axon terminals upon an AP invasion can or cannot reach the calcium sensor necessary for transmitter release. If more than one AP with high frequency invade the terminals, the intrabouton calcium concentration can reach the threshold that is necessary for triggering neurotransmitter release (Goswami et al., 2012; Hefft and Jonas, 2005).

Our knowledge about CCKBCs so far is mostly based on data obtained in rodent hippocampal slice preparations. The investigation of this cell type is largely hampered by the fact that there is no proper tool to selectively manipulate CCKBC function in the brain, because every attempt to create a transgenic animal selective for CCK/CB1-expressing inhibitory cells resulted in simultaneous expression of reporter molecules and light gated channels in PNs as well as in other CCK-containing GABAergic cells (Mate et al., 2013; Taniguchi et al., 2011). Therefore, to reveal the function of CCKBCs in network operations it requires novel in vitro and in vivo strategies.

1.2.5 PV-expressing BCs

PVBCs are one of the most investigated cell types in cortical networks. Their unique electrophysiological and morphological characteristics largely facilitated the experimenters to acquire a deep knowledge about this cell type and their roles in network functions. Similarly, to the aforementioned CCKBCs, PVBCs also have several spine-free dendrites and one axon, which densely arborizes locally (Freund and Buzsaki, 1996; Hu et al., 2014; Kubota et al., 2011; Tukker et al., 2013; Vereczki et al., 2016). Interestingly, PVBCs often form synaptic contacts and gap junctions with other nearby PVBCs thereby forming a functional syncytium (Fukuda and Kosaka, 2000; Galarreta and Hestrin, 2002; Kohus et al., 2016; Pfeffer et al., 2013; Tamas et al., 2000; Tamas et al., 1998). PVBCs characteristically express a calcium binding protein, the PV, which has a role in shaping the temporally precise inhibition together with other factors (Baimbridge et al., 1992; Bucurenciu et al., 2008; Caillard et al., 2000; Eggermann et al., 2011). Besides of PVBCs in cortical networks, other GABAergic cell types also express PV, such as AACs, dendrite-targeting bistratified cells and the distal dendritic tuft-innervating oriens lacunosum moleculare cells in the CA1. The latter two cell types also express SOM (Ferraguti et al., 2004; Katona et al., 2014). Surprisingly in the neocortex and BA, the coexpression of PV and SOM could not be demonstrated, suggesting that the neurochemical content of IN types may have region specificity (Ma et al., 2006; McDonald and Mascagni, 2002; Xu et al., 2013). In the rodent BA, PVBCs coexpress PV with another calcium binding protein, CB, which is missing from the PV-expressing AACs, thereby helping to distinguish PVBCs and AACs in this structure (McDonald and Betette, 2001). PVBCs provide strong inhibition onto the perisomatic region of PNs in a distance dependent manner, since the probability and strength of the inhibition decrease with the increasing intersomatic distance (Fino and Yuste, 2011; Packer and Yuste, 2011). PNs receive large and fast inhibition from PVBCs with apparently small jitter and marked short-term depression. The short-term depression is an indicator of an initially large release probability and the faithful synaptic transmission, which endows PVBCs to be capable of providing a temporally precise control over a large PN population (Bucurenciu et al., 2008; Daw et al., 2009; Doischer et al., 2008; Glickfeld and Scanziani, 2006; Hefft and Jonas, 2005;

Kraushaar and Jonas, 2000; Szabo et al., 2010; Veres et al., 2017). The fast spiking profile of PVBCs is one of their most apparent feature, because due to their specific potassium channels (Kv 3.1), PVBCs are able to fire at frequencies higher than 100 Hz (Lien and Jonas, 2003; Rudy and McBain, 2001). Altogether the fast firing capability and the faithful and precise inhibition make them suitable to initiate or follow fast oscillations in concert with PNs, as it was demonstrated in two types of synchronous network activities, in gamma oscillations and in sharp wave ripples, respectively (Buzsaki and Chrobak, 1995; Cobb et al., 1995; Gulyas et al., 2010; Mann et al., 2005; Oren et al., 2010; Schlingloff et al., 2014; Sohal et al., 2009). The somatic and dendritic surface of PVBCs are densely covered predominantly by excitatory inputs, but inhibitory inputs can be also found, though in a smaller number (Gulyas et al., 1999; Matyas et al., 2004). The high K^+/Na^+ channel ratio in PVBC dendrites and the fast membrane time constant support and enhance signal propagation from synapses to soma (Aponte et al., 2008; Glickfeld and Scanziani, 2006; Hu et al., 2010; Norenberg et al., 2010). Compared to the dendrites of CCKBCs that are prone to integrate signals, PVBC dendrites are rather designed for conveying individual synaptic events, which is facilitated by the relatively large density of the fast activating and fast inactivating potassium channels, thereby making them ideally responsive to even one or only a few excitatory inputs (Aponte et al., 2008; Evstratova et al., 2011; Glickfeld and Scanziani, 2006; Hefft and Jonas, 2005; Molnar et al., 2016; Norenberg et al., 2010). Furthermore, excitatory synapses on PVBC dendrites often contain a special GluR4-containing, but GluR2-lacking, calcium permeable AMPA (α-amino-3-hydroxy-5-methyl-4-isoxazolepropionic acid) receptor type, which can play a role in a non-Hebbian form of LTP expression in PVBCs (Geiger et al., 1995; Lamsa et al., 2007; Nissen et al., 2010). PVBCs express only a few types of neuromodulatory receptors (e.g. μ-opioid, M1 and M2), which is another striking difference from CCKBCs (Drake and Milner, 2002; Hajos et al., 1998; Yi et al., 2014). Thus, the different neuromodulator sensitivity of the two BC types strongly suggests a markedly different function in network operations (Freund, 2003; Freund and Katona, 2007).

1.2.6 Axo-axonic cells

A peculiar cell type in cortical structures is the PV-expressing AAC that selectively innervates the AIS of PNs (Fairen and Valverde, 1980; Han et al., 1993; Somogyi, 1977; Soriano et al., 1990; Veres et al., 2014). This GABAergic cell type can be uniformly found in all cortical regions. Notably, they innervate exclusively that part of the PN axon where the AP is generated with the highest probability (Veres et al., 2014). Inhibiting or facilitating the AP initiation at the site of the AP generation is one of the most effective position in PNs to control their spiking (Debanne et al., 2011; Kole and Stuart, 2012; Palay et al., 1968; Peters et al., 1968; Rasband, 2010; Veres et al., 2014). Regarding their morphology, AACs are similar to PVBCs, however, in the neocortex their axons form apparent "candle sticks" like structures, which is the origin of their other common name: the chandelier cell (Szentagothai, 1975). However, their dendritic arbor is significantly shorter compared to PVBCs and CCKBCs (Papp et al., 2013; Vereczki et al., 2016). In the BA, the chandelier-like structures are not easily distinguishable from those axons innervating dendrites and soma of PNs, which originate from other INs. Moreover, the electrophysiological properties of AACs are also very similar to that of PVBCs. For instance, AACs respond to current injections with very high firing frequency and their intrinsic membrane properties characterized by the relatively low input resistance and fast membrane time constant are reminiscent to PVBCs (Kohus et al., 2016; Papp et al., 2013; Povysheva et al., 2013; Woodruff et al., 2010; Zhu et al., 2004). Comparing to PVBCs or other INs, AACs never innervate other GABAergic cell types. Individual AACs give rise to 2-7 bouton onto single AISs, where the likelihood of AP generation is the highest due to the accumulation of the voltage gated sodium channels, therefore innervation of this domain is one of the most effective site for controlling the PN activity (Muller et al., 2006; Veres et al., 2014). The function of AACs in cortical regions is a hot topic in neuroscience research, but the lack of specific tools to separately investigate and manipulate PVBCs and AACs significantly decelerates researchers. Accumulating evidence from in vivo recordings suggests that the AAC activity during different brain functions and oscillations does not overlap with PVBC activity (Bienvenu et al., 2012; Klausberger et al., 2003; Lu et al., 2017; Massi et al., 2012; Viney et al., 2013; Zhu et al., 2004). During theta rhythm,

AACs fire at the ascending phase of oscillatory activity, while PVBC spiking increases during its descending phase, suggesting that AACs and PVBCs may have different excitatory drive (Bienvenu et al., 2012; Klausberger et al., 2003; Massi et al., 2012). This theory is further strengthened by the fact that unconditioned stimulus (US) applied during fear conditioning evoke a dramatic increase in AAC firing, while PVBC spiking is less and more variably affected (Bienvenu et al., 2012; Massi et al., 2012). In order to fully understand how AACs are recruited, their connection map and wiring principles in cortical networks have to be revealed in detail.

1.3 The amygdala

The amygdala in the mammalian brain is located in the mediotemporal lobe and is often referred as the structure responsible for fear and emotional memory formation in addition to reward learning, food intake and the expression of social aggression (**Fig. 2A**)(Aggleton, 1993; Armony et al., 1995; Douglass et al., 2017; Fanselow and Gale, 2003; Haller, 2018; Herry et al., 2008; LeDoux, 2000; Pape and Pare, 2010; Phelps and LeDoux, 2005; Tovote et al., 2015; Yamamoto, 2007). These functions represent evolutionally fundamental capabilities, which are required for survival. On the other hand, dysfunctions of the amygdala highly contribute to the development and expression of various mental disorders such as anxiety-related disorders, Alzheimer disease, Fragile-x syndrome and autism (Coghlan et al., 2012; Lee et al., 2017; Nuss, 2015; Olmos-Serrano et al., 2010; Prager et al., 2013; Schumann et al., 2011; Terburg et al., 2012; Vereecken et al., 1994)

1.3.1 The amygdaloid complex

Anatomical studies distinguished 13 different nuclei that make up the amygdaloid complex. These structures display a large heterogenity in terms of their cytoarchitecture, developmental origin and function (Pitkanen et al., 2000; Sah et al., 2003). Conventionally, three main parts are distinguished within the amygdala: the basolateral complex, the cortical amygdala nuclei and the centromedial nuclei

(Pitkanen et al., 2000; Sah et al., 2003). Notably, these parts can be further divided into subdivisions along functional and anatomical aspects.

Within the basolateral complex three main regions can be distinguished, namely the LA, BA/BLA and BMA (**Fig. 2B**)(Pitkanen et al., 2000; Sah et al., 2003). These nuclei have cortical origin and their cytoarchitecture and physiology are equivalent to that observed in other cortical structures (Carlsen and Heimer, 1988; Faber et al., 2001; Sah et al., 2003). The BLA complex is thought to be the site of fear learning and fear extinction and targeted by cortical and subcortical afferents, which control the function of this region (**Fig. 4**)(Armony et al., 1995; Herry et al., 2008; LeDoux, 2000; Pape and Pare, 2010; Tovote et al., 2015). Cortical afferents and thalamic inputs convey processed sensory information into the BLA complex and induce long-term physiological changes in PNs, thereby establishing fear memory (**Fig. 4**)(Bocchio et al., 2017; Li et al., 1996b; Pape and Pare, 2010; Rogan et al., 1997; Romanski and LeDoux, 1992; Szinyei et al., 2000). The BLA complex receives and processes multimodal sensory information, therefore it is thought that it represents the input site of the amygdala in fear learning. Furthermore, this structure forward the processed information into striatal structures such as central amygdala (CeA), dorsal and ventral striatum as well as into cortical areas, including the PFC and ventral hippocampus (**Fig. 4**)(Haubensak et al., 2010; Herry et al., 2008; Likhtik et al., 2008; Pape and Pare, 2010).

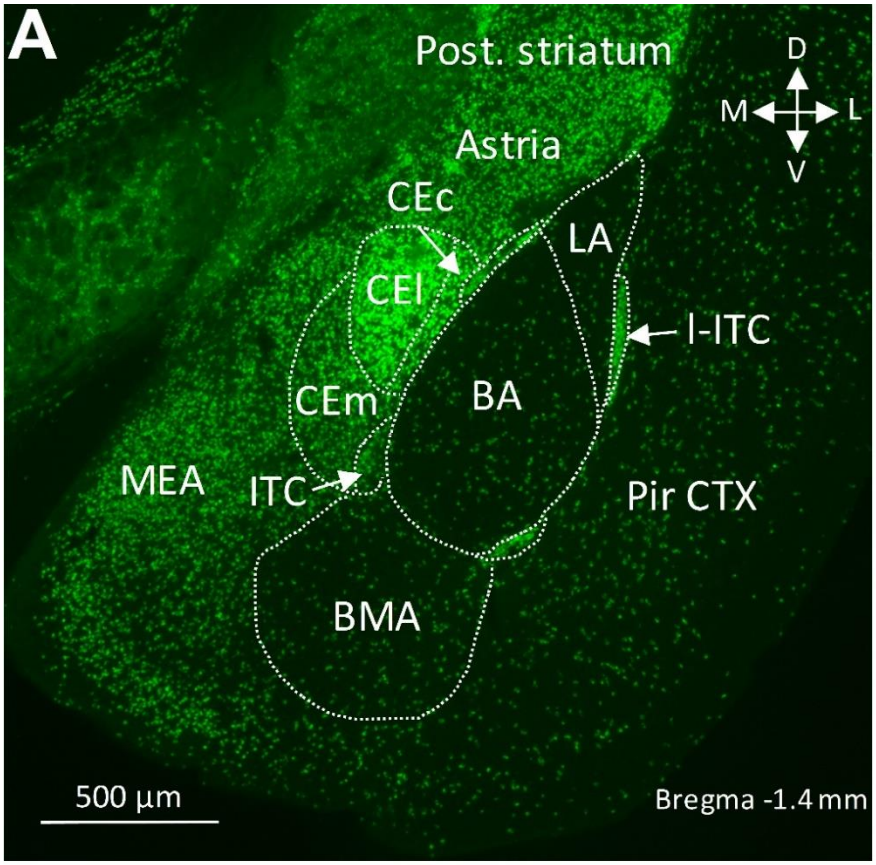
A
Post. striatum
D
M
L
V
Astria
CEc
LA
CEl
l-ITC
CEm
BA
MEA
ITC
Pir CTX
BMA
500 µm
Bregma -1.4 mm

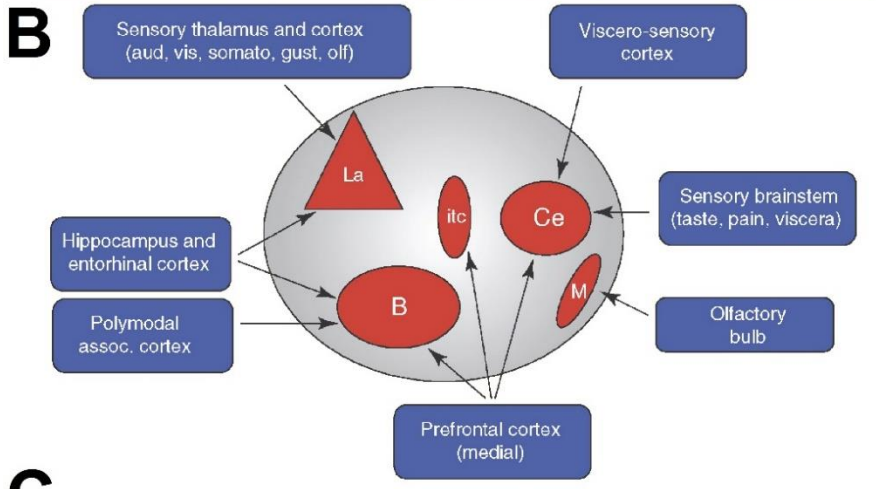
B
Sensory thalamus and cortex (aud, vis, somato, gust, olf)
Viscero-sensory cortex
La
itc
Ce
Sensory brainstem (taste, pain, viscera)
Hippocampus and entorhinal cortex
B
M
Polymodal assoc. cortex
Olfactory bulb
Prefrontal cortex (medial)

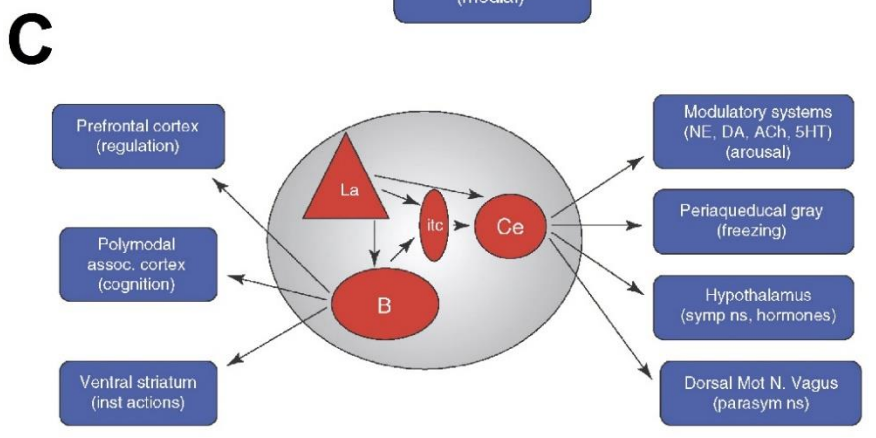
C
Prefrontal cortex (regulation)
Modulatory systems (NE, DA, ACh, 5HT) (arousal)
La
itc
Ce
Periaqueducal gray (freezing)
Polymodal assoc. cortex (cognition)
B
Hypothalamus (symp ns, hormones)
Ventral striatum (inst actions)
Dorsal Mot N. Vagus (parasym ns)

Figure 2. ***The rodent amygdala.*** *(**A**) ZsGreen fluorescent protein expression demonstrates the GABAergic cell distribution in the coronal section of the amygdala region from a VGAT-cre transgenic mouse crossed with a reporter line. Amygdala nuclei are delineated with dashed lines. (D, dorsal; V, ventral; M, medial; L, lateral; Post. striatum, posterior striatum; Astria, Amygdalo-striatal transition area; CEc, capsular part of the central amygdala; CEl, lateral part of the central amygdala; CEm, medial part of the central amygdala; MEA, medial amygdala; LA, lateral amygdala; BA, basal amygdala; BMA, basomedial amygdala; ITC, intercalated cells; l-ITC, lateral intercalated cells; Pir CTX, piriform cortex) (**B**) Inputs to some specific amygdala nuclei. Abbreviations of amygdala areas: B, basal nucleus; Ce, central nucleus; itc, intercalated cells; La, lateral nucleus; M, medial nucleus. Sensory abbreviations: aud, auditory; vis, visual; somato, somatosensory; gust, gustatory (taste). (**C**) Outputs of some specific amygdala nuclei. Abbreviations of amygdala areas: B, basal nucleus; Ce, central nucleus; itc, intercalated cells; La, lateral nucleus. Modulatory arousal system abbreviations: NE, norepinephrine; DA, dopamine; ACh, acetylcholine; 5HT, serotonin). Other abbreviations: parasym ns, parasympathetic nervous system; symp ns, sympathetic nervous system. (Panels (B) and (C) are adapted from (LeDoux, 2007))*

The cortical amygdala comprises the nucleus of the lateral olfactory tract (NLOT), bed nucleus of the accessory olfactory tract, the anterior and posterior cortical nucleus and the periamygdaloid cortex. Many of these nuclei are located at the surface of the brain and show cortical characteristics (Pitkanen et al., 2000; Sah et al., 2003).

The centromedial group consists of the CeA, medial amygdala and the amygdaloid part of the bed nucleus of the stria terminalis (Pitkanen et al., 2000; Sah et al., 2003). In contrast to the BLA complex and cortical amygdala the centromedial group has a striatal origin and the principal neuron type is GABA releasing inhibitory cells, which are reminiscent to the medium spiny cells (MSNs) in the striatum. The central nucleus can be further subdivided to centrolateral part (CeL) and centromedial part (CeM) (**Fig. 2B**)(Cassell et al., 1986; Jolkkonen and Pitkanen, 1998; McDonald, 1982a). Information flow in the amygdala during fear learning is considered

unidirectional. The CeA receives processed information from the BLA complex and send efferents to downstream effector structures, predominantly to the brainstem, thalamus and hypothalamus, therefore this structure is thought to be the output interface of the amygdala region (**Fig. 4**)(Tovote et al., 2015).

There are additional structures, which are difficult to classify into either of the main groups although they belong to the amygdala (Sah et al., 2003). For example, the intercalated cell mass (ITC), which are groups of GABA releasing cells located in the fiber bundles bordering the BLA complex and centromedial nuclei (**Fig. 2B**) (Millhouse, 1986). Two different cell types are distinguished in the ITC, cells with small soma and spiny dendrites similar to the striatal MSNs give rise to the majority of the population and a smaller number of cells can be characterized by large soma and smooth dendrites. These latter cells, however, might belong functionally to the BLA in spite of the fact that some of them are intermingled among small ITC cells (Pape and Pare, 2010). Based on the morphological analysis and electrophysiological characterization of the ITC cells, the current idea is that these cell groups form an interface between the BLA complex and central amygdala, because electrical stimulation of the basolateral complex evokes disynaptic inhibitory potentials in CeA neurons thereby shaping the output of the CeA (**Fig 4**)(Bienvenu et al., 2015; Jungling et al., 2008; Likhtik et al., 2008; Morozov et al., 2011). However, a recent study showed that ITC neurons might impact the neuronal activity in the basolateral complex (Asede et al., 2015). Other, less well-defined regions are also considered to belong to the amygdaloid complex or extended amygdala, such as the amygdalohippocampal region and anterior amygdala area whose contribution to the brain function is poorly understood (Pape and Pare, 2010; Pitkanen et al., 2000; Sah et al., 2003).

In our study, we investigated the wiring principles and functional organization of the BA, which is a key structure in fear learning and extinction, therefore in the next sections this structure will be characterized in detail.

1.3.2 The basal nucleus of the amygdala

In order to be able to understand the complex function of the BA that plays a role in different cognitive processes, including emotional learning, it is necessary to reveal in detail the wiring principles of the structure at synaptic, cellular and network levels. The BA is a part of the BLA complex located in the mediotemporal lobe, bordered dorsally by the LA, laterally by the capsula externa, medially by the CeA and ITC and ventrally by the BMA. Within the amygdala, the basal nucleus is interconnected with several other nuclei. According to the accepted view, during fear learning afferent sensory information is received by the LA, which forwards it to the BA, where fear memory engrams are evolved and stored (**Fig. 4**)(Anglada-Figueroa and Quirk, 2005; Haubensak et al., 2010; Herry et al., 2008; LeDoux, 2000; Likhtik et al., 2008). The BA forwards the processed information directly and indirectly via ITCs to the CeA, which subsequently activates downstream effector regions (**Fig. 4**). Additionally, the BA is reciprocally interconnected with the ventral hippocampus (vCA1) and subiculum as well as with the medial prefrontal cortex (mPFC). The BA receives unidirectional input from the midline thalamic nuclei, and projects to the striatal structures (McDonald, 1992; Pape and Pare, 2010; Pitkanen et al., 2000; Sah et al., 2003; Tovote et al., 2015). Moreover, the BA is intimately connected to the parts of the olfactory system, such as the NLOT, accessory olfactory bulb and olfactory bulb via unidirectional or reciprocal projections (Pitkanen et al., 2000; Sah et al., 2003).

1.3.3 Excitatory circuits in the BA networks

The cytoarchitecture of the BA shows cortical-like characteristics since glutamate releasing excitatory PNs give rise to the majority of the BA neuron population (80-85%), while the remaining neurons belong to different GABA releasing inhibitory cell types (15-20%)(McDonald, 1982a, b). BA PNs typically display a cortical pyramidal cell like appearance with relatively large soma and 3-7 spiny dendrites. However, in the BA, somata of PNs are seemingly distributed randomly instead of being organized into a layered structure. Additionally, a fraction of PNs can emanate 1-2 apical-like dendrites, while others are more similar to cortical stellate cells.

Although, there is no convincing evidence proving that the presence of apical dendrite-like structures is directly related to any orientation or afferent input selectivity compared to other cortical regions (Faber et al., 2001; McDonald, 1992; Muller et al., 2006; Washburn and Moises, 1992). Excitatory inputs predominantly target the spines of the PNs, which densely cover the dendritic surface and can serve as individual computational units. In contrast, inhibitory terminals, which originate mostly from local GABAergic cells, innervate dendritic shafts and the perisomatic region of PNs. The axon of PNs is typically grown from the soma or from a proximal dendritic segment and sends recurrent collaterals targeting other PNs and GABAergic cells in the BA, while other braches project to distal cortical or subcortical regions for example to the CeA, mPFC and vCA1 (Carlsen and Heimer, 1988; McDonald, 1992; Tovote et al., 2015). PNs in the BA similarly to other cortical PNs display regular firing pattern with broad APs and relatively slow membrane time constant (Washburn and Moises, 1992). In the healthy amygdala, the balance of excitation and inhibition is tightly and precisely regulated by the orchestrated activity of excitatory and inhibitory neurons and once this balance is acutely or chronically shifted, it will cause dysfunction in the system. Based on in vivo electrophysiological recordings it has been suggested that PNs in the BA are under strong inhibitory control, because in normal conditions the activity level of PNs is very low (0.1-0.3 Hz)(Bienvenu et al., 2012; Gaudreau and Pare, 1996). This theory is strongly supported by many studies, showing increased excitatory activity of PNs in different mental disorders like posttraumatic stress disorder (PTSD) or anxiety-related disorders due to the impaired or loss of inhibitory control (Herry et al., 2010; Lewis et al., 2012; Marin, 2012; Prager et al., 2016; Tye et al., 2011).

1.3.4 Inhibitory circuits in the BA networks

Although GABAergic inhibitory cells constitute only the minority of the BA neuron population, similarly to other cortical areas, they show a large diversity in their morphological and electrophysiological properties as well as in their functions (Capogna, 2014; Lee et al., 2013; Spampanato et al., 2011). In the hippocampus and

neocortex, the layered structure of PNs provides a fair basis for classification of GABAergic cell types. The location of their soma and dendritic arbor can be distinctive characteristics as well as the area covered by their axonal arbor, which often indicates the preferentially targeted membrane domain of the PNs. In contrast, in the BA the lack of the layered organization and the seemingly random distribution of neurons make the identification of the distinct GABAergic cell types difficult. Special anatomical methods, such as multicolor immunostaining and electronmicroscopic (EM) analysis are required for a satisfying and precise classification of cell types. Most of the studies in the literature classify GABAergic cells in the BA based on their neurochemical marker content and electrophysiological properties, methods which are also accepted and widely used in the neocortex and hippocampus (Ascoli et al., 2008; Capogna, 2014; DeFelipe et al., 2013; Freund and Buzsaki, 1996; Jiang et al., 2015; Klausberger and Somogyi, 2008; Lee et al., 2013; Markram et al., 2004; Pelkey et al., 2017; Spampanato et al., 2011).

According to this approach, the GABA releasing neuron population can be separated into two major, non-overlapping groups by their Ca2+ binding protein expression, the CB and the CR expressing inhibitory cells. The CB expressing GABAergic cells represent ~55 percent and the CR expressing GABAergic cells represent ~17 percent of the total GABAergic neuron population in the BA. Together with a small fraction of PV expressing neurons, which colocalize neither with CB, nor with CR, these groups cover the vast majority of the GABAergic population. Taking into account other types of neuropeptides and Ca^{2+} binding proteins expressed in distinct GABAergic cell types, the two main group can be further subdivided into those expressing PV, CCK, VIP, SOM or NPY (Davila et al., 2008; Kemppainen and Pitkanen, 2000; Mascagni and McDonald, 2003; McDonald, 1989; McDonald and Betette, 2001; McDonald and Mascagni, 2001a, 2002). The vast majority of the GABAergic cells expressing PV typically targets the perisomatic subcellular domains of PNs. These cells are mostly referred as fast spiking BCs and AACs, since they display fast non-adapting firing characteristics and narrow APs (< 0.50 ms). These INs are analogs of those PV-expressing BCs and AACs in the neocortex and hippocampus. (Bienvenu et al., 2015; McDonald and Betette, 2001; McDonald and Mascagni, 2001a; Rainnie et al., 2006; Vereczki et al., 2016; Veres et al., 2017; Veres et al., 2014;

Woodruff and Sah, 2007b). PV-expressing inhibitory neurons receive strong feedback excitation from local PNs and only a small portion of their excitatory inputs originate from cortical afferents, indicating their significant participation in feedback inhibition (Smith et al., 2000; Veres et al., 2014). Activity of PVBCs and AACs in the BA is not tightly phase coupled to hippocampal theta oscillation in contrast to e.g. other CB-expressing inhibitory and Astria cells. PV-expressing AACs and Astria cells, but not PVBCs are strongly activated by noxious stimuli, further supporting the view that the PV population is not homogenous, but rather shows cell type specific contribution to network functions (Bienvenu et al., 2012). Interestingly, the special ability of AACs to excite PNs has also been demonstrated in the BA similarly to the neocortex (Szabadics et al., 2006; Woodruff et al., 2006).

In addition to the PV-expressing BCs and AACs, there is another group of GABAergic cells, which targets the perisomatic region, but differ from those expressing PV in many aspects. This cell type has typically a large soma and express CCK and CB1 receptor, as well as they can be characterized by accommodating regular firing and broad APs (Jasnow et al., 2009; Katona et al., 2001; Mascagni and McDonald, 2003; McDonald and Mascagni, 2001b; Rovira-Esteban et al., 2017; Vereczki et al., 2016; Veres et al., 2017). Additionally to the CCK expression, different subsets of these INs contain either CB, CR or VIP, but their somata tend to be smaller and their axons preferentially innervate the dendrites of PNs or other GABAergic cells (Mascagni and McDonald, 2003; Rovira-Esteban et al., 2017; Vereczki et al., 2016). Although the role of inhibitory cell types in the regulation of PN and network activity is under intensive research, the current knowledge about the function of CCKBCs is largely incomplete not only in the BA, but in all the cortical regions. Comparing CCKBCs to PVBCs, which are evidently involved in the generation and maintenance of network oscillations, information coding, and the clockwork-like control of PN activity, the literature serves much less information about the in vivo activity of CCKBCs and their impact on circuit function. Early studies, which examined CCKBCs, suggested that ascending subcortical neuromodulatory afferents innervate these INs, thereby may underlie for fine-tuning of network operations. This theory was partially based on the presence of a rich set of neuromodulatory receptors in their membranes (Freund, 2003). It is also reported that CCK-containing cells expressing

CB1 receptors in the BA have a regulatory role in fear extinction in an endocannabinoid-mediated way (Katona et al., 2001; Marsicano et al., 2002), although it cannot be ruled out that, the observed effects were mediated by CB1 receptors expressed by PNs (Ruehle et al., 2013). An additional support for the "mood cell" theory has come from a recent study showing that during fear extinction, those PNs that participated in extinction memory encoding received inhibition from CCKBCs with different short-term dynamics and reduced endocannabinoid-mediated retrograde control of synaptic transmission - the so-called DSI - compared to those PNs that were active during fear learning (Vogel et al., 2016). Interestingly, even more profound target selectivity of CCKBCs has been found in cortical regions, where defined PN populations are specifically innervated and avoided, respectively (Bodor et al., 2005; Varga et al., 2010).

In addition to INs targeting the perisomatic region of PNs, there are several types of GABAergic cells innervating preferentially the dendrites of neurons. Similarly to the neocortex and hippocampus, SOM-expressing inhibitory neurons also exist in the BA and preferentially target dendrites (Muller et al., 2007; Wolff et al., 2014), thus they can regulate the dendritic computation in local PNs. In a subset of SOM cells CB or NPY can be also found. It has been found that this group of cells often sends axon collaterals outside of the amygdala projecting to the basal forebrain or entorhinal cortex (McDonald et al., 2012; Truitt et al., 2009).

Unfortunately, a detailed description and classification of BA GABAergic cell types are advancing slowly and many types of GABAergic cells revealed by immunohistochemical stainings are waiting for further examination. For example, the existence for the IN-selective inhibitory cell types that are typically expressing VIP and/or CR has just been characterized in the BA (Rhomberg et al., submitted). Furthermore, there is a special inhibitory cell type in cortical regions that is distinguished from "classic" GABA releasing cell types in many aspects, called neurogliaform cells (Olah et al., 2009; Tamas et al., 2003). They can be characterized by a small soma and short dendritic arbor and with an extremely dense local axonal ramification. GABAergic neurons with morphology identical to this cell type exist in the BA and express NPY (Manko et al., 2012). They form non-classical, so-called „loose" inhibitory synapses, which conduct slow $GABA_A$ (and in some cases $GABA_B$)

receptor-mediated responses in the postsynaptic partners and their inhibitory action is rather between the real synaptic inhibition and volume transmission of GABA (Olah et al., 2009; Price et al., 2005; Tamas et al., 2003). In summary, as in other cortical areas, almost all types of GABAergic cells have been defined in the BA.

Recently our group have also studied IN functions in the amygdala. Detailed anatomical and electrophysiological investigations have provided valuable data about the features of the PTIs and comparative analysis has shed light on some common and distinctive properties of the different BC types and AACs in the BA (**Fig. 3**). Surprisingly, it was found that AACs possess much smaller dendritic and axonal arbor in the BA in comparison to that found in the hippocampus, but these INs still innervate exclusively the AIS of the PNs (Papp et al., 2013; Vereczki et al., 2016; Veres et al., 2014). It has also been demonstrated that cell type specific morphological and physiological differences occur between the different types of PTIs, yet their inhibitory efficacy is similarly large though (Rovira-Esteban et al., 2017; Vereczki et al., 2016; Veres et al., 2017). In addition to the careful classification of BA PTIs, CCK/CB1-expressing INs can be further subdivided by their neurochemical profile, as a portion of these INs coexpressing Vglut3 preferentially target the perisomatic region of PNs, while those coexpress CB tend to innervate dendrites adding further complexity to the BA network (Rovira-Esteban et al., 2017), but comparable to that observed in the hippocampus (Klausberger et al., 2005; Lasztoczi et al., 2011).

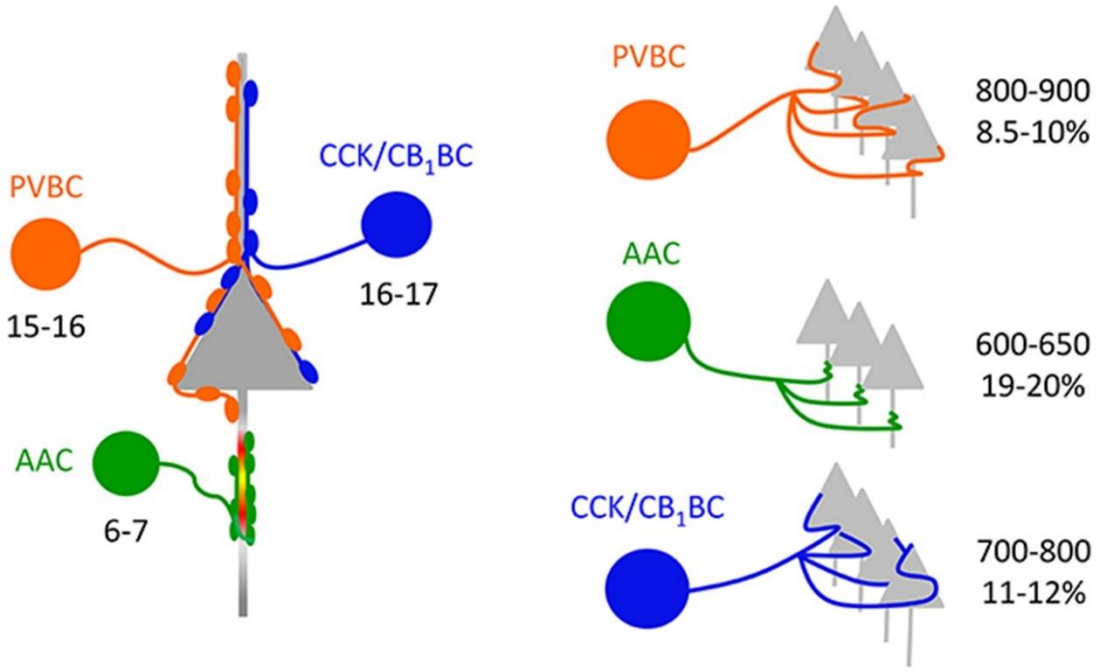

Figure 3. ***Convergence and divergence in the microcircuits composed of PTIs and PNs in the BA***. *Left, Similar numbers of PVBCs and CCKBCs converge on a PN in the BA. In contrast, fewer AACs innervate the AIS of single PNs (Veres et al., 2014). Right, The number of PNs targeted by singe BCs is comparable, while individual AACs innervate fewer PNs. The percentage refers to the fraction of PNs that are innervated by single INs within their axonal cloud. (Adapted from (Vereczki et al., 2016))*

Although our knowledge about the anatomical and functional properties of BA INs is dynamically accumulating, a large gap still exists to compose a realistic network model of the BA. Therefore, further investigations of the BA circuit are necessary to provide the bases for computational approaches aiming to understand the circuit operation in this cortical region. While research tools are obviously developing and opening new ways to have more insights into the brain working in vivo, in parallel, many of these novel technical approaches still suffer from the lack of satisfying specificity. A good example for supporting this notion is the fast spread of the different transgenic rodent strains. One of the original purposes of the genetic modification was to help selectively visualize specific cell groups and to allow the specific modulation

of their activity in order to understand their function. Unfortunately, the main goal, to selectively target certain cell types based on their most characteristic neurochemical profile, has partially failed, because as we can conclude from classification studies this approach resulted in broader categories (Capogna, 2014; DeFelipe et al., 2013; Freund and Buzsaki, 1996; Jiang et al., 2015; Klausberger and Somogyi, 2008; Lee et al., 2013; Markram et al., 2004; Spampanato et al., 2011). For example, PVBCs, AACs, bistratified cells and OLM cells are all expressing PV or PV and SOM in hippocampal CA1, but morphological studies showed that they target different membrane domains of PNs, thereby together they fully cover the somatodendritic surface of PNs. Furthermore, it was also revealed that these cell types are differently coupled to network oscillations, observations that suggest different roles for these INs in network operation (Klausberger et al., 2003; Klausberger et al., 2005). Therefore, in transgenic mouse lines where a fluorescent protein or cre-induced expression is under the control of either Ca^{2+} binding protein or neuropeptide promoter (e.g. PV-cre, SOM-cre, VIP-cre and NPY-cre lines), for instance, it is not possible to accurately manipulate the perisomatic inhibition without simultaneously affecting the distal dendritic inhibition of PNs. The level of IN diversity reported so far is mainly determined by the available anatomical, electrophysiological and molecular biological methods, which were applied during the classification process. Notably, it must to be also taken into account that the border between the natural variability of biological systems and the artificial resolution of our research methods is very thin. In order to fully map neuronal circuits responsible for different tasks in the brain, multidisciplinary approaches are necessary from the molecular level even to behaviour. In our studies, we have attempted to reveal the organizing principles of the PN-perisomatic inhibitory cell subnetworks in cellular, synaptic and network levels using the combination of the eligible classic and latest cutting-edge research methods.

1.3.5 The role of BA in emotional memory formation

Amygdala has been implicated in emotional memory formation, especially in acquiring fear memory and its extinction. The majority of our knowledge comes from

investigations of the rodent amygdala and behaviour using the classic Pavlovian fear conditioning approach (Amano et al., 2010; Quirk et al., 1997; Quirk et al., 1995). By using this task in combination with functional magnetic resonance imaging (fMRI), it has been also demonstrated that amygdala and mPFC are involved in fear memory formation also in humans (LaBar et al., 1998; Morris et al., 1998; Phelps et al., 2004). This paradigm is one of the most powerful approaches to investigate associative learning as well as to observe the function of dedicated neuronal circuits along with the resulting behavioural output (Davis and Shi, 2000; Fanselow and Poulos, 2005; LeDoux, 2000; Maren, 2001). The power of this method is given by its relative simplicity that a tone-shock pairing results in a long-lasting robust and reproducible fear response. In classic fear conditioning models, a conditioned neutral stimulus (CS, usually a tone) is paired with an aversive US (usually a mild electrical shock), which may lead to the expression of fear behavior (e.g. freezing) recalled by the subsequent presentation of the CS alone. Although the freezing response can be reproduced across several trials, repeated exposure to the CS gives rise to a marked decrease of freezing behaviour both in rodents and humans, therefore this phenomenon is called fear extinction (Amano et al., 2010; Herry et al., 2010; Milad and Quirk, 2002; Phelps et al., 2004).

According to the dominant concept, during fear learning the information unidirectionally flows in the amygdala, since the afferent information enters at the LA and is relayed through the BA toward the CeA, which region is proposed to be the output site (**Fig. 4A**). The PNs in the LA receive processed sensory information from several cortical areas including higher order auditory, visual or somatosensory cortices and thalamus, respectively (LeDoux, 2000; Li et al., 1996b; McDonald, 1998; Turner and Herkenham, 1991). Under normal conditions, local inhibitory circuits might significantly suppress the impact of the afferent excitatory projections to the LA, but in a fearful context, disinhibition of the LA networks can induce LTP at the afferent and/or local excitatory fibers. Thus, a gating function of inhibitory neurons during associative learning may be fundamental in fear memory formation (**Fig. 4A**)(Bissiere et al., 2003; Lang and Pare, 1997; Lee et al., 2013; Li et al., 1996a; Tully et al., 2007; Woodruff and Sah, 2007a). It has been hypothesized that the processed information from the LA is transferred to the BA, where fear responsive PNs will be recruited (**Fig.**

4A)(Amano et al., 2011; Herry et al., 2008). These fear cells are also called fear memory engram cells as it was nicely demonstrated that during repetition of the same fear task, the same population and pattern of fear encoding PNs were activated upon fear memory retrieval (Kim et al., 2016; Kitamura et al., 2017). Besides fear cells, extinction memory is also encoded and stored in the BA, although in a different population of PNs. The "extinction" neurons display different firing activity in response to the CS compared to fear neurons during fear learning vs. extinction memory formation (Amano et al., 2011; Herry et al., 2008). Acquisition of fear extinction memory is an active process, not simply the depotentiation of synapses conveying fear-related information, nor a forgetting process suggested by early studies (**Fig. 4B**). The animal learns that the previously threatening CS is not dangerous anymore, therefore this new memory rather suppresses the previously acquired fear memory, than erases that (Amano et al., 2011; Herry et al., 2010; Kim et al., 2007). This idea is further supported by observations showing that extinguished fear memory can be spontaneously retrieved or can be experimentally renewed by presentation of either the context or the US (Rescorla, 2004; Rescorla and Heth, 1975). In addition to the central role of the BA in fear and extinction memory expression, accumulating evidence indicates that BA has an important role in reward learning behaviour, which likely involves its reciprocal connection with the NAcc (Beyeler, 2016; Gore et al., 2015; Namburi et al., 2015; Tye and Janak, 2007; Tye et al., 2008). Altogether, these data imply that BA has a crucial role in association of both negative and positive valence with sensory information.

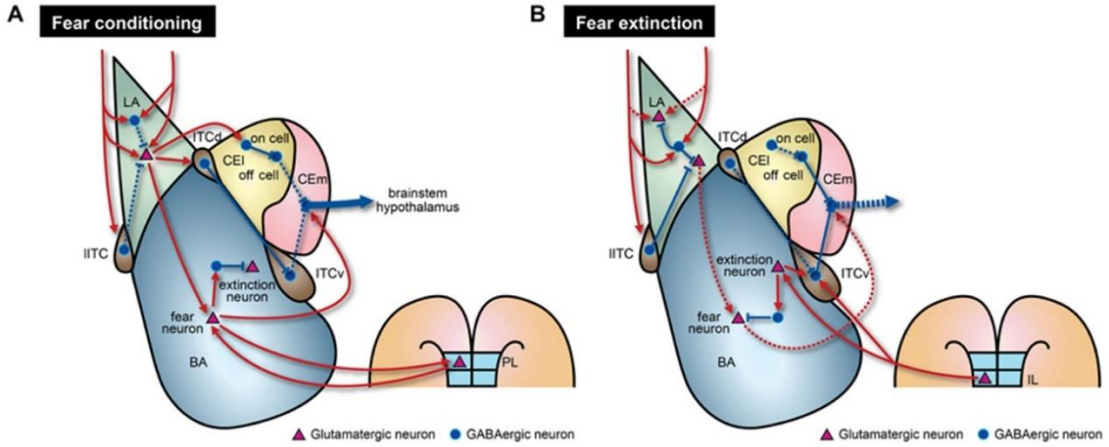

Figure 4. ***Model of amygdala circuitries during fear conditioning and extinction.*** *The model contains both known and hypothetical neural connections. Solid and dashed lines indicate strengthened and weakened connections, respectively, during the learning processes. (**A**) During fear conditioning, CEm output activity is enhanced by two intra-amygdala pathways. First, there are enhanced excitatory signals that originate from LA. In LA, there is disinhibition of local inhibitory circuits due to the effects of several biogenic amines. This disinhibition leads to increased neural activity in BA, ITCd, and CEl. Fear neurons in BA may receive direct excitatory inputs from LA. Augmented activity of fear neurons, mediated through reciprocal connections with prelimbic (PL) regions, is necessary to activate CEm output neurons. Second, strong inhibition of CEloff neurons and signaling from ITCv to CEm output neurons are reduced by the LA–CElon–CEloff–CEm and LA–ITCd–ITCv–CEm pathways, respectively. (**B**) During fear extinction, enhanced neural activity in LA is reduced by increased suppression from local inhibitory circuits and depotentiation of glutamatergic synapses. Decreased connectivity between extinction-resistant neurons in LA and fear neurons in BA could also contribute to fear extinction. Furthermore, infralimbic cortex (IL) sends glutamatergic projections to ITCv and possibly extinction neurons of BA. These IL projections may participate in suppression of BA fear neurons via local inhibitory circuits. (Adapted from (Lee et al., 2013)).*

A recent study using a „state of the art" combination of molecular biology, optogenetics and behavioural approaches has put into context the amygdala function in the systematic consolidation of fear memory (Kitamura et al., 2017). During the early phase of contextual fear conditioning BA receives contextual information from entorhinal and hippocampal regions, and the fear response is driven primarily by the amygdala. However, in parallel with this, the BA sends information toward the mPFC. As it is already known, the PL and IL regions of the mPFC have a reciprocal connectivity with the BA, and these pathways are implicated in the expression of fear and fear extinction, respectively (**Fig. 4**). Surprisingly, with time the regulation of fear response tends to be shifted into the PFC in parallel with the "maturation" of a well-defined fear related neuron population in this region, while fear-related neuronal populations in the hippocampus and entorhinal cortex tend to be less active in response to fear memory retrieval. In the BA fear engram cells preserve their responsiveness independently from the time, as they are activated both in early and remote fear memory retrieval (Kitamura et al., 2017; Maren and Fanselow, 1996). These findings together suggest that, when the animal encounters to a dangerous situation at the first time, fear engram is forming in the BA, as well as the fear response will be primarily driven by the amygdala. However, with time fear memory also evolves in the mPFC and repeated occurrence of the same dangerous situation will be evaluated first in this region, thereby the mPFC take over the regulation of BA function. This top-down process may control whether the fear response is adequate, or extinction memory should be induced (Kitamura et al., 2017).

In the past few years, amygdala research highly accelerated thanks to the new opto- and chemogenetic methods. In parallel, the focus has shifted from the synaptic and cellular levels toward the "loss of function" and "gain of function" manipulations of large neuronal populations in behaving animals, but in order to understand how the information is processed and converted into a behavioural response it requires the full exploration of the amygdala circuits at the network level.

2 AIMS

The aim of this study was to unravel the mechanisms underlying the recruitment of the perisomatic inhibitory neurons in the basal nucleus of the amygdala by local collaterals of PNs. To address this question, we needed to reveal the connectivity between CCKBCs, PVBCs, AACs and PNs in the BA and the properties of these connections. In the three main parts of the study, we aimed to answer the following specific questions:

1. Characterization of the input-output properties of the PTIs in the BA.

1.1 Identification and classification of the PTIs in the BA.

1.2 Determining the intrinsic electrophysiological properties of the PTIs.

1.3 Characterization of the output synaptic properties of the PTIs.

1.4 Comparison of the inhibitory efficacy of CCKBCs and PVBCs on PN spiking.

2. Investigation of the local feedback excitation received by the PTIs.

2.1 Determining the activation threshold of the different types of PTIs in the BA.

2.2 Comparison of the local excitatory input properties received by the distinct BC types.

2.3 Mapping the excitatory innervation received by the distinct BC types.

2.4 Comparison of the feedback excitation received by PVBCs and AACs.

3. Unraveling the wiring principles of PTIs and PNs in the BA circuits.

3.1 Mapping the connectivity among PTIs using immunocytochemical methods.

3.2 Functional mapping of connectivity among PTIs.

3.3 Proposing a model for the connectivity between PTIs and PNs in the BA.

3. MATERIALS AND METHODS

3.1 Experimental animals

All experiments were approved by the Committee for the Scientific Ethics of Animal Research (22.1/360/3/2011) and were performed according to the guidelines of the institutional ethical code and the Hungarian Act of Animal Care and Experimentation (1998; XXVIII, section 243/1998, renewed in 40/2013) in accordance with the European Directive 86/609/CEE and modified according to the Directives 2010/63/EU. Transgenic or double-transgenic mice of either sex (3 weeks to 10 weeks old) expressing enhanced green fluorescent protein (eGFP) under the control of the Pvalb promoter (BAC-PV-eGFP, (Meyer et al., 2002)), expressing DsRed under the Cck promoter (BAC-CCK-DsRed, Mate et al 2013), or expressing both eGFP and DsRed under the Pvalb and Cck promoter, respectively, were used in in vitro experiments.

3.2 Slice preparation and electrophysiological recordings

3.2.1 Slice preparation for electrophysiological recordings

For acute slice preparation, mice were deeply anesthetized with isoflurane and decapitated. The brain was quickly removed and placed into ice-cold solution, containing (in mM): 252 sucrose, 2.5 KCl, 26 $NaHCO_3$, 0.5 $CaCl_2$, 5 $MgCl_2$, 1.25 NaH_2PO_4, 10 glucose, bubbled with 95% O_2/5% CO_2 (carbogen gas). Horizontal slices of 200 μm thickness containing the BA were prepared with a Leica VT1000S or VT1200S vibratome and kept in an interface-type holding chamber containing artificial cerebrospinal fluid (ACSF) at 36°C that gradually cooled down to room temperature. ACSF contained the following (in mM): 126 NaCl, 2.5 KCl, 1.25 NaH_2PO_4, 2 $MgCl_2$, 2 $CaCl_2$, 26 $NaHCO_3$, and 10 glucose, bubbled with carbogen gas.

After at least one hour-long incubation, slices were transferred to a submerged type of recording chambers perfused with 32°C ACSF at approximately 2-2.5 ml/min flow rate. Recordings were performed under visual guidance using differential interference contrast microscopy (DIC)(Olympus BX61W or Nikon FN-1) using a 40x

or 16x water immersion objective. Neurons expressing eGFP or DsRed were visualized with the aid of a mercury arc lamp or a monochromator (Till Photonics) and detected with a CCD camera (Hamamatsu Photonics or Andor Zyla). Patch pipettes (4-7 MΩ) for whole-cell recordings were pulled from borosilicate capillaries with inner filament (thin walled, OD 1.5) using a DMZ-Universal Puller (Zeitz Instruments) or a P1000 pipette puller (Sutter Instruments). For loose-patch recordings 3-5 MΩ pipettes were filled with normal ACSF, and an incomplete seal was formed during the recording with the cell membrane of the targeted neuron in order to monitor spiking activity. In whole-cell paired recordings the patch pipette contained a K-gluconate-based intrapipette solution containing the following (in mM): 110 K-gluconate, 4 NaCl, 2 Mg-ATP, 20 HEPES, 0.1 EGTA, 0.3 GTP (sodium salt), and 10 phosphocreatine adjusted to pH 7.3 using KOH, with an osmolarity of 290 mOsm/L. In IN-PN paired recordings, the presynaptic intrapipette solution additionally contained 0.2% biocytin and 10 mM GABA and the postsynaptic intrapipette solution additionally contained 100 μM AlexaFluor-488 hydrazide sodium salt (Invitrogen). In PN-IN paired whole-cell recordings, 0.2% biocytin and 10 mM glutamate were added to the presynaptic intrapipette solution, and 0.1 mM spermine and Cascade Blue hydrazide trisodium salt (0.1%), Lucifer Yellow CH potassium salt (0.1%), or Alexa 594 hydrazide sodium salt (100 μM, all from Life Technologies) was added to the postsynaptic intrapipette solution in order to visualize the recorded cells in different colors. In light stimulation experiments, in which only INs were recorded in whole-cell mode, the intrapipette solution contained 0.2% biocytin. In IN-IN paired whole-cell recordings, intrapipette solution for both cells contained the following (in mM): 54 K-gluconate, 4 NaCl, 56 KCl, 20 HEPES, 0.1 EGTA, 10 phosphocreatine, 2 Mg-ATP, 0.3 GTP (sodium salt), 10 mM GABA, and 0.2% biocytin adjusted to pH 7.3 using KOH and with an osmolarity of 290 mOsm/L.

Recordings were performed with a Multiclamp 700B amplifier (Molecular Devices), low-pass filtered at 2 kHz, digitized at 10-50 kHz, and recorded with an in-house data acquisition and stimulus software (Stimulog, courtesy of Prof. Zoltán Nusser, Institute of Experimental Medicine, Hungarian Academy of Sciences, Budapest, Hungary) or Clampex 10.4 (Molecular Devices). Recordings were analyzed with EVAN 1.3 (courtesy of Professor Istvan Mody, Department of Neurology and

Physiology, University of California, Los Angeles, CA), Clampfit 10.4 (Molecular Devices), Origin 8.6, or OriginPro 2015. Recordings were not corrected for junction potential. To test the firing characteristics, neurons were injected with 800-ms-long hyperpolarizing and depolarizing square current pulses with increasing amplitudes from -100 to 600 pA. The broad AP waveform, accommodating firing pattern, and slow after-hyperpolarization were characteristic for PNs. PN identity was further confirmed by the post hoc morphological analysis of their spiny dendrites. For PVBCs and AACs, fast spiking, nonaccommodating firing pattern together with eGFP expression were typical as well as post hoc analysis of their neurochemical marker profile. CCKBCs were characterized by their accommodating regular firing pattern together with strong DsRed expression as well as post hoc analysis of the expression of CB1 at their axon terminals (see below).

3.2.2 Measuring the intrinsic properties of PTIs

Using voltage responses to the hyperpolarizing current injections, we calculated the input resistance, membrane capacitance, membrane time constant, and the relative sag amplitude with a custom-made program written in MATLAB (Zemankovics et al., 2010).

The AP features and the firing characteristics were calculated from the voltage responses to the depolarizing current steps with an in-house analysis software SPIN 1.0.1 (courtesy of Prof. Zoltán Nusser; (Papp et al., 2013)). The amplitude of the AP was defined as the voltage difference between the threshold and peak of the AP, while the AP half-width refers to the full width at the half maximum of the AP. Accommodation index was calculated as the ratio of the values for the last and the first inter-spike intervals (**Table 1**).

3.2.3 Recording and analysis of inhibitory connections

For determining the output properties of PTIs, the presynaptic cell was an IN identified by its fluorescence signal and the postsynaptic cell was a randomly chosen

neighboring PN. The intrapipette solution used for the postsynaptic PN contained (in mM) 80 CsCl, 60 Cs-gluconate, 1 MgCl2, 2 Mg-ATP, 3 NaCl, 10 HEPES, and 5 QX-314 (2(triethylamino)- N-(2,6-dimethylphenyl) acetamine), adjusted to pH 7.3 with CsOH and the osmolarity was 295 mOsm/L. Presynaptic INs were held in current-clamp mode near a membrane potential of -65 mV, and stimulated by brief current pulses (1.5 ms, 1-2 nA) to evoke APs. PNs were clamped at the holding potential of -65 mV. Series resistance (between 5 and 20 MΩ) was frequently monitored and compensated by 65%. Cells where the series resistance has changed more than 25% during recording were discarded from further analysis. The kinetic properties of unitary inhibitory postsynaptic currents (uIPSCs) were calculated with excluding the transmission failures. The latency of synaptic transmission was calculated by subtracting the time of the AP peaks from the onset of the postsynaptic currents. This latter value was estimated by subtracting the rise time from the peak time of events calculated from the time of the AP peaks. Calculation of asynchronous release was achieved by the comparison of the average charge (area under the curve) of all currents in a 100-ms-long time window before and after the AP trains. To investigate the dynamics of the transmitter release, we calculated the average of uIPSC amplitudes in response to ten APs at different frequencies evoked in the presynaptic cell. These trains of APs were evoked at 0.05 Hz during each recording.

For recordings of inhibitory efficacy of BCs, the presynaptic IN was held near a membrane potential of -65 mV in current-clamp mode and injected by brief square current pulses (2 ms, 1.5-2 nA) to evoke spikes. As done before, the PN was clamped at a holding potential of -40 mV (Veres et al., 2014). Series resistance was monitored (range: 8-20 MΩ) and compensated by 65%. To record IPSPs, the presynaptic cell was stimulated in the same way, and the postsynaptic PN was held in current-clamp mode at approximately -55 mV. Bridge balance was adjusted throughout the recordings. Kinetic properties of IPSCs and IPSPs were analyzed on the average of 10 to 20 consecutive events. To test the capability of BCs to suppress PN firing, sinusoidal current pulses at theta frequency (3.53 Hz) with peak-to-peak amplitudes of 30 pA and 50 pA were injected into the postsynaptic PN. The membrane potential of PNs was set (approximately -55 mV) to trigger a spike at the peak of the sinusoidal current pulses with the amplitude of 50 pA but not with 30 pA (Veres et al., 2014). This adjustment

maintained the membrane potential of PNs near the spiking threshold. One trial consisted of 7 sinusoidal current waves (5 x 50 pA and 2 x 30 pA), repeated 10 to 20 times in each pair. Three APs at 30 Hz were evoked in the IN by brief square current pulses (2 ms, 1.5-2 nA) before the fourth sinusoidal current wave (50 pA) in each trial. To assess the reduction in spiking probability, the probability of AP generation in PNs under control conditions was determined from the average of the responses to 50 pA currents (first, third, fifth, and sixth sinusoidal wave), which was compared with that recorded during the fourth cycle. In IN-IN pair recordings, presynaptic INs were held in current-clamp mode at approximately -65 mV, and 3 to 10 APs were evoked by injection of brief square current pulses (2 ms, 1.5-2 nA) at 30 Hz or 40 Hz, while IPSCs in the postsynaptic cell were recorded at the membrane potential of -65 mV. To study the electrical coupling, a hyperpolarizing current of 100 pA or 200 pA in one IN was applied, and the change in the voltage was monitored in the other IN. This experiment was performed bi-directionally. IN pairs were considered electrically coupled when a change in the voltage of one IN could also be observed in the other one.

3.2.4 Recording and analysis of excitatory connections

For recordings of excitatory postsynaptic currents/potentials (EPSCs/EPSPs) in PN-IN pairs, postsynaptic INs were recorded at -65 mV, while 3 to 5 brief square current pulses (2 ms, 1.5-2 nA) were applied in the presynaptic PN held at approximately -65 mV in current-clamp mode. For constructing the connectivity map, PV-eGFP, CCK-DsRed, or PV-eGFP x CCK-DsRed transgenic mice (P30–35) were injected with 2/5 serotype adeno-associated virus (AAV) carrying CaMKII-ChR2-mCherry construct (for CaMKII and ChR2 see the chapter, List of abbreviations)(Penn Vector Core) bilaterally into the BA (anteroposterior: -1.5; mediolateral: 3.3; dorso-ventral: -4.4 mm from bregma, 50-100 nl into each hemisphere). At least 3 weeks after the injection, acute slices of 200-µm thickness were obtained from mice expressing ChR2 in PNs, as described above. For mapping the connection probability between PNs and perisomatic inhibitory INs using light stimulation, an eGFP- or a DsRed-expressing IN was recorded in whole-cell mode, while single PNs were sequentially

activated by a blue light spot having a diameter of the soma sized (15-20 μm) for 50 ms (447 nm blue laser, Roithner Laser Technik) using a Digital Mirror Device (DMD)-based pattern illuminator (Mightex Polygon 400)(**Fig. 5, Fig. 6**).

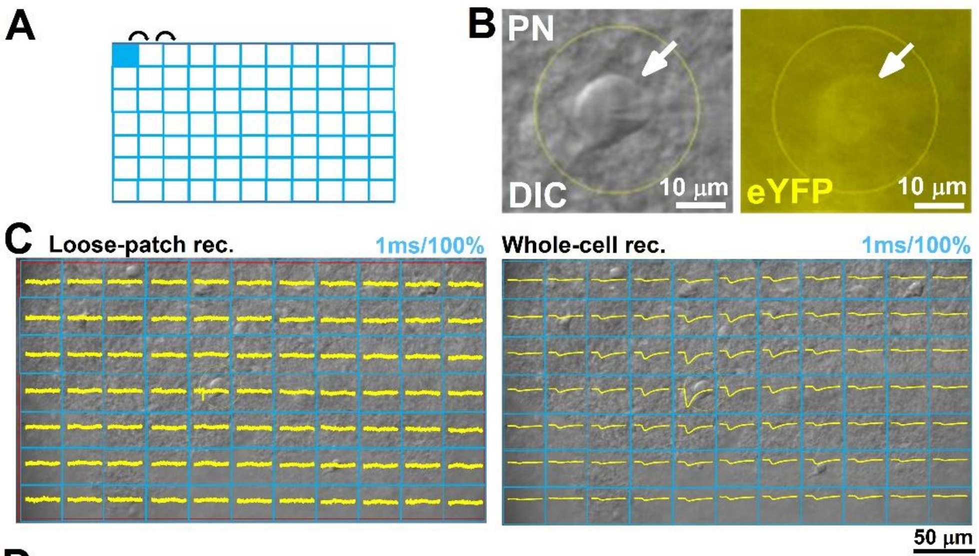

D Loose-patch rec. 1ms/100%

0	0	0	0	0	0	0	0	0	0	0
0	0	0	0	0	0	0	0	0	0	0
0	0	0	0	0	0	0	0	0	0	0
0	0	0	0	0	0	0	0	0	0	0
0	0	0	0	0	0	0	0	0	0	0
0	0	0	0	0	0	0	0	0	0	0
0	0	0	0	0	0	0	0	0	0	0

Whole-cell rec. 1ms/100%

-13	-21	-30	-50	-42	-44	-56	-52	-57	-26	-19
-19	-30	-34	-54	-61	-51	-79	-87	-52	-33	-23
-27	-53	-56	-90	-148	-105	-102	-42	-31	-35	-38
-29	-69	-91	-124	-438	-175	-115	-75	-52	-39	-29
-31	-59	-109	-133	-236	-118	-121	-83	-37	-26	-22
-19	-47	-63	-62	-136	-125	-77	-57	-32	-31	-24
-16	-26	-30	-30	-57	-86	-66	-44	-31	-24	-16

E Loose-patch rec. 2ms/100%

0	0	0	0	0	0	0	0	0	0	0
0	0	0	0	0	0	0	0	0	0	0
0	0	0	0	0	0	0	0	0	0	0
0	0	0	0	1	0	0	0	0	0	0
0	0	0	0	0	0	0	0	0	0	0
0	0	0	0	0	0	0	0	0	0	0
0	0	0	0	0	0	0	0	0	0	0

Whole-cell rec. 2ms/100%

-33	-19	-56	-71	-83	-82	-101	-106	-95	-45	-19
-34	-38	-66	-98	-116	-99	-140	-151	-89	-69	-36
-56	-90	-103	-171	-259	-192	-172	-84	-56	-67	-59
-54	-116	-125	-216	-596	-286	-195	-128	-85	-58	-52
-46	-113	-173	-217	-366	-223	-211	-132	-58	-46	-35
-39	-83	-99	-120	-198	-241	-145	-98	-58	-50	-39
-25	-39	-56	-62	-100	-158	-124	-83	-56	-40	0

F Loose-patch rec. 5ms/100%

0	0	0	0	0	0	0	0	0	0	0
0	0	0	0	0	0	0	0	0	0	0
0	0	0	0	1	0	0	0	0	0	0
0	0	0	1	2	1	0	0	0	0	0
0	0	0	0	1	0	0	0	0	0	0
0	0	0	0	1	0	0	0	0	0	0
0	0	0	0	0	0	0	0	0	0	0

Whole-cell rec. 5ms/100%

-38	-73	-108	-143	-168	-167	-191	-203	-172	-89	-40
-58	-95	-128	-189	-228	-204	-260	-258	-167	-128	-79
-97	-160	-203	-312	-420	-337	-312	-173	-123	-128	-109
-114	-215	-235	-380	-749	-479	-342	-241	-146	-112	-99
-98	-185	-292	-366	-574	-387	-377	-235	-117	-93	-73
-73	-157	-198	-232	-351	-387	-270	-186	-117	-102	-74
-50	-90	-119	-126	-203	-283	-199	-132	-123	-111	0

Figure 5. ***Illustration of spatial stimulation profile of a ChR2-expressing PN in response to sub-, near-, and over-threshold stimulation in the BA.*** *(**A**) Schematic illustration of the stimulation pattern. Squares were illuminated with 447 nm laser light sequentially in a "scanning"-like manner. (**B**) DIC image of a ChR2-*enhanced yellow fluorescent protein *(eYFP)-expressing PN in the BA (left), and epifluorescent image of the eYFP expression in the same cell (right). (**C**) Example threshold calibration of the ChR2-expressing PN shown in (**B**). (left) Loose patch recordings, overlaid with DIC image showing the area covered by the illumination pattern, show that at the activation threshold a PN fires an AP in response to light stimulation only in that square, which fully covers its somatic region. (right) Light evoked spatial EPSC profile of the same cell recorded in whole-cell voltage-clamp mode indicates that the largest response could be measured in the same square where PN fired an AP in response to light stimulation. (**D**) Spatial profiles of the same PN activation (number of light evoked AP(s)/square) (left), and light evoked EPSC amplitudes (pA) (right) using subthreshold stimulation parameters (light pulse length: 1 ms, light intensity 100%). With subthreshold stimulation parameters, no light evoked AP could be detected. (**E**, left) Increasing the light pulse length (light pulse length: 2 ms, light intensity: 100%) readily activates the same PN. Near-threshold stimulation parameters evoke firing in the PN, if the light beam targets only the square, which covers the somatic region of the PN. (right) Spatial near-threshold stimulation evoked EPSC profile recorded in the PN. (**F**) Increasing further the stimulation light pulse length (light pulse length: 5 ms, light intensity: 100%) extended the area where the PN could be activated. (left) Targeting the somatic region covering square with over-threshold stimulation parameters evokes multiple spikes in the PN, but stimulating the neighboring area can also activate the PN. (right) Spatial over-threshold stimulation evoked EPSC profile in the PN.*

PNs were randomly chosen and the light-evoked APs were simultaneously monitored with a pipette containing ACSF in loose-patch mode. The connectivity map was created using the XY coordinates of the recorded cells, and the inter-somatic distance was calculated between the tested presynaptic PNs and the postsynaptic IN (**Fig. 6A and B**).

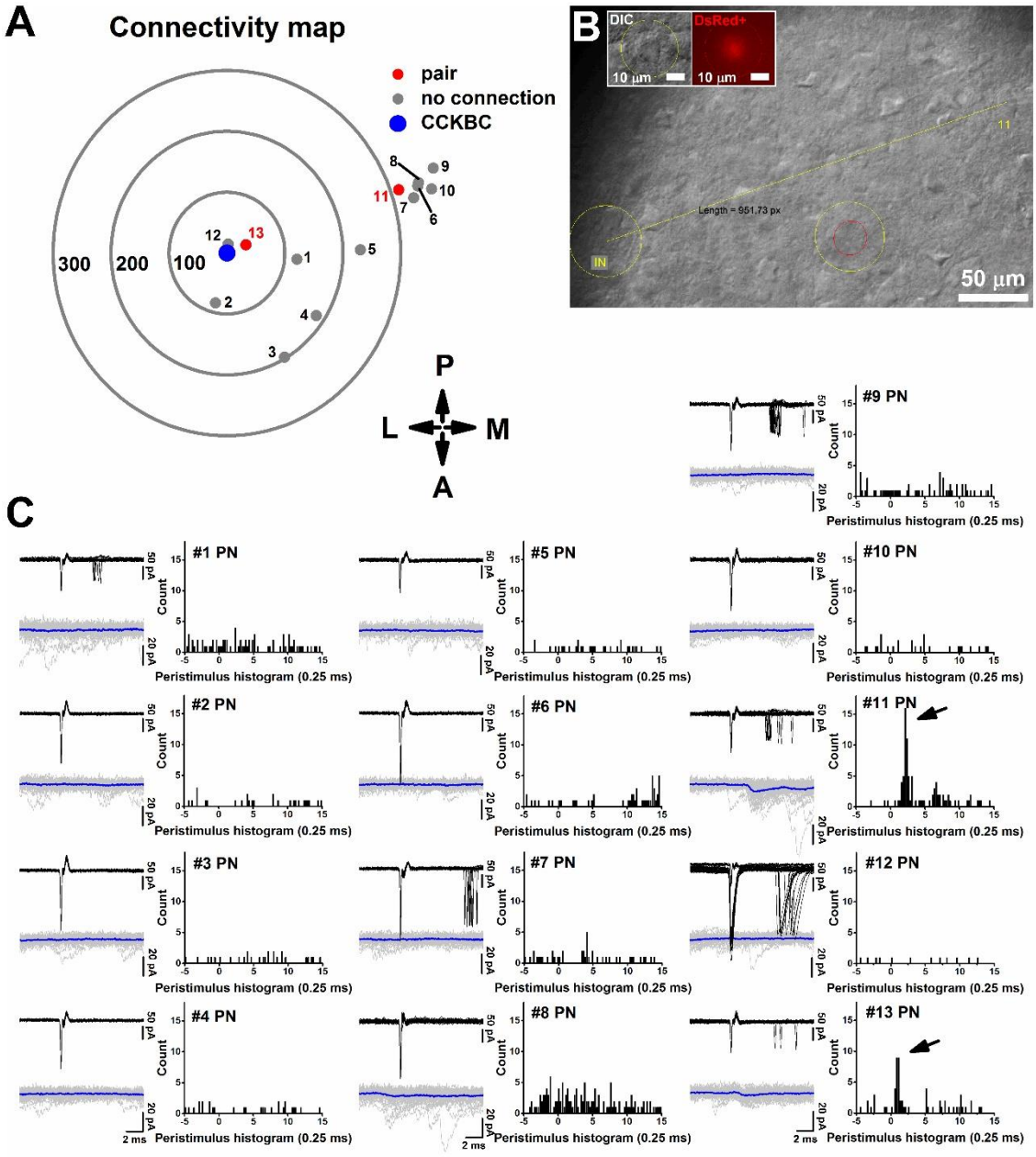

Figure 6. ***Mapping connectivity between single PNs and a CCKBC using optogenetics.*** *(**A**) Example experiment (t150422-01), where potential synaptic coupling between thirteen randomly selected PNs and the CCKBC (center, in blue) was tested. Two of the tested PNs innervated the CCKBC (red dots), while no response could be measured by activation of the remaining PNs (gray dots). Concentric circles indicate Δ100 µm distance from the CCKBC in the center. (**B**) DIC image shows the position and the distance of the recorded PN-CCKBC pair (PN #11). Red circle illustrates the size of the laser illumination spot over a PN soma. Insets, DIC and*

*epifluorescent images taken from the soma of the postsynaptic CCKBC. (**C**) Representative traces show recordings from all tested PNs (left panels). Ten consecutive traces (in gray) and averages (in blue). Peri-stimulus histogram was plotted for all tested PNs to reveal a monosynaptic connection between the PNs and the CCKBC (right panels). Arrows (PN #11, PN #13) indicate two monosynaptic connections out of thirteen PNs tested.*

Light stimulation intensity was set individually for each tested presynaptic PN to the minimal intensity value sufficient to evoke AP(s) (**Fig. 7C-D, Fig. 5**). We used 50-ms-long light pulses with low stimulus intensity to minimize the light scattering that might activate some neighboring PNs expressing ChR2 and/or their axons. Since the activation threshold of individual ChR2-expressing PNs highly depends on the ChR2 expression level (**Fig. 7C-D, Fig. 5**), it is expected that in some cases more than one PN is stimulated by the applied method. To overcome this limitation, we peak aligned the light-evoked APs in the PN, recorded in loose-patch mode in order to exclude uEPSCs that originated from the light-activated neighboring PNs (**Fig. 7C-D**).

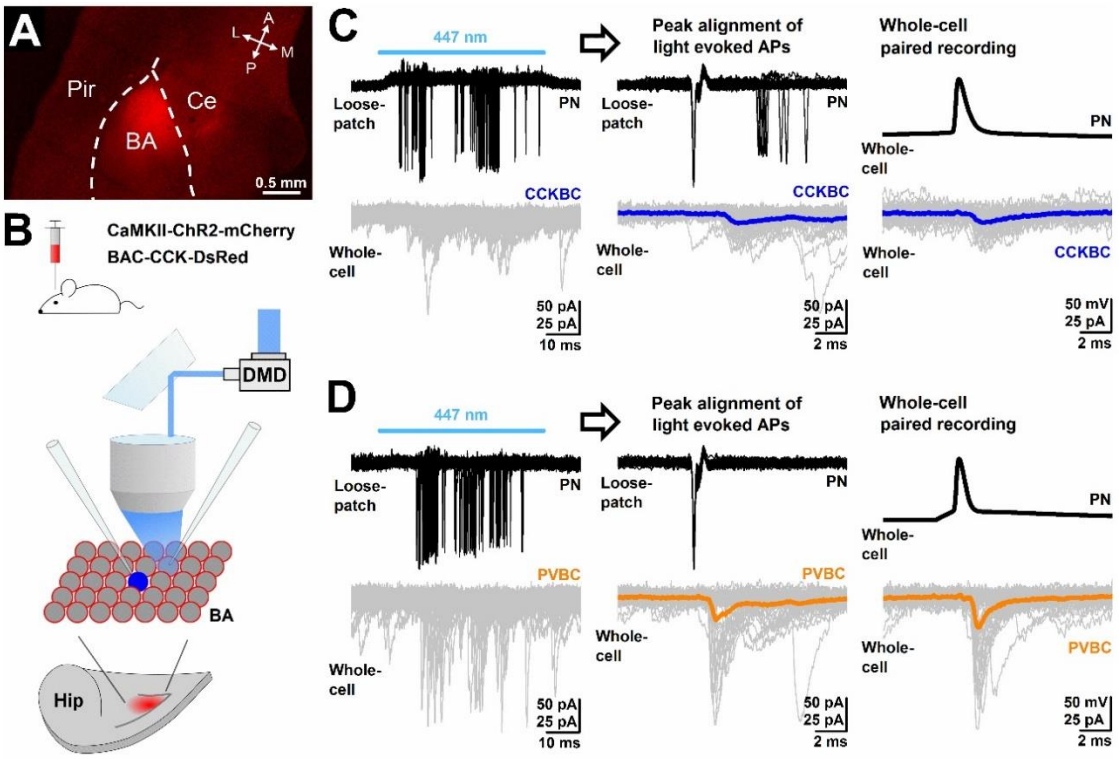

Figure 7. ***Basic properties of the uEPSCs in CCKBCs (blue) and PVBCs (orange) evoked by light stimulation of single PNs and by electrical stimulation of the same PNs in whole-cell mode are not different.*** *(**A**) Low magnification confocal image shows the ChR2-mCherry expression site in the BA after AAV injection. (Pir, piriform cortex; Ce, central amygdala) (**B**) Schematic illustration of the experiment design to record uEPSCs using blue light stimulation. (**C**) Representative traces showing light evoked APs in a PN recorded in loose-patch mode, a potential synaptic partner to a CCKBC recorded in whole-cell voltage-clamp mode (left). Peak alignment of the light evoked APs revealed a monosynaptic excitatory connection to the postsynaptic CCKBC (middle). Whole-cell paired recording of the same monosynaptically coupled PN-CCKBC pair shows similar characteristics of the EPSCs compared with the light stimulation method (right). n = 50 traces. (**D**) Representative traces showing light evoked APs in a PN recorded in loose-patch mode, a potential synaptic partner to a PVBC recorded in whole-cell voltage-clamp mode (left). Peak alignment of the light evoked APs revealed a monosynaptic excitatory connection to the postsynaptic PVBC (middle). Whole-cell paired recording of the same PN-PVBC pair shows similar characteristics of EPSCs compared to the light evoked events (right). n = 50 traces.*

To test a connection, 50-200 sweeps were recorded, and a peristimulus histogram was calculated in order to reveal monosynaptic excitatory connections between the PNs and BCs. In some cases, whole-cell recordings were obtained from the presynaptic PN that was proved to be connected to the BC upon light stimulation, and EPSCs in the postsynaptic BC were recorded upon electrical stimulation of the same PN. This approach allowed us to compare the properties of the unitary events evoked by light and electrical stimulation of the presynaptic PNs. No significant difference was found between the results obtained by the two methods (**Fig. 8**; (**A**) Potency: CCKBC: ChR2 stim: 18.52 ± 1.43 pA, Pair. rec.: 17.23 ± 1.62 pA; Paired Sample Wilcoxon Signed Rank Test, p = 0.53; PVBC: ChR2stim: 82.39 ± 13.44 pA, Pair. rec.: 82.51 ± 14.02 pA; Paired Sample Wilcoxon Signed Rank Test, p = 0.75; (**B**) Peak amplitude: CCKBC: ChR2 stim: 6.24 ± 1.23 pA, Pair. rec.: 6.42 ± 1.51 pA; Paired Sample Wilcoxon Signed Rank Test, p = 1; PVBC: ChR2 stim: 70.66 ± 14.39 pA, Pair. rec.: 67.9 ± 14.38 pA; Paired Sample Wilcoxon Signed Rank Test, p = 0.2; (**C**) Failure rate: CCKBC: ChR2 stim: 0.65 ± 0.07, Pair. rec.: 0.63± 0.08; Paired Sample Wilcoxon Signed Rank Test, p = 1; PVBC: ChR2 stim: 0.22 ± 0.05, Pair. rec.: 0.26 ± 0.05; Paired Sample Wilcoxon Signed Rank Test, p = 0.06; (**D**) Rise time 10-90%: CCKBC: ChR2 stim: 0.74 ± 0.09 ms, Pair. rec.: 0.83 ± 0.06 ms; Paired Sample Wilcoxon Signed Rank Test, p = 0.06; PVBC: ChR2 stim: 0.39 ± 0.04 ms, Pair. rec.: 0.4 ± 0.04 ms; Paired Sample Wilcoxon Signed Rank Test, p = 0.97; (**E**) Decay tau: CCKBC: ChR2 stim: 2.76 ± 0.23 ms, Pair. rec.: 2.99 ± 0.34 ms; Paired Sample Wilcoxon Signed Rank Test, p = 0.67; PVBC: ChR2 stim: 1.57 ± 0.21 ms, Pair. rec.: 1.41 ± 0.15 ms; Paired Sample Wilcoxon Signed Rank Test, p = 0.2). Therefore, the optical stimulation approach was applied for mapping the connectivity between PNs and BCs (**Fig. 6, Fig. 7**). The amplitude of uEPSCs was measured in an individually defined time window calculated from the peristimulus histogram for each pair, including both events and transmission failure. For the potency of the events, uEPSC amplitudes excluding failures were averaged.

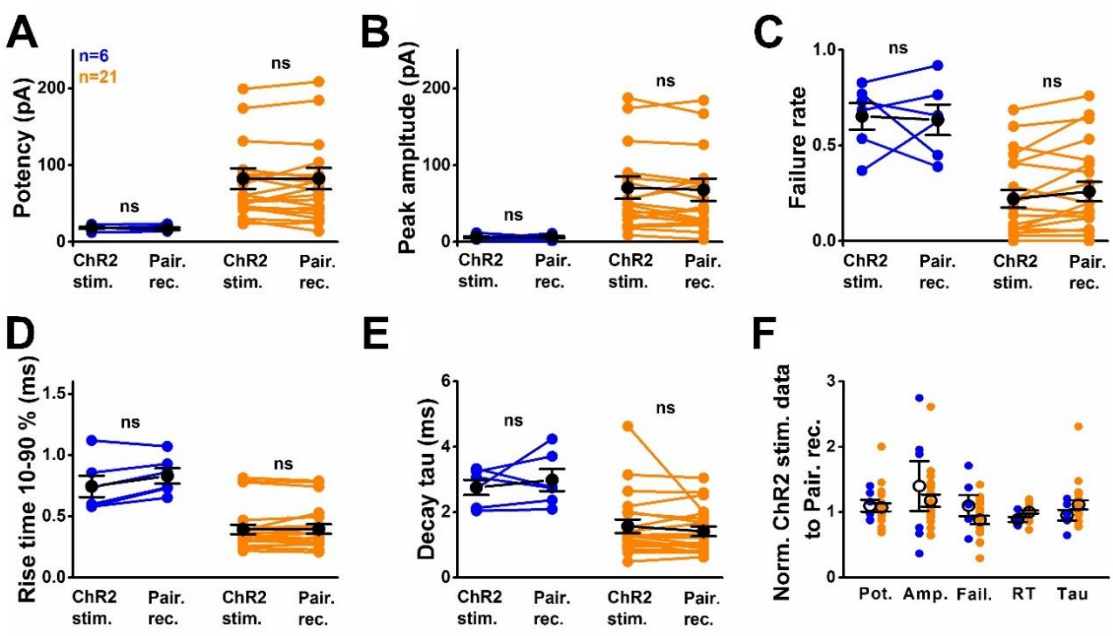

Figure 8. ***Validation of the optogenetic paired recording approach.*** *Comparison between the light stimulation method and the paired whole-cell recording shows no significant difference in the potency (**A**), in the peak amplitude (**B**), in the failure rate (**C**), in the rise time 10-90% (**D**), in the decay tau (**E**) of uEPSCs either in CCKBCs (blue) or in PVBCs (orange). (**F**) The data obtained by light stimulation (ChR2 stim.) normalized to those collected in paired recordings (Pair. rec.) show no major difference. Each pair of data points represents an average obtained in paired recordings. Mean ± SEM is shown in black.*

3.2.5 Determining the activation threshold of PTIs

To define the spiking threshold of the INs by population excitation originating from local PNs, double-transgenic mice (PV-eGFP x CCK-DsRed) were crossed with VGluT1-cre homozygote mice (type 1 vesicular glutamate transporter), and offsprings were injected with 2/5 serotype AAVs carrying DIO-ChR2-mCherry construct bilaterally into the BA (the same coordinates as described above) in order to obtain ChR2 expression selectively in PNs. At least 3 weeks after the injection, acute slices were prepared from injected mice. To investigate the excitability of the INs, firing

threshold in PVBCs and CCKBCs were always simultaneously measured in loose-patch mode, while the whole area of the BA in the slice was stimulated with 10-ms-long blue (447 nm laser) light pulses with gradually increasing intensity (typically delta +5% steps). Spiking threshold was defined as the lowest light intensity (%), in which INs fired single APs in response to the light stimulation of a PC population. After determining the firing threshold in loose-patch mode, INs were repatched in whole-cell mode, and the same protocol was performed to measure the magnitude of the light-evoked currents at the intensity values used for loose-patch recordings.

3.2.6 Recording and analysis of miniature events

For miniature event analysis, CCKBCs and PVBCs were recorded in whole-cell mode at a holding potential of -65 mV (i.e., at the reversal potential of $GABA_A$ receptor-mediated conductance using low intrapipette Cl^-) in the presence of 0.5 μM tetrodotoxin (TTX, Hello Bio). In these experiments, the intrapipette solution contained (in mM): 110 K-gluconate, 4 NaCl, 2 Mg-ATP, 20 HEPES, 0.1 EGTA, 0.3 GTP (sodium salt), 10 phosphocreatine, 0.2% biocytin, and 0.1 spermine adjusted to pH 7.3 using KOH, with an osmolarity of 290 mOsm/L. During the offline analysis, individual miniature events were detected automatically using an algorithm, and, after visual inspection of each detected event, the peak amplitude and interevent interval of mEPSCs were measured in Clampfit 10.4 (n = approximately 300 consecutive events/IN).

3.3 Morphological investigations

3.3.1 BA delineation in BAC-CCK-DsRed mice

BAC-CCK-DsRed mice (n = 2) were intracardially perfused with 4% paraformaldehyde (PFA) in 0.1 M phosphate buffer (PB). The brain was removed from the skull and re-sectioned to 50-μm-thick horizontal slices. To reveal cholinergic fibers, rabbit anti-vesicular acetylcholine transporter (VAChT), 1:1000, Frontier Institute) was used, which was visualized using an Alexa488-conjugated donkey anti-rabbit antibody

(1:500, Jackson). Single-plane fluorescent images were obtained using a Nikon C2 confocal microscope (Plan Fluor 4x objective, N.A. 0.13, xy: 0.8 μm/pixel)(Ben-Ari et al., 1977; Carlsen et al., 1985).

3.3.2 Immunostainings for identification of the recorded cells

After the recordings, slices were fixed overnight in a solution containing 4% PFA in 0.1 M PB (pH 7.4). In the case of the ultrastructural analysis of the connections with EM, the fixative solution additionally contained 0.05% glutaraldehyde and 15% picric acid. Biocytin-filled recorded cells were visualized either with Cy3, Alexa488 or Alexa647-conjugated streptavidin (1:3000, Molecular Probes or Life Technologies). In those cells in which the fluorescent dyes Alexa488 or Cascade Blue were used for labeling, the signal was amplified by an immunostaining against the fluorophores (rabbit anti-Alexa488 (Invitrogen), rabbit anti-Cascade Blue (Molecular Probes), all 1:1000). Confocal images were taken using a Nikon A1R or C2 microscope (CFI Super Plan Fluor 20X objective, N.A. 0.45; z step size: 1 μm, xy: 0.31 μm/pixel). Using the confocal images, the postsynaptic IN was fully reconstructed in 3D with the Neurolucida 10.53 software (MBF Bioscience), and the putative contact sites from the presynaptic PN were labelled. For the detailed analysis of the putative synaptic sites, higher magnification images were acquired using the same microscopes (CFI Plan Apo VC60X Oil objective, N.A. 1.40; z step size: 0.13 μm, xy: 0.08 μm/pixel). The location analysis of the contact sites was obtained by the Neurolucida Explorer software. Values were corrected for shrinkage and flattening of the tissue (x and y axis: no correction, z axis: 1.7). For confirmation of the presence of putative contact sites determined by confocal microscopy, some of the samples were further processed for EM analysis. Biocytin in PNs was revealed using avidin-biotinylated horseradish peroxidase reaction (Avidin-biotin complex (ABC); Vector Laboratories) with nickel-intensified 3,3-diaminobenzidine (DAB-Ni), giving a dark reaction product. Rabbit anti-Cascade Blue primary antibody in INs was visualized with biotin-conjugated goat anti-rabbit secondary antibody, with ABC reaction visualized by DAB giving a light brown chromogen. Next, sections were post fixed in 0.5% OsO_4 (1% for IN only) with 7%

glucose, treated in 10% uranyl acetate (1% for IN only), dehydrated in a graded series of ethanol, and embedded in epoxy resin (Durcupan; Sigma, Fluca). Ultrathin sections of 60 nm thickness were cut, and putative synaptic sites, in which the presynaptic axon formed close appositions with the labelled IN, were examined in serial sections, and the presence of the synapses could be clearly verified.

Post hoc confirmation of the identity of the INs was performed based on their neurochemical content as follows. After imaging the cell using a confocal laser scanning microscope (Nikon C2 or A1R), only those INs that preserved the axon collaterals were further processed for anatomical identification. For CCKBC identification, an immunostaining using goat anti-CB1 (1:1000; Frontier Institute) or rabbit against CB1 (1: 2000; Cayman Chemicals) was performed, and only those cells in which CB1 receptor expression was found in their boutons were included in the study. To distinguish PVBCs and AACs, an immunostaining against Calb was performed (rabbit anti-Calb, 1:3000, Swant, see (Vereczki et al., 2016)). PV-containing cells with Calb expression in the soma and/or axon terminals were considered BCs, whereas those cells that showed no Calb expression and displayed characteristic cartridges of terminals surrounding putative AISs were considered AACs. In some cases, the identity of AACs was strengthened by ankyrin G staining visualizing AISs, as the boutons of biocytin-labeled cells formed close appositions predominantly with ankyrin G stained profiles (Vereczki et al., 2016). To assess the connection probability between different IN types, we included in the final data set only those recordings in which both cells could be unequivocally identified and had axonal arbor.

For illustration purposes, one IN from each group was used for reconstruction. In this case, biocytin was visualized using avidin-biotinylated horseradish peroxidase complex reaction (ABC; Vector Laboratories, Burlingame, CA, USA) with nickel-intensified 3,3-diaminobenzidine as a chromogen. After dehydration and embedding in Durcupan (Fluka), neurons with the most complete axonal and dendritic arborizations were reconstructed with the aid of a drawing tube using a 40x objective.

3.3.3 Comparison of excitatory input density of BCs

The estimation of the density of excitatory inputs received by BCs was done as previously described (Papp et al., 2013). Biocytin was revealed in in-vitro-filled INs with Alexa488-coupled streptavidin (1:3000, Molecular probes), then, after fixation, slices were resectioned into 40-µm-thin sections. Samples were incubated for 4 nights at 4°C in a solution containing the following primary antibodies and reagents: mouse anti-bassoon (1:1000, Abcam), guinea pig anti-VGluT1 (1:1000, Millipore), 2% normal donkey serum (NDS), 0.5% Triton-X 100, and 0.05% Na-azide in 0.1 M PB. Primary antibodies were visualized with Cy3 conjugated donkey anti-mouse and Cy5 conjugated donkey anti-guinea pig secondary antibodies (Jackson Laboratory, 1:500) incubated for 2 hours at room temperature. Sections were then washed and mounted on slides in Vectashield (Vector Laboratories). Confocal images were taken using a Nikon A1R microscope (CFI Plan Apo VC60X Oil objective, NA: 1.40, z step size: 0.13 µm; xy: 0.06 µm/pixel), and analyzed with Neurolucida 10.53 software.

3.3.4 Super-resolution microscopy on identified IN dendrites

To estimate the content of AMPA receptors at synapses of identified IN dendrites, 3D direct stochastic optical reconstruction microscopy (3D-STORM) was performed. For this study, identified CCKBCs and PV-containing INs were intracellularly filled with biocytin as described above. After the electrophysiological experiments, slices were fixed overnight in 4% PFA and re-sectioned to 30-µm-thick sections. Next, an immunostaining to label AMPA receptors was performed as previously described (Fukaya et al., 2006). Briefly, sections were treated for 10 minutes with a solution containing pepsin 1 mg/ml in 0.1 M PB and HCl 0.2 N at 37°C for antigen retrieval and then a solution containing 0.2% Triton-X and NDS 10% together with bovine serum albumin 2% in 0.1 M PB to prevent unspecific binding of the antibodies. Then, sections were incubated for 5 days at 4°C in a 0.1 M PB solution containing 0.2% Triton-X, 1% NDS, 0.05% Na-azide and the following mixture of primary antibodies: guinea pig anti-pan-AMPAR (Frontier Institute, 1:200) and mouse anti-bassoon (Abcam, 1:3000). The staining was visualized using Alexa488-

conjugated streptavidin (Molecular Probes, 1:10000), Alexa647-conjugated donkey anti-guinea pig (Jackson, 1:400) and Cy3-conjugated donkey anti-mouse (Jackson, 1:500).

Sections were prepared for dSTORM imaging as follows. After the staining, they were flat mounted on coverslips and stored dried at 4°C. Samples were embedded in freshly prepared imaging medium immediately before the STORM imaging session (Dudok et al., 2015). Once a dendritic segment of interest was selected, a high-resolution confocal stack (512x512 pixels, xy: 0.08 μm/pixel, z step size: 0.15 μm) followed by 3D-STORM imaging was performed with an APO TIRF 100x objective, using a Nikon Ti-E inverted microscope equipped with a Nikon C2 confocal scan head, an AndorXion Ultra 897 High Speed EMCCD camera, and a Nikon N-STORM system.

For STORM imaging, a 300 mW laser was used (VFL-P-300-647, MPB Communications). The imaging process for each sample consisted of 5000 cycles of the reporter Alexa647 activation at maximum laser intensity of 30-ms-long frames, with a continuous low-intensity illumination using the 405 nm laser to enhance the activation. To minimize out-of-focus background and focus drift during imaging, all samples were bleached similarly using the 488 nm, 568 nm and 647 nm laser lines in all the z depth of the sample, and TIRF illumination angle and a Perfect Focus System were applied. Localization points (LPs) were collected within 600 nm centered in a focal plane contained in a 1–3 μm range from the surface. The resulting coordinates were acquired using the N-STORM module in the NIS Elements software, setting the intensity height detection range of the bright points from 1000 to 20000 and the CCD baseline to 100. Confocal stacks from the imaged areas were deconvolved using Huygens software (SVI), and transformed in ImageJ software. The manual alignment of deconvolved confocal and STORM images, as well as the analysis of the number, 2D Convex Hull area and density of LPs was performed using VividSTORM software (Barna et al., 2016). To quantify the number of LPs, a region of interest (ROI) was manually drawn around those puncta observed along the dendrite in single focal planes restricted to the central 300 nm, which contained bassoon in close apposition. Puncta depicting AMPA receptors not apposing bassoon were also analyzed (11 out of 30 for CCKBCs, 13 out of 53 for PV-expressing INs), and, as there were no significant differences in the number of LPs compared with the bassoon-apposing puncta ($p = 0.16$

for PV-containing INs and $p = 0.70$ for CCKBCs), data were pooled. To avoid biasing the analysis, all images were processed equally, and a normalizing factor was introduced in the number of LPs to account for possible technical differences in the staining or imaging sessions. The normalizing factor was obtained as follows: a cluster analysis was performed in a large area immediately surrounding the analyzed dendrite, using the same parameters used for the analysis of the ROIs. The mean number of LPs from all the automatically identified clusters was calculated for every analyzed image and scored based on the averages obtained in all images. The number of LPs in the ROIs was normalized by dividing the raw data obtained for INs by the normalizing factor. In addition, to avoid introducing errors derived from the size/shape of the clusters, analyzed puncta fulfilled two additional criteria: (1) normalized number of LPs higher than 8, and (2) puncta area larger than 0.07 μm^2.

3.3.5 Morphological investigation of IN-IN connectivity

To investigate the connectivity among INs, CCK-DsRed mice ($n = 2$) and wild-type mice ($n = 2$) were transcardially perfused with 4% PFA in 0.1 M PB, and areas containing the amygdala region were sectioned into 50-μm-thin slices, then freeze thawed above liquid nitrogen in 30% sucrose solution. To label connections between CCKBCs and PV-expressing cells, samples from CCK-DsRed mice were incubated for 6 nights at 4°C in the following primary antibody mixture: mouse anti-gephyrin (Synaptic Systems, 1:1000), rabbit anti-PV (Swant, 1:10.000), guinea pig anti-CB1 (Frontiers Institute, 1:1000), 2% NDS, and 0.05% Na-azide in 0.1 M PB. Primary antibodies were visualized with the mixture of the following secondary antibodies: Alexa488-conjugated donkey anti-mouse (Molecular Probes, 1:500), Alexa647-conjugated donkey anti-rabbit and Dylight405-conjugated donkey anti-guinea pig (both Jackson Laboratory, 1:500) incubated 1 night at 4°C. To label PV-PV cell connections, samples from wild-type mice were used, and besides labeling gephyrin and PV as described above, guinea pig anti-VGAT (vesicular GABA transporter)(Frontiers Institute, 1:1000) and goat anti-GAD65/67 (pan-GAD, Frontiers Institute, 1:500) primary antibodies were also applied that were visualized with Cy3-

conjugated donkey anti-guinea pig and Cy3-conjugated donkey anti-goat secondary antibodies. Sections were then washed and mounted on slides in Vectashield. Confocal images were taken using a Nikon A1R microscope (CFI Plan Apo VC60X Oil objective, NA: 1.40, z step size: 0.13 μm; xy: 0.06 μm/pixel), and analyzed with Neurolucida 10.53 software. Appositions were only identified as contacts if the postsynaptic anchoring protein of $GABA_A$ receptors, gephyrin, was localized at the side of the immunolabeled terminal, which faced the somatic membrane, otherwise the terminals were regarded to form contacts on neighboring structures. In case of PV-immunoreactive terminals on PV-immunostained somata, the presence of VGAT and GAD65/67 immunolabeling identified the PV-containing structure as an axon terminal. CCKBC somata were visualized by the expression of the genetically encoded DsRed fluorescent protein.

3.4 Statistical analysis

In the case of data with non-normal distribution according to the Shapiro-Wilk test, the Mann-Whitney *U* test, Wilcoxon Signed Rank test, Kolmogorov-Smirnov test, and Kruskal-Wallis ANOVA were used for analysis of the data. To correlate variables from normal distributions, the Pearson's correlation coefficient was used. All statistics were performed using Origin 8.6 or OriginPro 2015. Data are presented as mean ± SEM.

3.5 Personal contribution

Optogenetics, electrophysiological experiments and analysis of excitatory connections, as well as the connectivity map were performed and created by me. Inhibitory connections were measured and analyzed partially by me and by other members of the group (Boglárka Barsy, Gergely Szabó, Judit Veres, Laura Rovira and Attila Vikór). Morphological and anatomical analysis, including EM reconstructions and STORM analysis were done by other members of the group (Noémi Holderith, Judit Veres, Laura Rovira, Richárd Kozma and Erzsébet Gregori).

4 RESULTS

4.1 Different output properties of PTIs in the BA

4.1.1 Identification of different types of PTIs

All INs in this study were filled with biocytin for further *post hoc* morphological analysis. The identity of the different types of PTIs were determined by their firing pattern, neurochemical phenotype and morphological characteristics. (**Fig. 9A**) PV expressing BCs and AACs were selected by their PV-eGFP expression during recordings. In order to undoubtedly distinguish AACs from PVBCs, further investigations were necessary. The biocytin-filled axon terminals of AACs and the AIS of the PNs were visualized by double immunostaining, therefore the AIS targeting terminals could be easily recognized by their close appositions on the AISs visualized by Ank-G immunostaining (n = 29)(**Fig. 9E**). Further EM analysis of the putative synapses made by AAC terminals confirmed the presence of symmetrical synaptic contacts on the AISs (**Fig. 9F**). Based on our previous study, those PV/eGFP expressing cells, which avoided the AIS of the PNs were categorized as PVBCs ((Vereczki et al., 2016); **Fig. 9C and D**, n = 34). CCKBCs were identified by their DsRed and CB1 coexpression (**Fig. 9B**, n = 22).

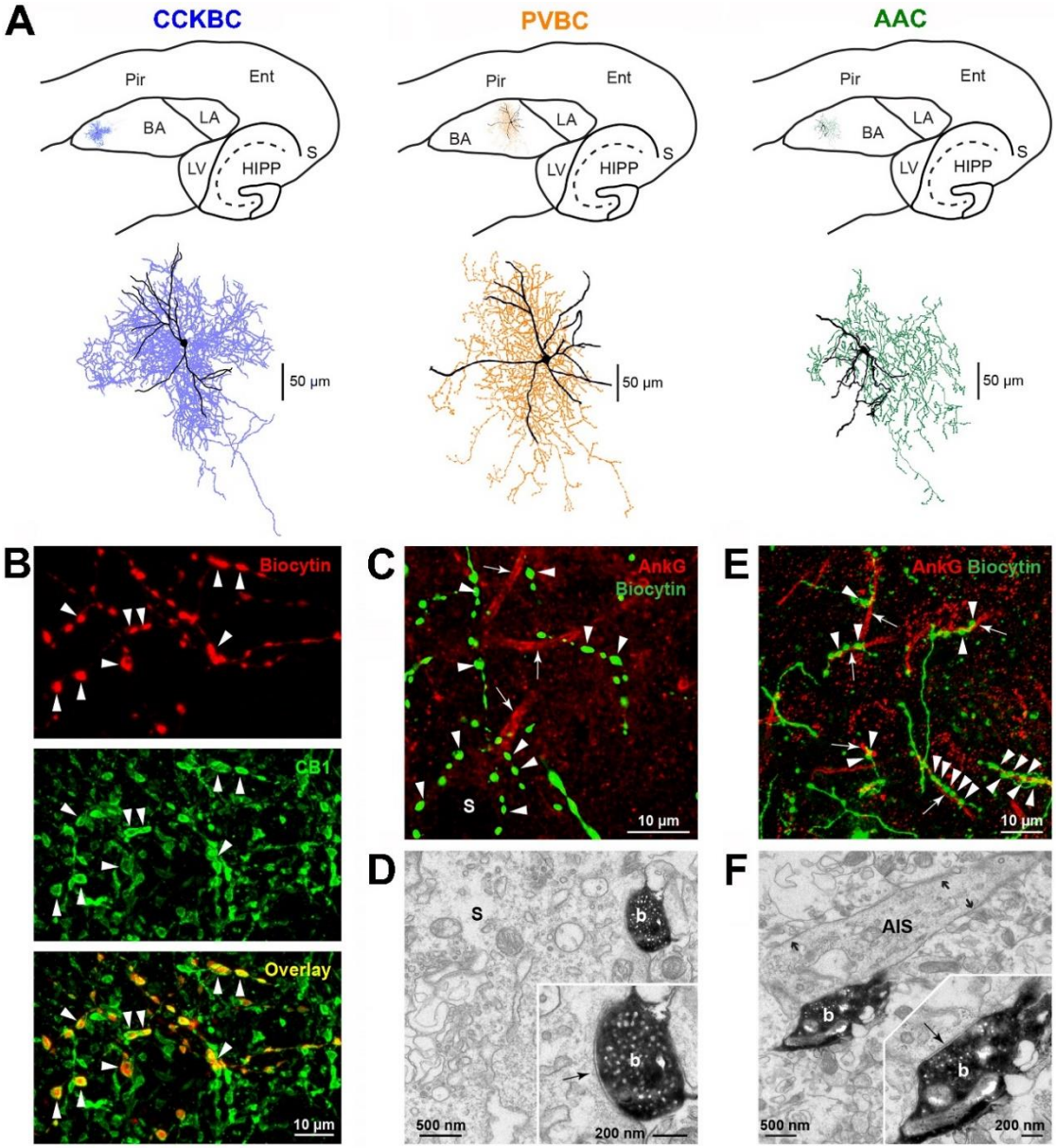

Figure 9. ***Morphological properties and identification of CCKBCs, PVBCs and AACs in the BA of the mouse amygdala.*** *(**A**) Camera lucida reconstructions and the localization of representative biocytin-labeled neurons in horizontal slices prepared from the mouse amygdala region. BA; basal amygdala; Ent, entorhinal cortex; HIPP, hippocampal formation; LA, lateral amygdala; LV, lateral ventricle; Pir, piriform cortex; S, subiculum. Soma and dendrites are shown in black and axonal arbor in blue (CCKBC), orange (PVBC) or green (AAC). (**B**) Confocal images indicate that biocytin-filled axon terminals of a DsRed-expressing cell (arrowheads, in red) co-express CB1*

*receptor (green). (**C**) Double immunofluorescent labeling shows that biocytin-filled axon terminals of a PVBC cell (green; arrowheads) avoid Ankyrin G-labeled AISs (red; arrows), but surround soma (s). (**D**) A bouton (b) of the same PVBC forms a symmetrical synapse (marked by an arrow in the inset) on the soma (s) of a postsynaptic cell. (**E**) Double immunofluorescent labeling as in (**C**) shows close appositions of boutons (arrowheads) belonging to a biocytin-filled PV-eGFP neuron with AISs (arrows), identifying this cell type as AAC. (**F**) An electron micrograph shows a biocytin-labeled axon terminal (b) of an AAC forming a symmetrical synapse (arrow; inset) on an AIS. Small arrows point to the undercoating in the AIS.*

4.1.2 Intrinsic membrane properties of PTIs in the BA

To test the passive and active membrane characteristics of the three different types of perisomatic inhibitory cells, we performed whole-cell patch clamp recordings. Voltage responses were obtained by gradually increasing depolarizing and hyperpolarizing current steps, that were injected into the cells in current-clamp configuration and the responses were compared between groups (**Fig. 10A**). Comparison of the three cell types revealed that the intrinsic membrane properties of PV-expressing BCs and AACs were markedly different from those expressing CCK/CB1, however PVBCs and AACs appeared to be rather similar. PVBCs and AACs typically displayed fast spiking phenotype with narrow AP half width and without apparent accommodation (**Table 1**). By contrast, CCKBCs have an accommodating regular spiking profile and significantly wider spike half-width (**Table 1**). Interestingly, we found differences in the membrane capacitance between PVBCs and AACs, although their membrane kinetics were similarly fast (**Fig. 10D, Table 1**). In CCKBCs the membrane time constant was significantly lower, compared to that measured either in PVBC or in AAC (**Fig. 10D, Table 1**). Surprisingly, our results showed that the AP afterhyperpolarization (AHP) half- width was dissimilar in the three different cell types, measured at the half-maximum amplitude (**Fig. 10D, Table 1**).

Table 1. ***Single-cell properties of the three PTI types in the BA.*** *Data are presented as the median with the first and third quartiles in parentheses. Significant differences shown in bold were determined by Kruskal-Wallis ANOVA and Mann-Whitney (MW) U test. (AP, action potential; AHP, after hyperpolarization; ISI, inter-spike interval.)*

Parameters	**AAC (n=18-19)**	**PVBC (n=22-26)**	**CCKBC (n=14)**	**Kruskal-Wallis ANOVA**	**AAC-PVBC MW test**	**AAC-CCKBC MW test**	**PVBC-CCKBC MW test**
Rheobase (pA)	150 (100, 150)	300 (150, 400)	90 (70, 150)	**<0.001**	<0.001	0.049	<0.001
AP threshold (mV)	-38.1 (-39.7, -36.9)	-37.2 (-40.7, -33.6)	-41 (-43.9, -37.5)	0.06387	n/a	n/a	n/a
AP amplitude (mV)	63.7 (58.1, 75.5)	55.85 (49.9, 64.2)	73.65 (62.3, 78.6)	**0.003**	0.039	0.13	0.001
AP half-width (ms)	0.3 (0.3, 0.4)	0.3 (0.3, 0.4)	0.7 (0.6, 0.8)	**<0.001**	0.15	<0.001	<0.001
Spike rate (Hz)	177.5 (157.5, 193.8)	110 (92.5, 138.75)	30 (27, 40)	**<0.001**	<0.001	<0.001	<0.001
Accommodation ratio	2 (1.89, 2.23)	1.445 (1.29, 1.65)	4.755 (4.07, 5.69)	**<0.001**	<0.001	<0.001	<0.001
Input resistance (MOhm)	113.45 (109.3, 120.8)	77.15 (62.28, 107.9)	160.3 (130.3, 200.6)	**<0.001**	0.002	<0.001	<0.001
AHP amplitude (mV)	16.9 (16.2, 19.7)	21 (18.9, 23.4)	17.9 (15.4, 19.4)	**0.0031**	0.004	1	0.005
AHP 25% decay (ms)	9.1 (4.8, 21.8)	9.9 (6.7, 15.9)	45.6 (33.3, 58.4)	**<0.001**	0.82	<0.001	<0.001
AHP 50% decay (ms)	27.3 (18.9, 35)	17.4 (14.6, 28.1)	76.95 (60.2, 119.9)	**<0.001**	0.036	<0.001	<0.001
AHP 75% decay (ms)	33.9 (26.1, 43.1)	26.9 (21.2, 37.7)	113.85 (87.9, 156.6)	**<0.001**	0.16	<0.001	<0.001
Ratio of AP amplitude adaptation	0.7 (0.62, 0.75)	0.8 (0.68, 0.88)	0.83 (0.75, 0.91)	**0.003**	0.011	0.001	0.48
Membrane time constant (ms)	12.63 (10.56, 13.6)	9.53 (8.26, 12.1)	16.9 (13.48, 18.18)	**<0.001**	0.057	0.001	<0.001
Membrane capacitance (pF)	100.82 (84.56, 120.7)	137.95 (93.62, 174.7)	104.6 (92.41, 110.2)	**0.04**	0.035	0.81	0.033
Relative sag amplitude	0.123 (0.096, 0.168)	0.1 (0.068, 0.14)	0.196 (0.112, 0.235)	**0.035**	0.19	0.06	0.024
ISI between the first two spikes	3 (2.8, 3.4)	6.1 (5, 9)	6 (5.7, 7.4)	**<0.001**	<0.001	<0.001	0.91
ISI between the last two spikes	6.2 (5.4, 7.4)	10.7 (8.2, 11.8)	33.6 (23.6, 38.2)	**<0.001**	<0.001	<0.001	<0.001

Further detailed analysis of the firing features of PTIs revealed differences in their input-output characteristics. In current-clamp mode, gradually increasing depolarizing and hyperpolarizing current steps were injected to the cell, and the firing rate was plotted as a function of the current steps (**Fig. 10A**). Smaller current steps resulted in a similar response curve in all the three cell types, however, the injection of larger depolarizing currents clearly divided the different cell types, as AACs displayed the highest firing rate and CCKBCs showed the lowest (**Fig. 10B**; PVBC, n = 8; AAC, n = 8; CCKBC, n = 13). Significant difference was found between the three groups (a), between PVBC and CCKBC, and between AAC and CCKBC (b), between AAC and CCKBC (c), and between PVBC and AAC (d). (at 100 pA: ANOVA $p = 0.041$, AAC vs. PVBC: $p = 0.043$; at 200 pA: ANOVA $p = 0.01$, AAC vs. CCKBC: $p = 0.003$; at 250 pA: ANOVA $p < 0.001$, PVBC vs. AAC: $p = 0.037$, PVBC vs. CCKBC: $p = 0.046$, AAC vs. CCKBC: $p < 0.001$; at 300 pA: ANOVA $p < 0.001$, PVBC vs. AAC: $p = 0.049$; PVBC vs. CCKBC: $p = 0.027$; AAC vs. CCKBC: $p < 0.001$; at 400 pA: ANOVA $p < 0.001$, PVBC vs. AAC: $p = 0.037$; PVBC vs. CCKBC: $p < 0.001$; AAC vs. CCKBC: $p < 0.001$; at 500 pA: ANOVA $p < 0.001$, PVBC vs. CCKBC: $p < 0.001$; AAC vs. CCKBC: $p = 0.004$). Moreover, the maximal firing rate in response to the highest current step was significantly different among the three cell types (**Table 1**). We found differences in membrane time constant and half width of the AHP. Interestingly, comparing the interspike interval of the first two and last two APs from the train showed significant difference between AACs and BCs, namely AACs had shorter interspike intervals (**Fig. 10C, Table 1;** Membrane time constant: $p < 0.001$, Kruskal-Wallis ANOVA; AHP 50%, $p < 0.001$, Kruskal-Wallis ANOVA; Interspike interval $p < 0.001$, Kruskal-Wallis ANOVA).

Our results clearly demonstrated that the passive and active membrane properties of CCKBCs markedly differ from the PV-expressing INs, and PV-expressing GABAergic cells are rather similar irrespectively whether they are BCs or AACs.

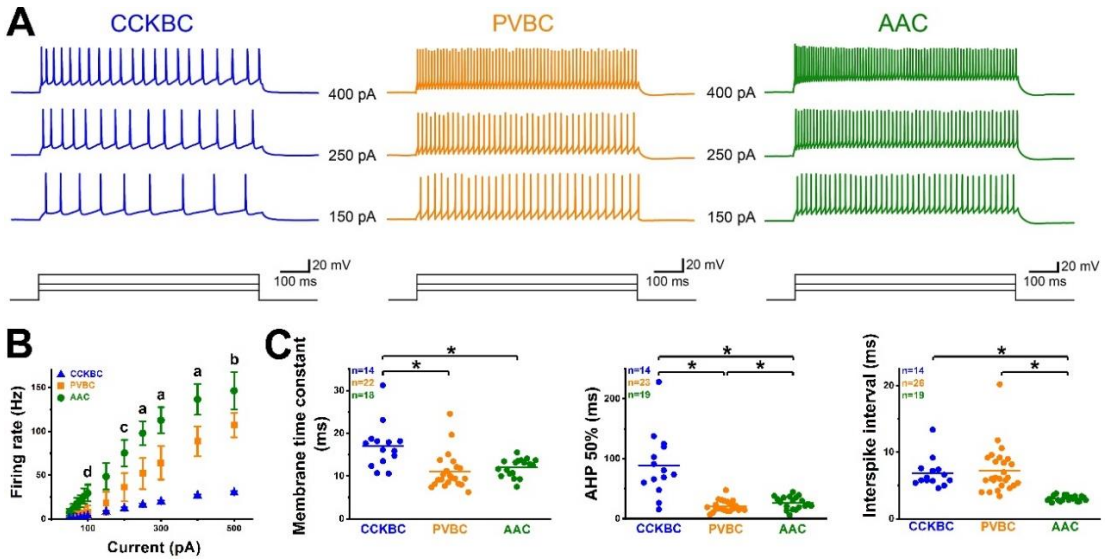

Figure 10. ***Distinct single-cell electrophysiological properties of the three IN types targeting the perisomatic region of the PNs in the BA.*** *(**A**) Voltage responses to depolarizing current steps (150, 250, and 400 pA) injected at a holding potential of -65 mV. (**B**) Average frequency-input current relationships of the three IN types measured at a membrane potential of -65 mV. (**C**) Single-cell properties are distinct in the three cell types. On the graphs, each line represents a value from an individual cell. Bars show the median values in each group and asterisks indicate significant differences. Comparison for membrane time constant, AHP half-width and interspike interval for the first two spike at maximal firing rate are shown. Significance levels are *p < 0.05. For more details, see* ***Table 1***.

4.1.3 The synaptic properties of the perisomatic inhibition of PNs in the BA

Besides the similarities or differences in the input-output features of the distinct types of PTIs, we investigated the properties of their inhibitory synaptic transmission onto PNs, which may help to understand how they impact the network operation. In order to address this question, we made dual whole-cell recordings from fluorescently identified PTIs and local PNs in the BA. In order to determine the basic properties of the synaptic transmission, APs were evoked in the presynaptic IN and the resulting uIPSCs were recorded in the postsynaptic PN **(Fig. 11A)**. Analyzing the uIPSCs, we

determined the peak amplitude, potency (excluding failures) and transmission failure of the IPSCs, as well as the kinetics of the IPSCs, such as the 10-90 % rise time, decay time constant and latency (**Fig. 11B-G**). The statistical analysis of the results revealed that the CCKBCs give IPSCs with slower rise time and latency onto PNs compared to PV-expressing cells, although the decay kinetics were not significantly different between the cell types (**Fig. 11D, F and G, Table 2**). Moreover, the failure in CCKBC synaptic transmission was significantly different from those in AAC synapses on PNs (**Fig. 11E, Table 2**). Interestingly, the magnitude of the amplitude and potency showed no significant differences between the cell types, however IPSCs from CCKBCs tend to be smaller compared to PVBCs and AACs under such recording conditions (**Fig. 11A and B, Table 2**). It should be noted that the recording solution did not contain any CB1 receptor antagonist, thus the presence of the tonic endocannabinoid effect might reduce the IPSC amplitude originating from CCKBCs (see (Rovira-Esteban et al., 2017)). The properties of the synaptic transmission from PVBCs and AACs tended to be similar except the latency of the IPSCs, which was significantly shorter in PVBCs (**Fig. 11B-G, Table 2**).

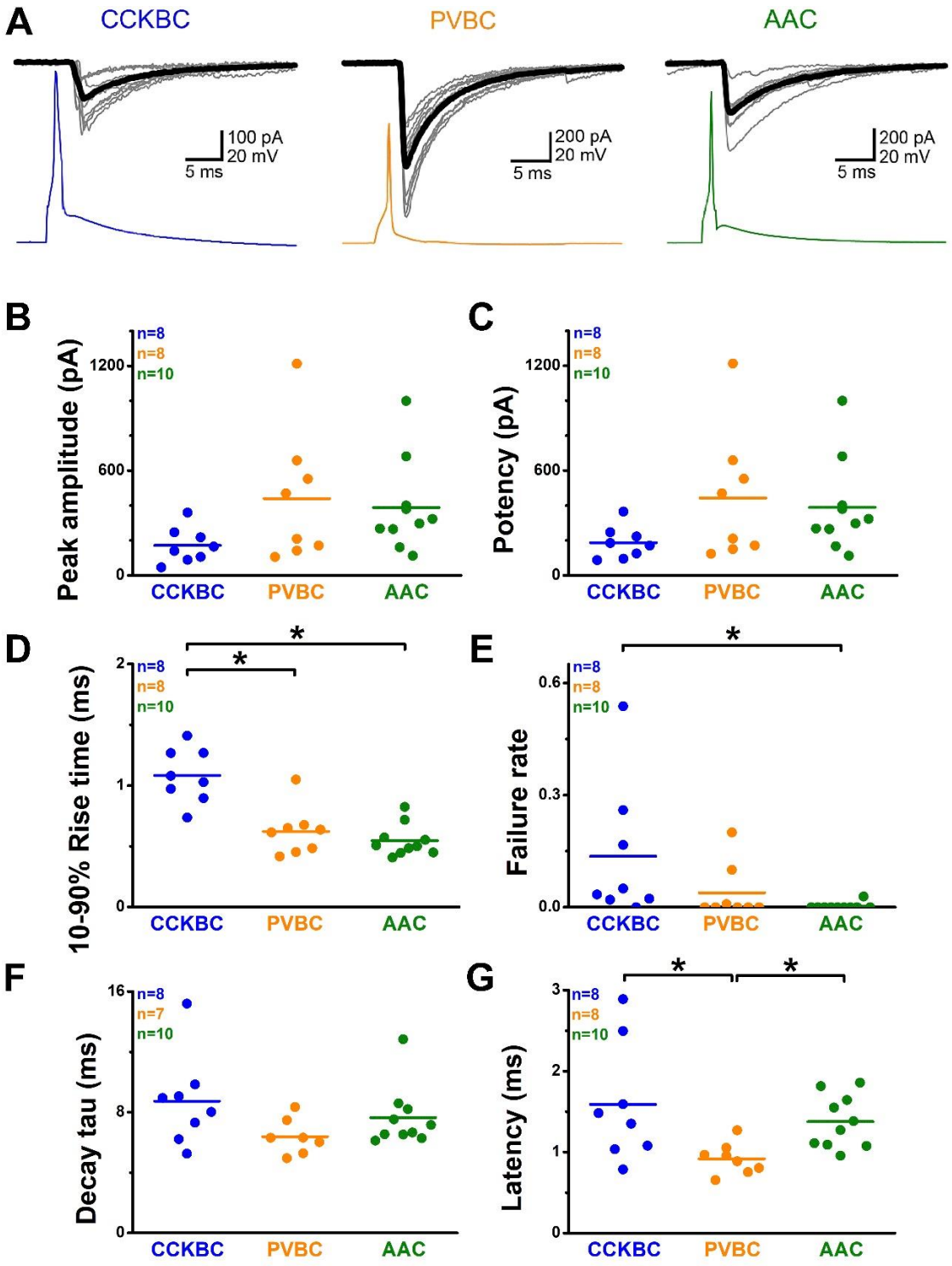

Figure 11. ***Basic properties of synaptic transmission in PTI-PN pairs***. *(**A**) Examples obtained in paired recordings, where single APs were evoked in the three distinct types of INs (bottom traces), and the postsynaptic currents were recorded in the PNs (top traces). Ten consecutive traces are superimposed (gray) with the average of all traces*

*(black). (**B-G**) Comparison of the peak amplitude, the synaptic potency, 10-90% rise time, the failure rate, the decay tau, and the latency measured at unitary connections between INs and PNs. Asterisks indicate significant differences, *p < 0.05. For more details, see **Table 2**.*

Next, we determined the short-term kinetics of the synaptic transmission in response to 10 APs at various frequencies, where the second and tenth IPSC amplitudes were compared to the first (**Fig. 12A**). Our results showed that in average short-term depression could be observed at all the three IN types, however the strength of the depression was highly dependent on the firing frequency, as higher frequency resulted stronger depression (**Fig. 12B and C**). Comparison of these data showed that PVBCs displayed a strong depression in the $IPSC_2/IPSC_1$ ratio over 5 Hz firing frequency, while there is no change in the magnitude of the depression measured at the synaptic outputs of AACs and CCKBCs (**Fig. 12C**). By contrast, comparison of the $IPSC_{10}/IPSC_1$ ratio between the three cell types showed a similarly profound depression at their outputs (**Fig. 12C**). These results together suggest that, in spite of the similarity in the basic properties of the uIPSCs at all the three types of PTIs, differences in their short-term dynamics can be distinctive regarding their function in the regulation of PN activity. For instance, at a low activity level of INs, when doublets of APs mediate inhibition onto PNs, PVBCs immediately show marked depression, which might be related to their suggested function in the temporally precise control of PN discharge. In contrast, the three different types of PTIs show similarly strong short-term depression at higher activities, but the relevance of this ability still must be addressed.

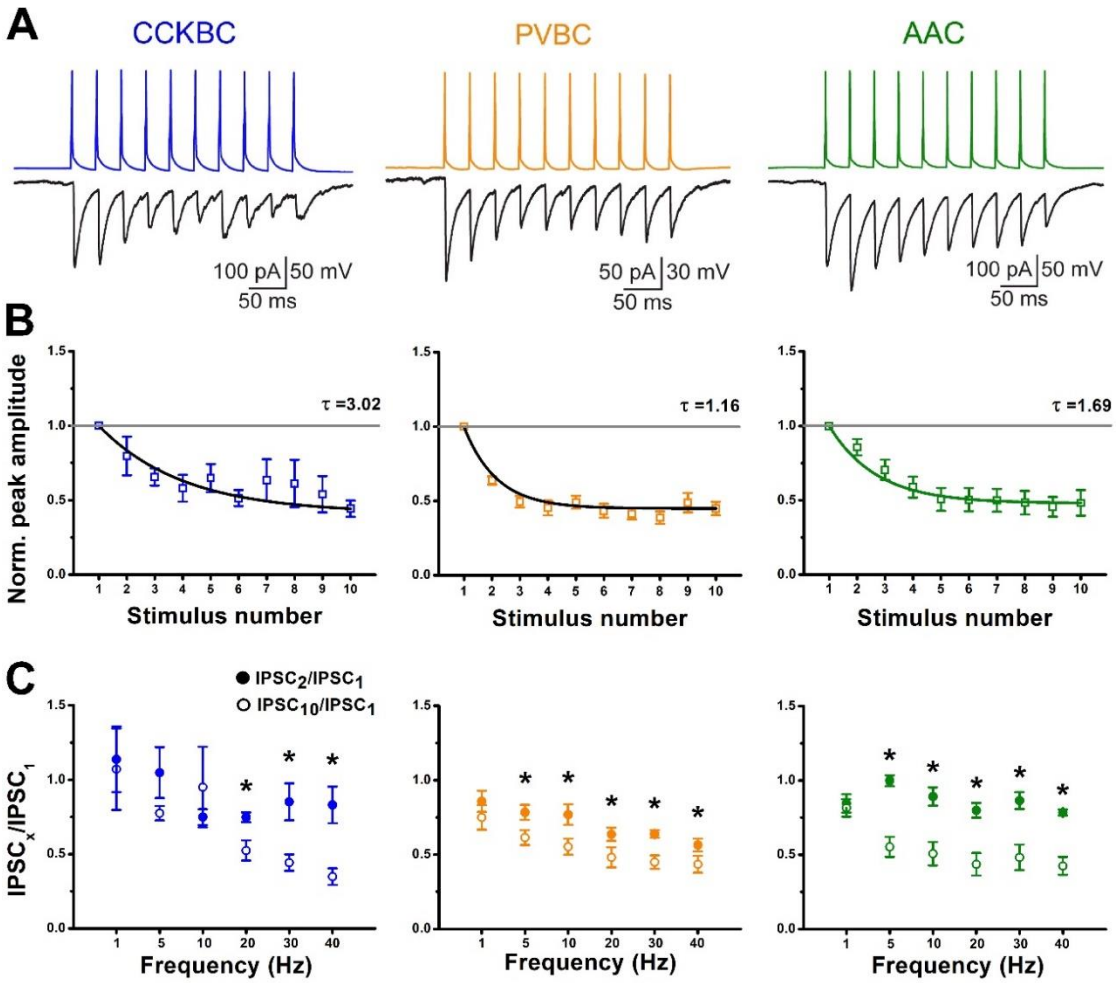

Figure 12. ***Short-term dynamics of transmitter release at the output synapses of the three PTIs.*** *(**A**) Representative average IPSCs (bottom traces) in response to ten APs evoked at a frequency of 30 Hz (upper traces). (**B**) Summary of the release dynamics evaluated at 30 Hz in PVBC- (n = 10), AAC- (n = 12) and CCKBC-PN pairs (n = 7). Amplitude values in each case were normalized to the first peak. Tau values were obtained by exponential fit to data points in summary plots, showing distinct dynamical properties of events evoked at 30 Hz. (**C**) Frequency-dependent changes in short-term plasticity. Ratios of IPSC2/IPSC1 and IPSC10/IPSC1 calculated at distinct frequencies indicate the different properties in release at the unitary connections giving rise by the three IN types. *p < 0.05.*

Next, we tested whether, in addition to the phasic GABA release tightly locked to the APs, a higher IN activity is capable of producing asynchronous transmitter release from the axon terminals of these cells. To address this question, trains of APs were evoked in the presynaptic IN with various frequencies and charge transfer of the inhibitory response was recorded in the postsynaptic PN (**Fig. 13A**). We found that no asynchronous release could be detected at the output synapses of the AACs (**Fig. 13B and C**). Interestingly, a small charge could be observed at PVBC output synapses following the AP train (**Fig. 13B and C**). In contrast, CCKBC output synapses display an apparent and marked asynchronous release in response to an AP train, which was frequency dependent (**Fig. 13B and C**). These data indicate that, in contrast to PV-expressing PTIs, CCKBCs are able to prolong their inhibitory effect on PNs at high network activity levels, if they spike at high rates.

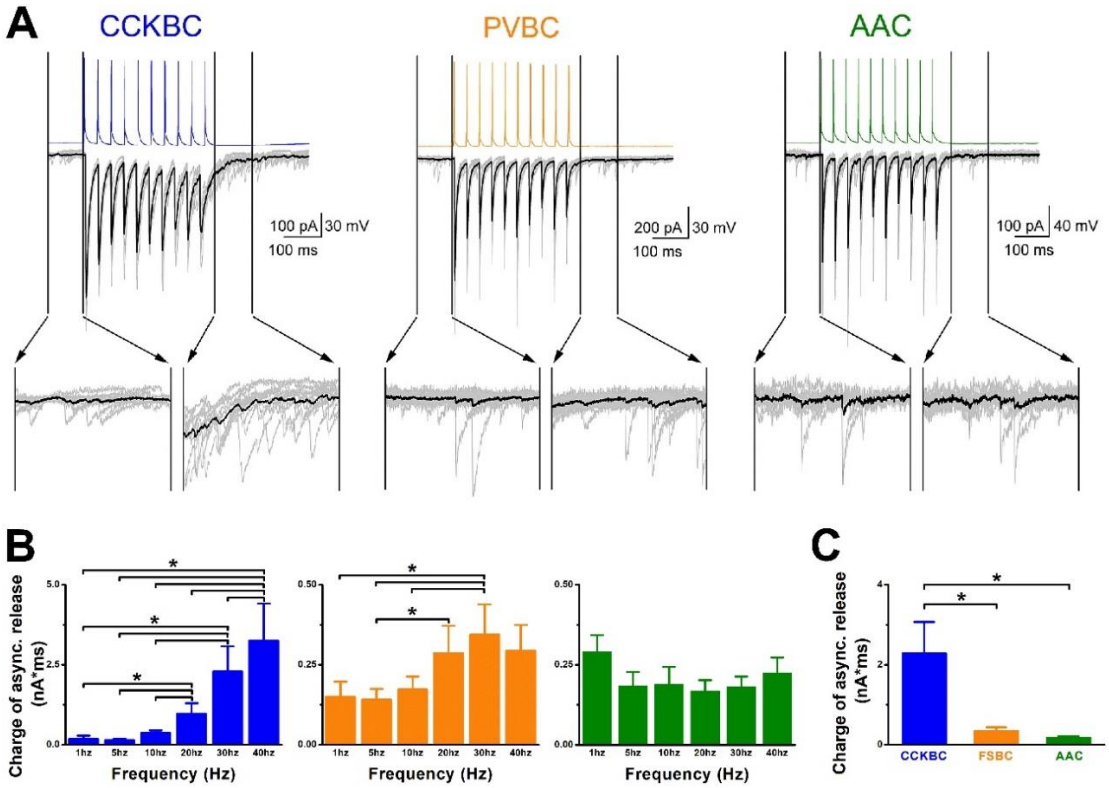

Figure 13. ***Asynchronous transmitter release at the output synapses of the three types of PTIs.*** *(**A**) Representative postsynaptic events in response to ten APs (upper traces) evoked at 30 Hz. Averaged traces in black are superimposed on ten consecutive events shown in gray. The magnified 100-ms-long periods before and after the AP trains used to estimate the amount of asynchronous transmitter release are shown. In CCKBC-PN pairs, the charge following the AP train is clearly larger than before. (**B**) Summary of the frequency-dependent asynchronous release in the three types of IN-PN pairs. A robust increase in release was characteristic at the output synapses of CCKBCs at 20 Hz or higher frequencies. (**C**) Comparison of the magnitude of asynchronous release in the three IN-PN pairs evoked by 30 Hz. *p < 0.05, ***p < 0.001.*

Table 2. ***Summary of uIPSC properties.*** *Data are presented as the median with the first and third quartiles in parentheses. p values represent the results of the statistical comparison of *PVBC vs. AAC, #AAC vs. CCKBC and +CCKBC vs. PVBC using the Mann-Whitney U test after Kruskal-Wallis ANOVA.*

	PVBC			**AAC**			**CCKBC**		
Parameter	Median	*p*-value*	n	Median	*p*-value#	n	Median	*p*-value+	n
Peak amplitude (pA)	339.4 (156.5-605.7)	0.056	8	310.3 (265.0-400.0)	0.056	10	152.6 (97.7-232.5)	0.056	8
Potency (pA)	340.0 (160.5-605.7)	0.094	8	310.3 (265.0-400.0)	0.094	10	177.6 (109.9-234.7)	0.094	8
Rise time (10-90%, ms)	0.63 (0.47-0.66)	0.450	8	0.50 (0.45-0.57)	**0.001**	10	1.05 (0.93-1.27)	**0.004**	8
Decay time constant (ms)	6.31 (5.30-7.48)	0.115	7	6.91 (6.52-8.21)	0.115	10	8.49 (6.77-9.45)	0.115	8
Probability of failure	0 (0-0.05)	0.180	8	0 (0-0)	**0.002**	10	0.04 (0.02-0.021)	0.067	8
Latency (ms)	0.92 (0.78-1.01)	**0.003**	8	1.33 (1.09-1.64)	0.965	10	1.42 (1.06-2.04)	**0.018**	8

4.1.4 Both CCKBCs and PVBCs can potently inhibit PN spiking in the BA

In order to compare the efferent features of BCs, we examined the characteristics of the output synapses of PVBCs and CCKBCs and their effects on the spiking of postsynaptic PNs using paired recordings in slices prepared from adult PV-eGFP or CCK-DsRed mice (**Fig. 14A**). Three APs evoked at 30 Hz (similar to in vivo spiking activity, (Bienvenu et al., 2012)) in a presynaptic BC resulted in postsynaptic responses in a PN (**Fig. 14C and D**). There was a high probability to find a monosynaptically connected pair in case of both BC types (CCKBC-PN, 86.5%, n = 16; PVBC-PN, 96.1%, n = 13). In addition, we found that IPSC/Ps evoked by the first APs of the trains were also similar (**Fig. 14E and F**). As in the hippocampus (Hefft and Jonas, 2005; Szabo et al., 2010), three APs evoked in PVBCs resulted in depressing inhibitory responses in the PNs, while there was no obvious change in the amplitude of

IPSC/Ps evoked by spike trains in CCKBC-PN pairs at the population level (**Fig. 14E**; CCKBC pairs: 80.53 ± 18.36 pA, n = 13; PVBC pairs: 150.38 ± 30.24 pA, n = 13, Mann-Whitney U test, p = 0.073). However, this difference in short-term plasticity was not apparent in the IPSP summation as the area under IPSPs evoked by three spikes in the two BC types were indistinguishable (**Fig. 14F**; CCKBC pairs: 121.83 ± 43.71 mV*ms, n = 13; PVBC pairs: 119.78 ± 30.35 mV*ms, n = 11, Mann-Whitney U test, p = 0.45). The similarities in the unitary events originating from the two BC types implied that these GABAergic cells might have comparable effects on the spiking of PNs. To test this prediction, we injected sinusoidal current trains into the PNs near their firing threshold and three spikes at 30 Hz were evoked in the presynaptic BCs at the peak of a sinusoidal wave, the point where PNs spiked with the highest probability (**Fig. 14G**). This reproducible approach allowed us to estimate the efficacy of inhibition for both GABAergic cell types by comparing the firing probability of PNs during evoked BC activity and during control epochs, when the presynaptic BC did not fire (**Fig. 14H**). This analysis fully supported our expectation based on the unitary event properties, namely, that the two BC types inhibited the PN firing with equal efficacy (**Fig. 14I;** CCKBC pairs: 72.53 ± 8.80%, n = 13; PVBC pairs: 78.70 ± 8.29%, n = 13, Mann-Whitney U test, p = 0.63). These results show that in this cortical network, PVBCs and CCKBCs provide similarly effective synaptic inhibition onto their neighboring PNs.

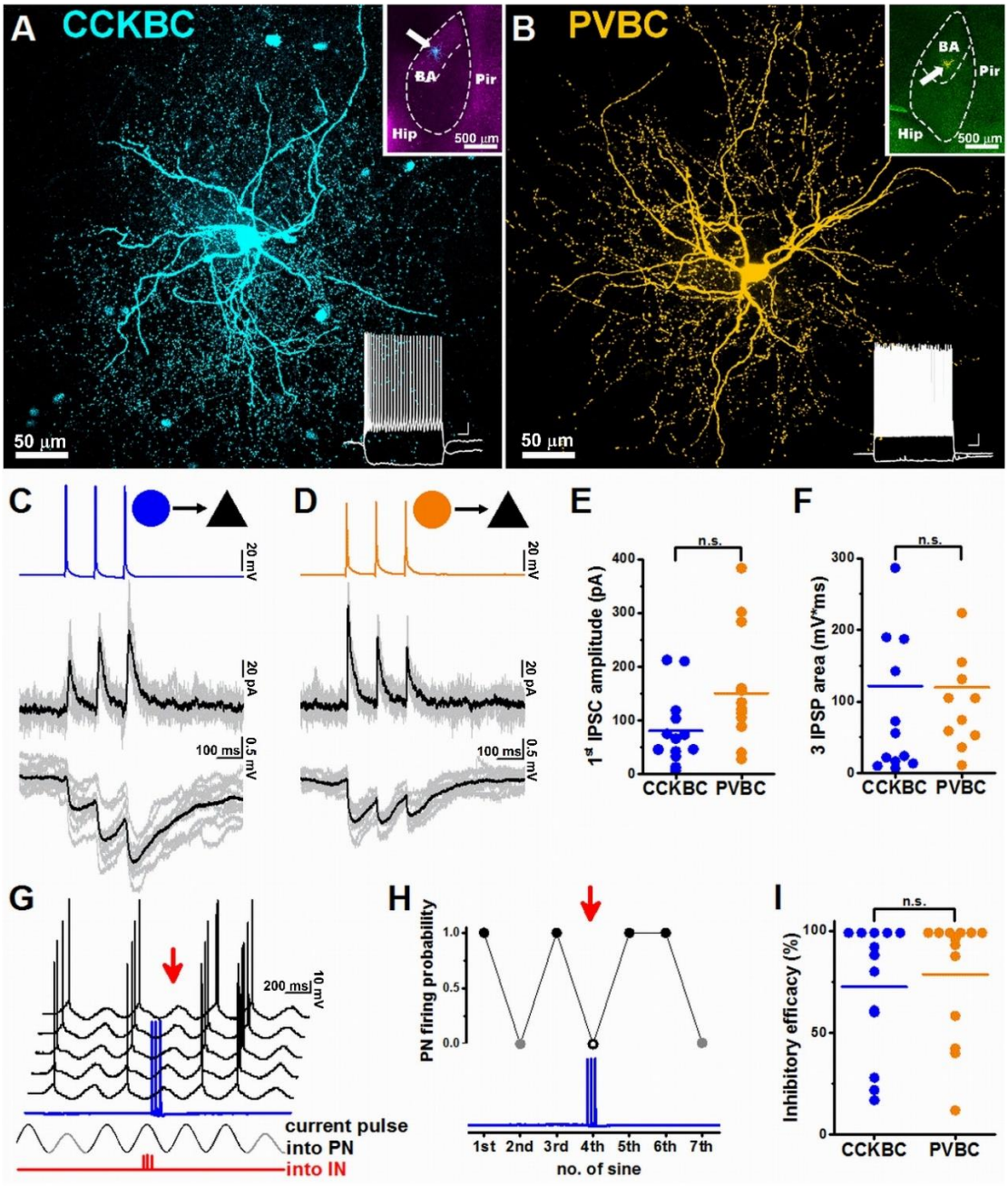

Figure 14. ***Similarly potent inhibition of PN activity by CCKBCs and PVBCs.*** *Maximum z intensity projection image of a CCKBC (**A**) and a PVBC (**B**). Upper insets in (**A**) and (**B**) indicate the positions of the recorded BCs (white arrows) in horizontal slices prepared from mice expressing CCK-DsRed and mice expressing PV-eGFP, respectively. Hip, hippocampus; BA, basal amygdala; Pir, piriform cortex. Lower insets show the firing patterns of the same BCs in response to a step current injection (+400 and -100 pA). Scales: 10 mV, 100 ms. (**C**, **D**) Representative IPSC (middle*

*traces) and IPSP (lower traces) recordings in a CCKBC (blue)-PN (black) pair (**C**) or in a PVBC (orange)-PN (black) pair (**D**) in response to three APs at 30 Hz (upper traces). Ten superimposed consecutive traces are in gray, average in black. (**E**) CCKBCs and PVBCs give rise to IPSCs with similar amplitude, and (**F**) 3 IPSPs with the similar area recorded in PNs. (**G**) Sinusoidal current trains with peak-to-peak amplitude of 30 pA (gray cycles) and 50 pA (black cycles) were injected into a PN to initiate firing, and 3 APs were evoked in the presynaptic CCKBC (blue) at the fourth cycle (red arrow). Schematic representation of the injection of three current pulses into the presynaptic IN at 30 Hz is shown in red. Voltage traces are offset for clarity. (**H**) Raw data of the experiments are shown in (**G**). Black and gray dots refer to the firing probability observed at the sinusoid current amplitudes of 50 pA and 30 pA, respectively. An open circle indicates the cycle when the presynaptic IN fired three APs. (**I**) Comparison of the inhibitory efficacy of CCKBCs and PVBCs. Each data point on the plots represents an average obtained in a pair recording, and lines represent means.*

4.2 Different recruitment of PTIs in the BA

4.2.1 A lower activity level of PN populations triggers spiking of PVBCs than CCKBCs

As PNs in cortical regions readily innervate INs in their vicinity (Jiang et al., 2015; Kullmann, 2011), the above data raises an intriguing question. Are the distinct PTI types excited similarly or distinctly by local PNs? To reveal the recruitment of these GABAergic cells by feedback excitation, we produced triple transgenic mice by crossing VGluT1-cre mice with PV-eGFPxCCK-DsRed double crossed mice, allowing simultaneous investigations of the different PTI types. An AAV carrying ChR2 fused to a red fluorescent protein (ChR2-mCherry) expressed in a cre-dependent manner was injected into the BA of these triple transgenic mice, allowing us to selectively excite PNs locally by blue light illumination (**Fig. 15A**). Three to five weeks after injection, acute slices containing the amygdala region were prepared, and simultaneous loose-patch recordings from a PV-containing IN and a CCK-expressing IN were obtained, while the intensity of light illumination was gradually increased (**Fig. 15B**).

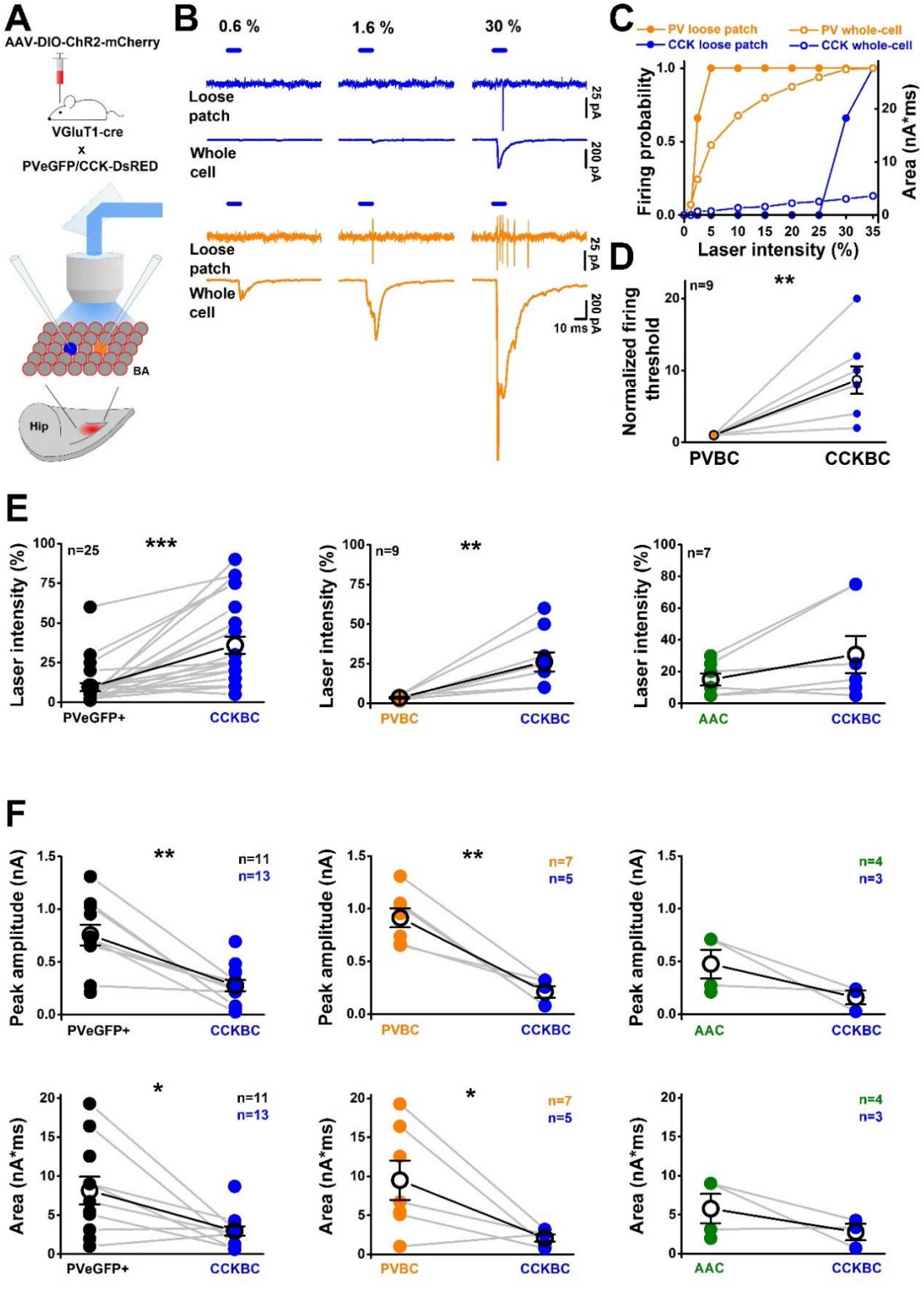
A
AAV-DIO-ChR2-mCherry
VGluT1-cre
x
PVeGFP/CCK-DsRED
BA
Hip
B
0.6 %
1.6 %
30 %
Loose patch
Whole cell
25 pA
200 pA
10 ms
C
PV loose patch
PV whole-cell
CCK loose patch
CCK whole-cell
Firing probability
Area (nA*ms)
Laser intensity (%)
D
n=9
**
Normalized firing threshold
PVBC
CCKBC
E
n=25
***
Laser intensity (%)
PVeGFP+
CCKBC
n=9
**
PVBC
CCKBC
n=7
AAC
CCKBC
F
**
n=11
n=13
Peak amplitude (nA)
PVeGFP+
CCKBC
n=7
n=5
PVBC
n=4
n=3
AAC
*
Area (nA*ms)

Figure 15. ***Spiking of PVBCs requires a lower activity level of PN population than CCKBCs and AACs.*** *(**A**) Experimental design. mCherry-containing construct was injected into the BA of triple transgenic mice (bottom drawing illustrates a horizontal slice showing the expression site in red; Hip, hippocampus; BA, basal amygdala). Among AAV-infected PNs (red circles), a CCKBC (blue) and a PVBC (orange) were simultaneously recorded first in loose-patch mode, followed by recordings in whole-cell mode, while neighboring PNs were excited by light illumination. (**B**) Representative traces of loose-patch and whole-cell recordings show different spiking thresholds and, concomitantly, larger light-evoked responses in a PVBC (lower traces) compared to a CCKBC (upper traces) in response to PN stimulation at different light intensities. Averages calculated from three consecutive events are shown in blue and orange for the CCKBC and the PVBC, respectively. (**C**) A summary graph of the experiment shown in (**B**); the firing probability (solid circles, left axis) and the integral of the light-evoked responses (open circles, right axis) detected in BCs upon gradually elevated stimulation intensities. (**D**) The activation threshold of PVBCs is significantly lower than that recorded simultaneously in CCKBCs. Firing threshold values are normalized to PVBC firing threshold (**E**) Comparison of the firing threshold in INs expressing eGFP under the control of the PV promoter (PVeGFP+) and CCKBCs upon the light stimulation of ChR2-expressing PNs in the BA. (Left) PV-expressing cells at a population level have a significantly lower activation threshold compared to the simultaneously recorded CCKBCs. (Middle) PVBCs identified post hoc by the CB content showed significantly lower spiking threshold compared to the simultaneously recorded CCKBCs. (Right) AACs, identified by the lack of CB expression, tend to have a lower activation threshold compared to the simultaneously recorded CCKBCs, but in this case the difference between the two cell types was not significant. (**F**) (Left) At the firing threshold PVeGFP+ INs received significantly larger light evoked EPSCs (both peak amplitude and area) compared to CCKBCs tested with the same stimulation protocol as in panel (**A**) (Area, lower row). (Middle) PVBCs displayed at their spiking threshold significantly larger EPSC amplitude and area compared to CCKBCs (Peak amplitude, upper row; Area, lower row). (Right) AACs at the AP generation threshold tend to have larger EPSC amplitude and area compared to CCKBCs, but the difference was not significant (Peak amplitude, upper row; Area, lower row). ***p < 0.001, **p*

*< 0.01, *p < 0.05. Mean ± SEM are shown in black. In (**B**), results of whole-cell recordings obtained only for single INs were also included.*

We noticed that spikes could be detected at significantly lower light power in PV-expressing cells in comparison to CCK-containing INs (**Fig. 15C and D**). To determine the magnitude of excitatory synaptic inputs necessary to evoke APs in these GABAergic cells, the illumination protocol was repeated while the same two INs were recorded in whole-cell mode (**Fig. 15B and C**), allowing the identification of neuron types post hoc (**Fig. 16A**). The results indicated that at the activation level of PNs where PV-containing INs reached their spiking threshold, they received significantly larger evoked excitatory synaptic input than CCKBCs (**Fig. 15E and F;** Activation threshold (**E**): (Left) PVeGFP+: 9.55 ± 2.55%, CCKBC: 36 ± 5.43%; Paired Sample Wilcoxon Signed Rank Test, (Middle) PVBC: 3.47 ± 0.5%; CCKBC: 26.11 ± 6%, Sample Wilcoxon Signed Rank Test; Peak amplitude (**F**), (upper row): (Left) PVeGFP+: 754.9 ± 98.1 pA, CCKBC: 275.1 ± 53.3 pA; Mann-Whitney U test, (Middle) PVBC: 914.1 ± 91.3 pA, CCKBC: 210.1 ± 54.7pA; Mann-Whitney U test; Area (**F**), (Lower row): (Left) PVeGFP+: 8.15 ± 1.78 nA*ms, CCKBC: 2.96 ± 0.59 nA*ms; Mann-Whitney U test, (Middle) PVBC: 9.51 ± 2.53 nA*ms, CCKBC: 2.07 ± 0.45 nA*ms; Mann-Whitney U test). This difference was preserved when we separately examined PVBCs, indicating that PVBCs are driven by lower PN activity levels than CCKBCs (**Fig. 15D;** CCKBC: 8.67 ± 1.91, n = 9 dual recordings; Paired Sample Wilcoxon Signed Rank Test, $p < 0.01$). When the PN population activity reached the level required to drive CCKBC firing, PVBCs already discharged multiple spikes (**Fig. 15B**, number of PVBC spikes at CCKBC firing threshold, 4.26 ± 0.21, n = 9). Surprisingly, the activation of AACs required a higher level of the PN activity compared to PVBCs, but they showed still substantially lower threshold than CCKBCs (**Fig. 15E and F**; Activation threshold (**E**): AAC: 15 ± 3.78%, CCKBC: 30.71 ± 11.67%; Sample Wilcoxon Signed Rank Test, p = 0.09; Peak amplitude (Upper row): (Right) AAC: 476.6 ± 135.8 pA, CCKBC: 159.8± 67.3pA; Mann-Whitney U test, p = 0.21; Area (Lower row): (Right) AAC: 5.77 ± 1.88 nA*ms, CCKBC: 2.78 ± 1.07 nA*ms; Mann-Whitney U test, p = 0.59). These

observations clearly showed that the PTI types are distinctly recruited by BA PNs, which can be primarily explained by the difference in their excitatory inputs.

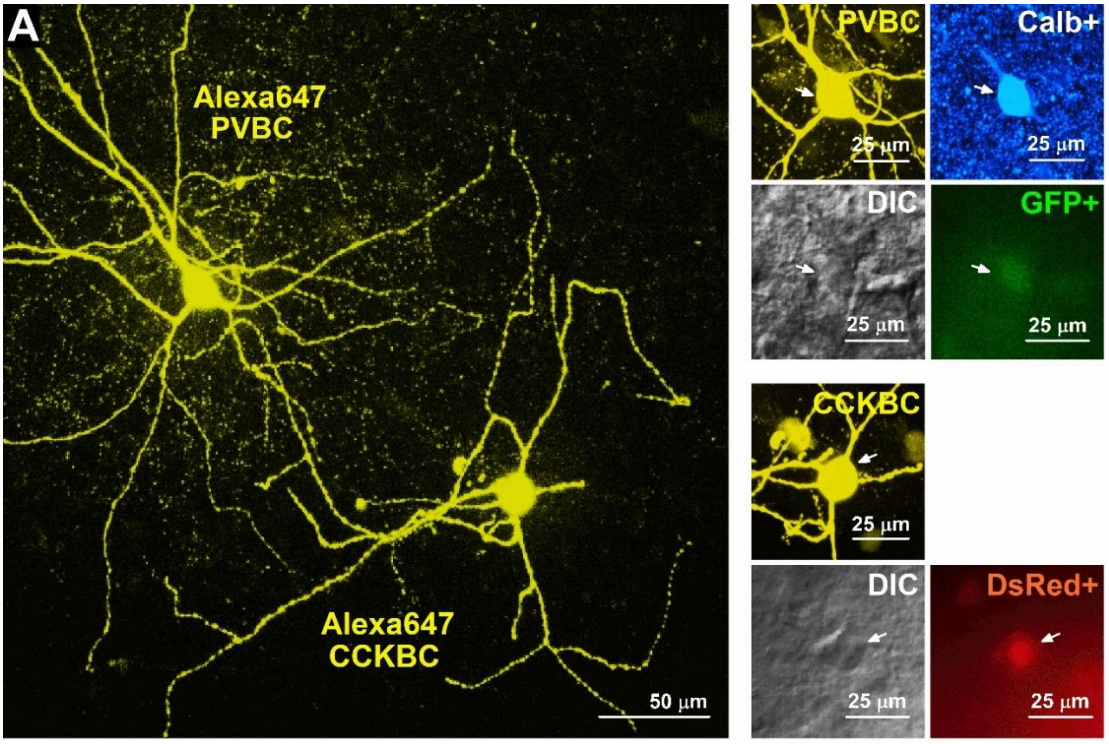

Figure 16. ***Post hoc anatomical identification of a simultaneously recorded CCKBC and a PVBC*** **(A)** *Maximum z intensity projection image of the in vitro biocytin-filled INs from which recording is shown in (**Fig. 15B**). Right, images illustrate the presence of CB (Calb+) immunopositivity in the PVBC (blue), while epifluorescent images show the expression of eGFP in the PVBC and red fluorescent protein (DsRed) in the CCKBC together with the corresponding differential interference contrast images.*

4.2.2 PNs distinctly innervate the distinct types of PTIs

To reveal the differences in synaptic excitation that can contribute to the distinct excitability of BCs by BA PNs, we first estimated the density of excitatory inputs received by intracellularly labeled BCs (**Fig. 17A and B**). This analysis showed that VGluT1-expressing boutons more densely covered the dendrites of PVBCs than those

of CCKBCs (**Fig. 17C**; VGluT1 input density: CCKBC 0.32 ± 0.06 /µm, PVBC 0.76 ± 0.06 /µm, Mann-Whitney U test). These results are in line with our observations that the activity of a smaller fraction of PNs should excite PVBCs more readily (**Fig. 15**), if there is no substantial difference in the unitary events received by the two BC types.

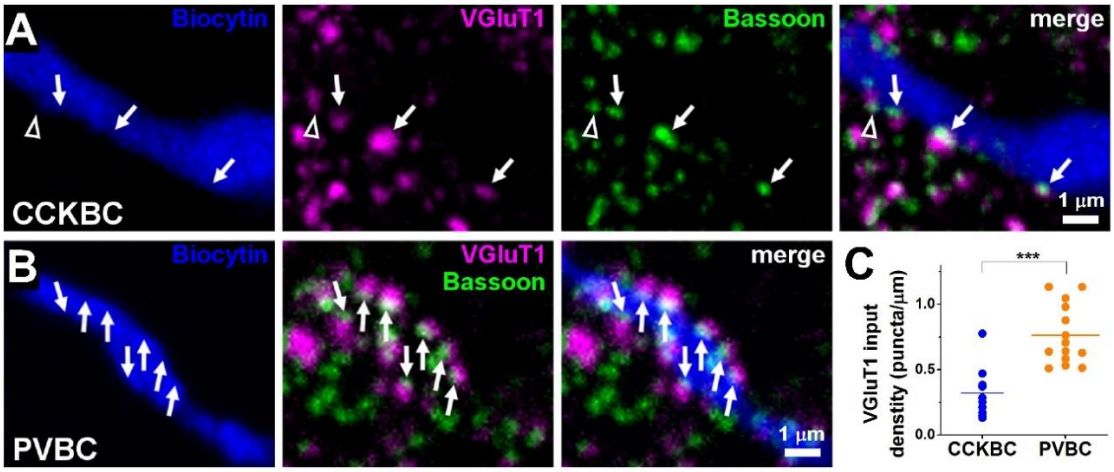

Figure 17. ***PVBCs receive a higher number of excitatory inputs than CCKBCs.*** *VGluT1-immunopositive puncta opposing the dendrite of a CCKBC (**A**) and a PVBC (**B**) and containing bassoon staining were regarded as a contact (arrows). Open arrowhead shows a VGluT1 immunoreactive bouton in which bassoon did not oppose the biocytin-labeled dendrite, presumably contacting a neighboring structure. (**C**) Each data point on the plot represents an average density obtained on a dendritic segment, lines represent mean. Biocytin-labeled dendritic segments of 5 CCKBCs and 6 PVBCs were investigated. ***p < 0.001.*

To address this latter assumption, we next investigated the properties of unitary events from individual PNs onto BCs and expanded the results with data from AACs. We made in vitro dual recordings from post hoc identified PN-CCKBC, PN-PVBC and PN-AAC pairs, where current pulse was injected into the presynaptic PN to evoke an AP and the postsynaptic response was detected in the postsynaptic IN (**Fig. 18A and B**). We found that the average potency and failure rate of uEPSCs were significantly

larger and lower, respectively, in PVBCs and AACs than in CCKBCs, moreover PVBCs and AACs received EPSCs with significantly faster kinetics (**Fig. 18D-I**; Potency (**D**) CCKBC: 21.5 ± 1.65 pA, PVBC: 94.25 ± 15.08 pA, AAC: 67.7 ± 11.77 pA, Peak amplitude (**E**): CCKBC: 10.16 ± 2.02 pA, PVBC: 81.78 ± 15.68 pA, AAC: 53.28 p ± 13.09 pA; Failure rate (**F**): CCKBC: 0.58 ± 0.05, PVBC: 0.25 ± 0.04, AAC: 0.31 ± 0.07; Rise time 10-90% (**G**): CCKBC: 0.77 ± 0.07 ms, PVBC: 0.4 ± 0.03 ms, AAC: 0.42 ± 0.06 ms; Decay tau (**H**): CCKBC: 3 ± 0.23 ms, PVBC: 1.41 ± 0.1 ms, AAC: 1.05 ± 0.14 ms; Latency (**I**): CCKBC: 1.75 ± 0.09 ms, PVBC: 0.92 ± 0.07 ms, AAC: 1 ± 0.05 ms, Mann-Whitney U test).

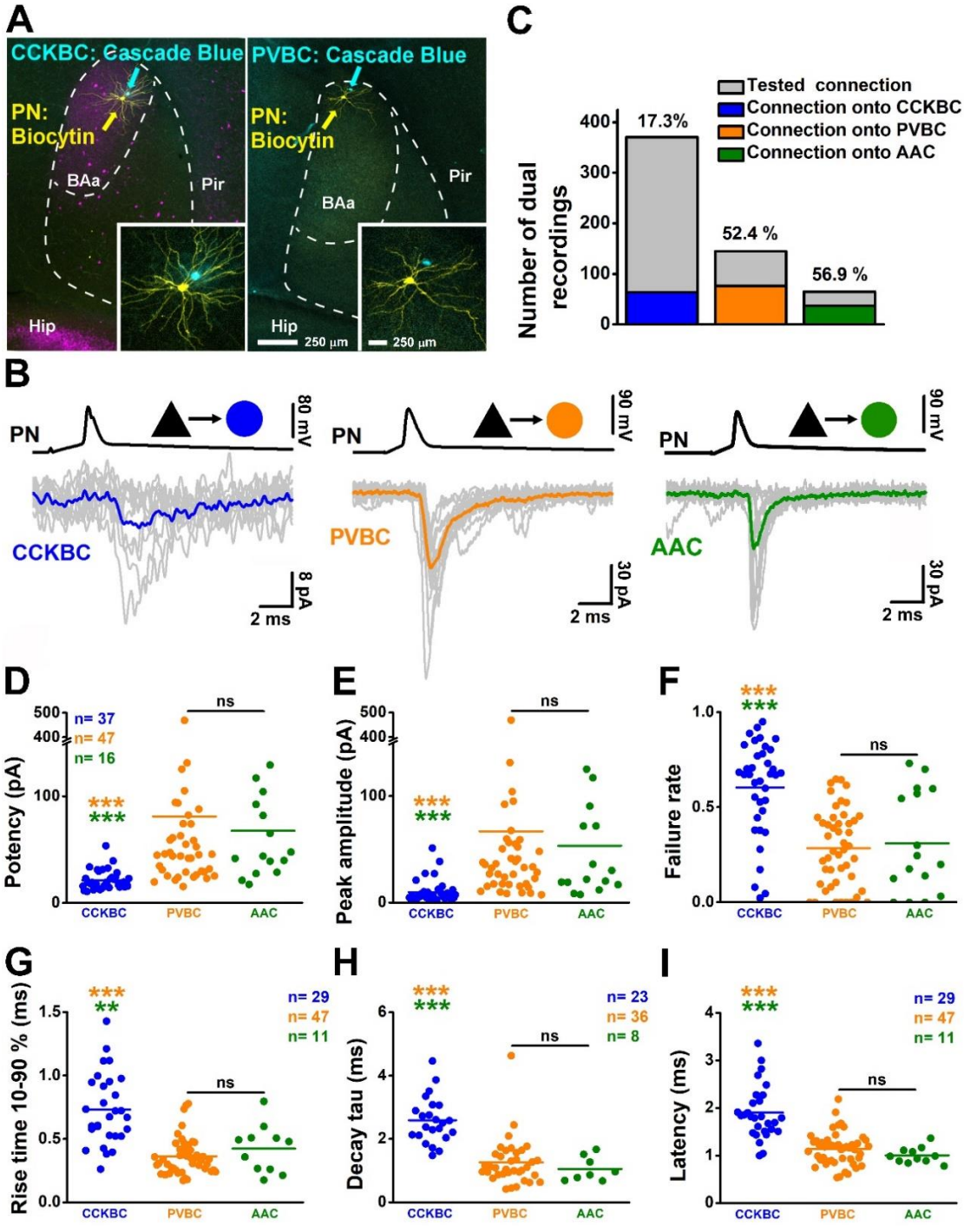

Figure 18. ***PNs give rise to distinct excitatory synaptic inputs onto the PTIs.*** *(**A**) Panoramic images showing a CCKBC-PN (left) and a PVBC-PN (right) pair in the anterior part of the BA. INs were filled with Cascade Blue and PNs with biocytin. Insets show a higher magnification of the cell pairs recorded. (**B**) Representative traces of unitary excitatory postsynaptic currents (EPSCs) evoked by APs in a PN-CCKBC (left*

*traces), PN-PVBC pair (middle traces) and PN-AAC pair (right traces). Ten superimposed consecutive traces are in gray, and averages are in blue, orange and green, respectively. (**C**) Comparison of the connection probability between the two BC types shows that local PNs target CCKBCs with a relatively low likelihood in comparison to PVBCs and AACs, whose are innervated similarly. (**D-I**) Basic properties of the uEPSCs received by the three types of perisomatic inhibitory neurons. The potency (**D**) and the peak amplitude (**E**) of the uEPSCs in CCKBCs are significantly smaller than those recorded in PVBCs and AACs. (**F**) The failure rate of the uEPSCs in CCKBCs are significantly larger than those recorded in PVBCs and AACs. The rise time 10-90% (**G**), the decay tau (**H**) and the latency (**I**) of the uEPSCs in CCKBCs are also significantly different than those recorded in PVBCs and AACs. Mean ± SEM. ***p < 0.001, **p <0.01.*

Next, we analyzed the connection probability between PNs and BCs. In paired recordings, we found a low chance to find connected PN partner to CCKBCs (**Fig. 18C**). Overcoming this drawback, we designed an optogenetic paired recording approach (**Fig. 19A,** see Materials and Methods). In this experiment, we used patterned light stimulation of individual ChR2 expressing PNs and tested their synaptic connection in postsynaptic BCs. We noticed that surprisingly, the connection probability showed distinct distance-dependence (**Fig. 19B and C**). The construction of a spatial map for PN-BC pairs uncovered that PVBCs were contacted preferentially by their neighboring PNs (<200-250 μm), but only rarely by more distal excitatory neurons. In contrast, PNs innervated CCKBCs with lower probability, but the chance to find a connected pair was distance-independent (**Fig. 19C**).

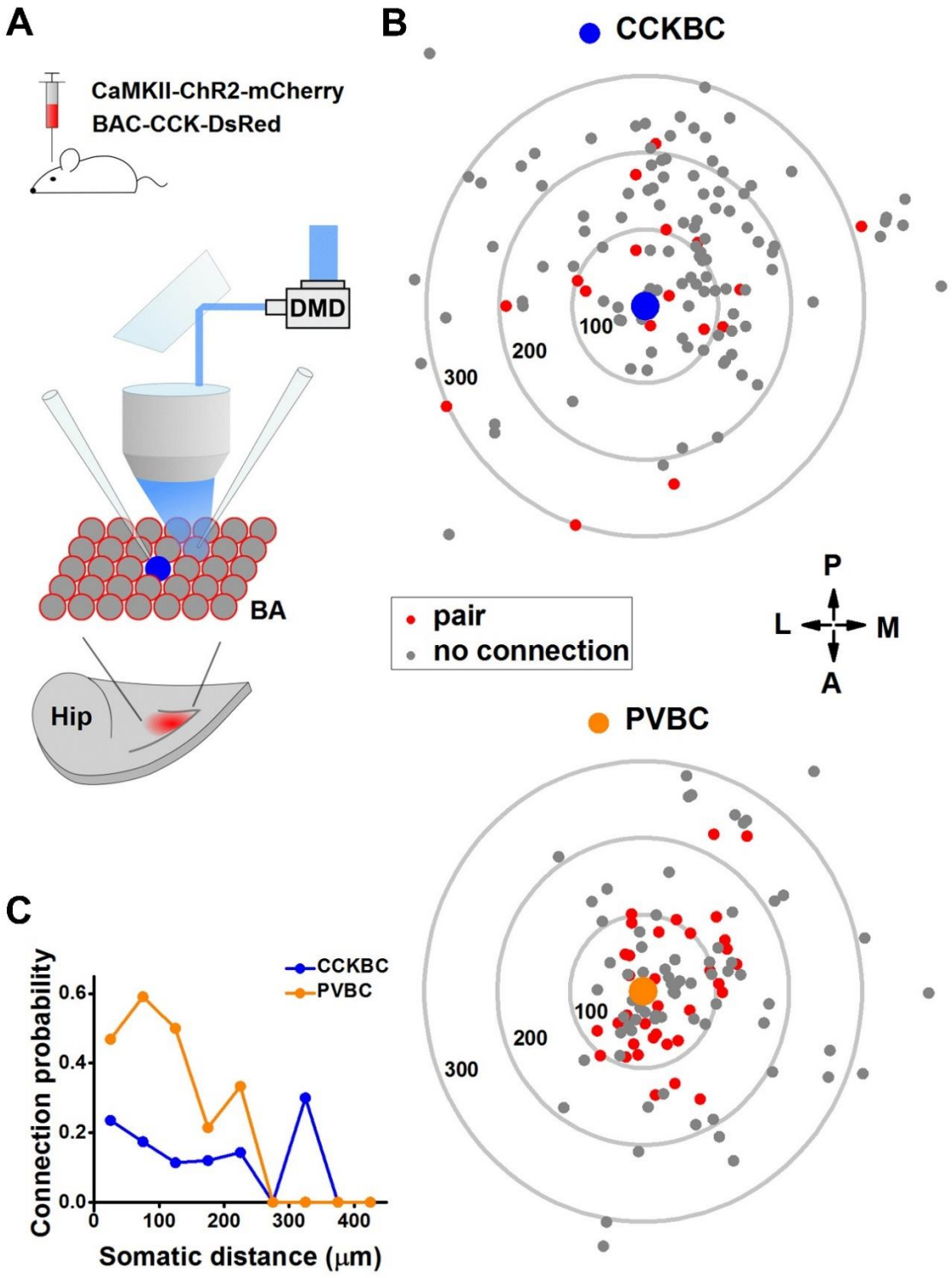

Figure 19. ***PNs innervate PVBCs, but not CCKBCs in a distant-dependent manner.*** *(**A**) Schematic illustration of the experimental design to excite PNs using blue light. ChR2-mCherry-containing construct was injected into the BA of transgenic mice*

*(bottom drawing illustrates a horizontal slice showing the expression site in red). Among AAV-infected PNs (red circles), a CCKBC (blue) was recorded in whole-cell mode, while its excitatory input from neighboring PNs was tested by light illumination and/or whole-cell recording. BA, basal amygdala; Hip, hippocampus. (**B**) Connectivity map. Concentric circles indicate Δ100 μm distance from the IN in the center. Each dot represents a tested PN soma location. (**C**) PVBCs receive excitatory synaptic inputs from their neighboring PNs with high probability, while CCKBCs are innervated by PNs via their local collaterals with low probability, independently of the inter-somatic distance.*

Next, we performed an analysis of contact sites between PNs and BCs. In order to identify the putative appositions between the presynaptic terminals and the postsynaptic partner, we used dual color labelling of the pre- and postsynaptic neurons during the recording (**Fig. 20A and F**). Subsequently, the cell pairs were reconstructed and putative contact sites were identified with high magnification confocal imaging (**Fig. 20B-E and Fig. 20G-J**). In both BC types, some of the close appositions were validated as synaptic contact at the EM level (**Fig. 20K and L**). This investigation has revealed that twice as many contacts could be identified from single PNs onto PVBCs on average, than onto CCKBCs (**Fig. 20J**; Number of contacts/pair: PN-CCKBC 1.79 ± 0.26, n = 14, PN-PVBC 3.23 ± 0.57, n = 13). However, the location of the contact sites along the somato-dendritic membrane surface of both BCs was similar (PN-CCKBC pairs: 104.34 ± 12.67 μm; PN-PVBC pairs: 77.49 ± 11.39 μm, p = 0.0871, Mann-Whitney U test). When the amplitude of unitary events was plotted as a function of the identified contact sites, a linear relationship was observed in the case of PN-CCKBC pairs, showing that an increase in the number of contacts results in a gradual increase in the unitary amplitude (**Fig. 20M**). In contrast, no relationship was found in the case of PN-PVBC pairs (**Fig. 20M**).

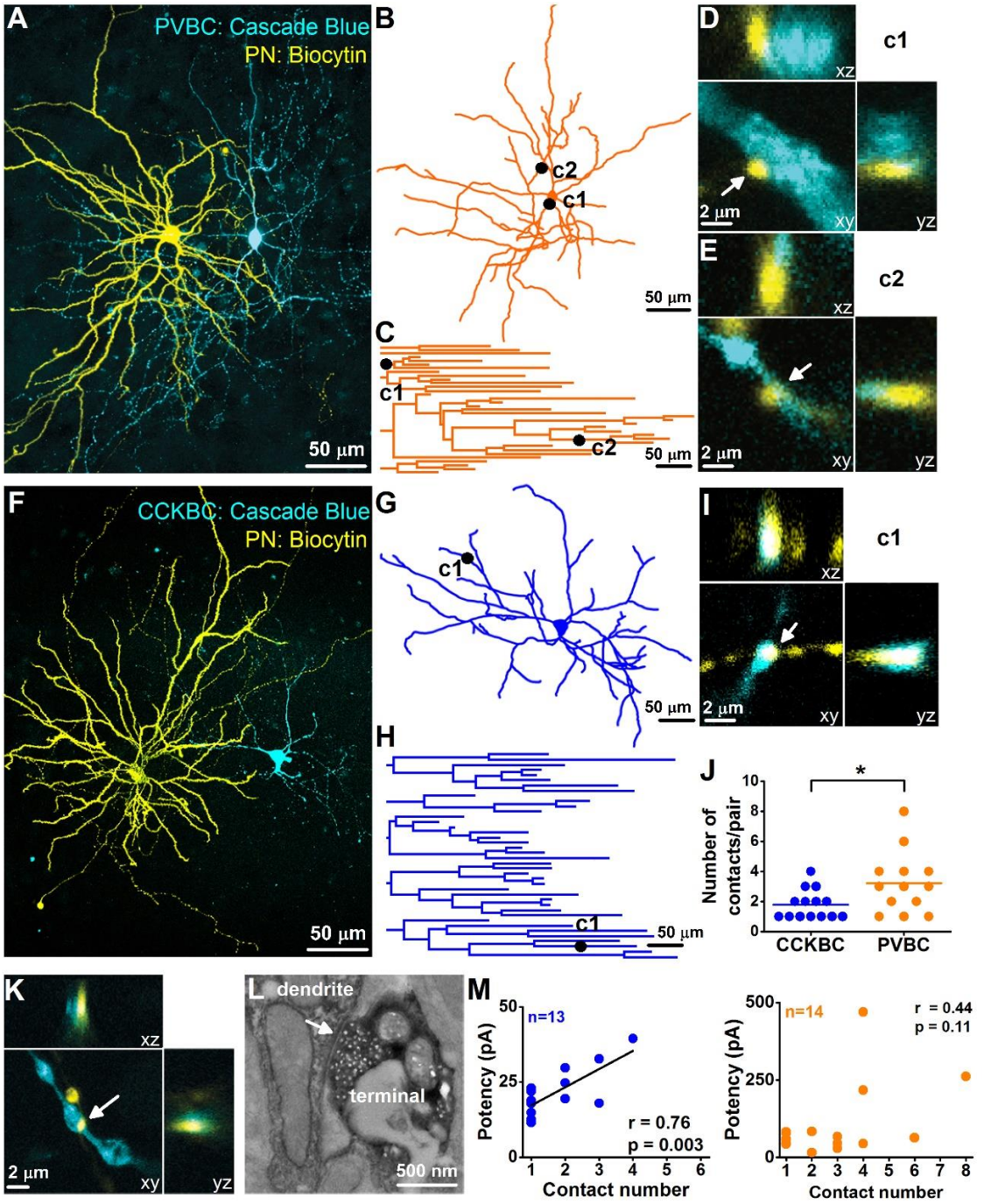

Figure 20. ***PNs differently innervate the two BC types.*** *Maximum z intensity projection image of a representative PN-PVBC pair (**A**) and a PN-CCKBC pair (**F**). Cascade Blue was used to label the BCs, while biocytin was introduced into the PNs to visualize them with streptavidin-conjugated Alexa647. Neurolucida reconstructions (**B** and **G**) and the resulted dendrogram analysis (**C** and **H**) of the PVBC and CCKBC*

*shown in (**A**) and in (**F**), respectively, marking the location of connections 1 and 2 (**c1** and **c2**) established by the monosynaptically connected presynaptic PNs. (**D** and **E**) High-power magnification 3D confocal images of putative contacts (**c1** and **c2**), showing close appositions between the dendrite-targeting boutons of the PN (yellow) and the PVBC dendrites (blue). (**I**) High power magnification 3D confocal images of a putative contact (**c1**), showing close appositions between the bouton of the PN (yellow) and the CCKBC dendrites (blue). (**J**) PNs establish significantly more contacts on PVBCs than on CCKBCs. Each data point on the plot was obtained from a pair recording, and lines represent means. (**K**) 3D confocal image showing a close apposition between a biocytin-labeled PN terminal (yellow) and a Cascade Blue-labeled BC dendrite (blue). (**L**) EM analysis of the contact shown in (**K**) confirmed the presence of the synaptic junction (arrow). (**M**) A strong relationship was found between the number of contact sites and the uEPSC potency in the case of PN-CCKBC pairs, while no correlation could be observed in the case of PN-PVBC pairs.* Mann-Whitney U test, *$p < 0.05$

4.2.3 PNs make cell type specific synaptic contacts on the two BC types at the level of individual synapses

To further strengthen the finding at the population level that excitatory synaptic inputs at individual release sites received by the two BC types are qualitatively and quantitatively different, we performed two sets of experiments. First, we recorded miniature (i.e. quantal) excitatory postsynaptic currents (mEPSCs) in the presence of 0.5 μM TTX and investigated the properties of single events (**Fig. 21A**). We found that the amplitude distribution of mEPSCs significantly differed in the two BC types (**Fig. 21B**). Importantly, mEPSCs in CCKBCs had small and largely uniform amplitudes (mini recordings: 12.62 ± 0.43 pA, n = 5 cells, CV = 0.07), data that were not markedly different from those obtained in paired recordings with single contacts (p = 0.047, Two sample t test), supporting the finding that BA PNs excite CCKBCs predominantly via a few (one or two) synaptic contacts, having small and uniform EPSC amplitudes. In contrast, mEPSCs in PVBCs had overall larger amplitudes and showed a more skewed

distribution (mini recordings: 21.19 ± 3.01 pA, n = 5 cells, CV = 0.31, **Fig. 21B**). These observations are in line with those obtained in paired recordings, namely that the synaptic conductance at single contacts is larger and more variable in PVBCs than in CCKBCs, and, notably, PNs innervate PVBCs via several (on average three) contact sites (**Fig. 20J and M**). In addition, we also observed a marked difference in the interevent interval distributions of mEPSCs (**Fig. 21B**; Interevent interval: CCKBCs, 86.97 ± 15.03 ms, n = 5; PVBCs, 34.87 ± 8.02 ms, n = 5). In CCKBCs, the time intervals between mEPSCs were significantly longer than between those events recorded in PVBCs. These results are in line with our findings, showing that the density of VGluT1-expressing axon terminals along the dendrites of CCKBCs was significantly lower than of PVBCs (**Fig. 17**).

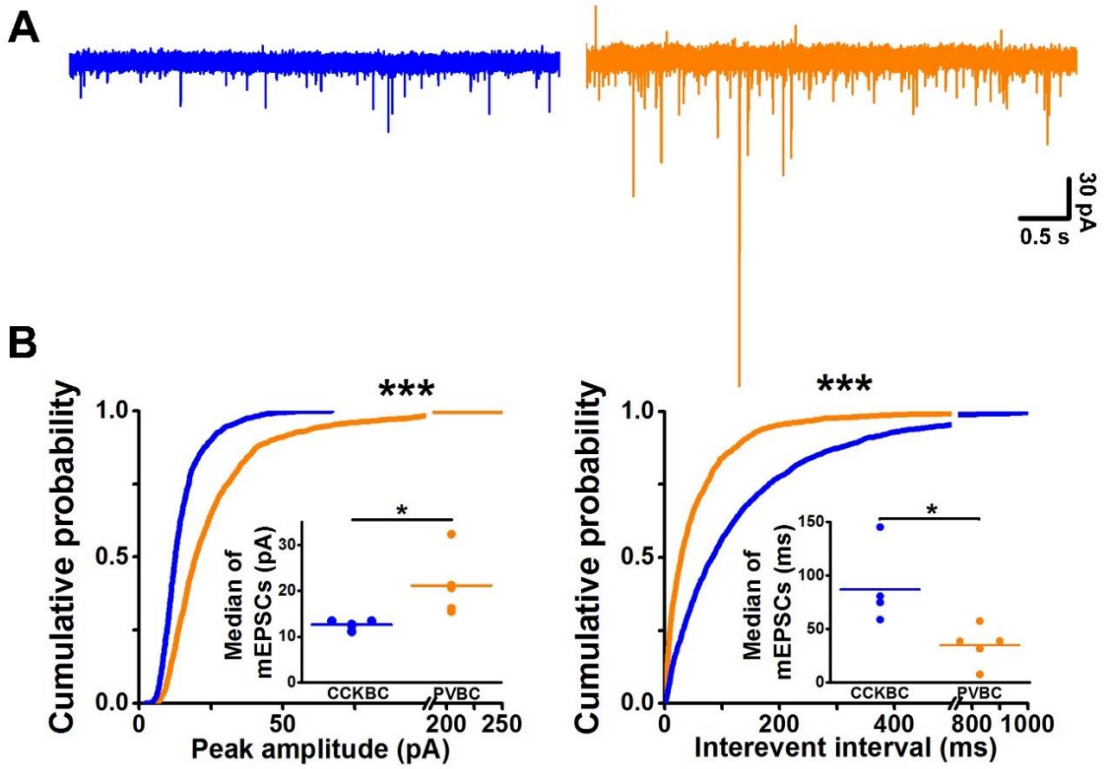

Figure 21. ***mEPSC properties recorded in PVBCs and CCKBCs are significantly different.*** *(**A**) Representative traces depicting mEPSCs in the presence of 0.5 µM TTX in a CCKBC (left, blue) and in a PVBC (right, orange) (holding potential, -65 mV). (**B**) Cumulative probability distributions of mEPSC peak amplitudes (left) and interevent*

*intervals (right) obtained in CCKBCs (blue, n = 5) and PVBCs (orange, n = 5). PVBCs receive mEPSCs with larger amplitude and at higher frequency than CCKBCs. Data points in the insets represent the median of the cumulative distributions obtained for each cell, and lines indicate means. Kolmogorov-Smirnov test, ***p < 0.001; (Insets) Mann-Whitney U test, *p < 0.05*

To reveal a potential reason why release of single vesicles causes significantly smaller mEPSCs in CCKBCs than in PVBCs, we estimated the AMPA receptor content at individual synapses along the CCK- and PV-expressing IN dendrites using super-resolution microscopy (**Fig. 22A and B**). These investigations uncovered that the number of LPs, representing AMPA receptors, at individual clusters apposed to bassoon labeling along the CCKBC dendrites was significantly lower than those observed along the IN dendrites expressing PV (**Fig. 22C**). In addition, there was a significant difference in the 2D convex hull area size of LP clusters along the dendrites of two IN types (**Fig. 22C**; Normalized number of LPs: CCKBCs, 53.13 ± 8.58, PV-containing INs 69.28 ± 8.90; 2D convex hull area: CCKBCs, 0.04 ± 0.007 μm^2, PV-containing INs, 0.08 ± 0.006 μm^2). These data collectively show that PNs innervate the two BC types via different principles and the characteristics of connections between the PNs and BCs favor the excitation of PVBCs at a lower activity level.

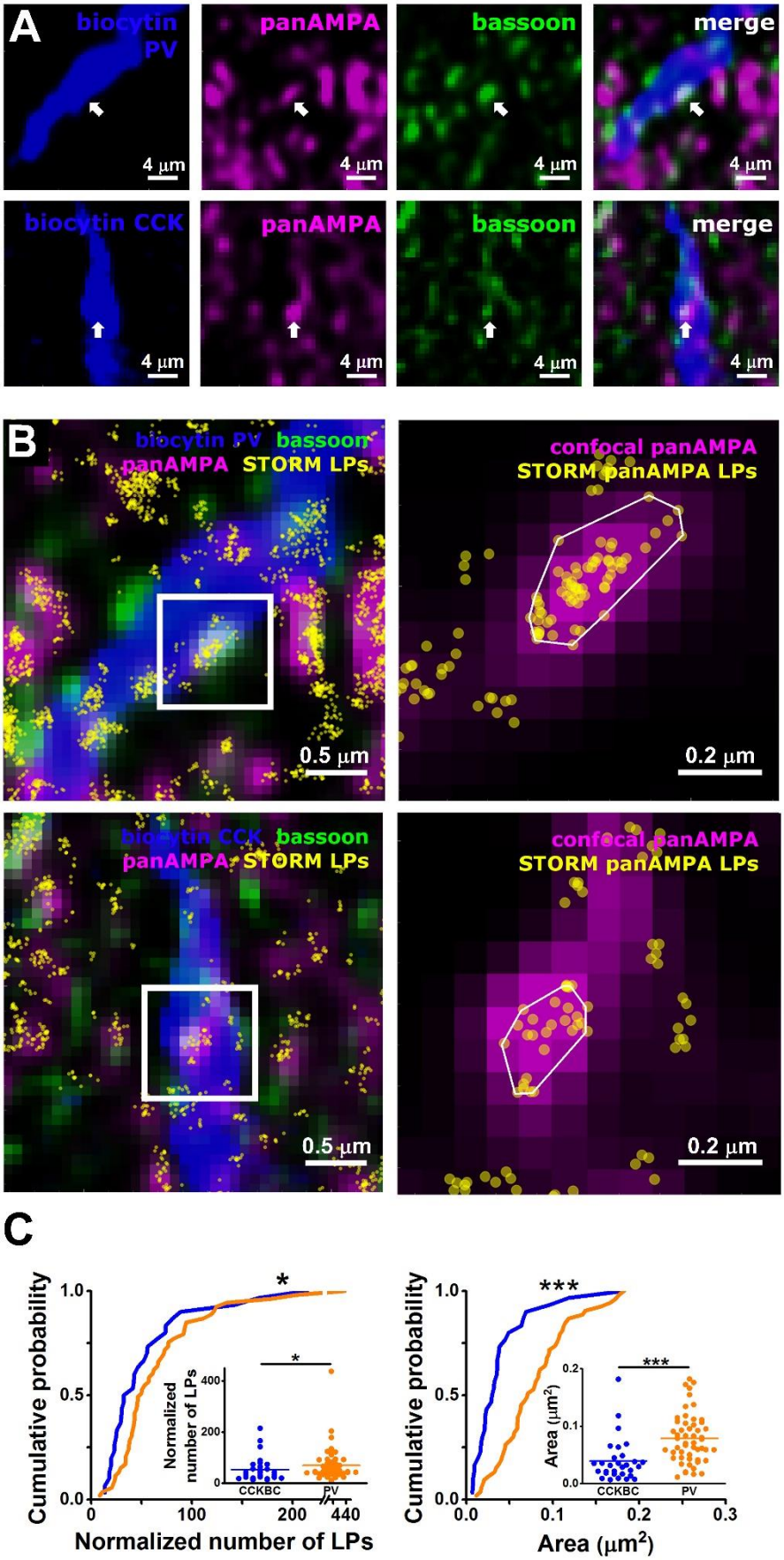
A
biocytin PV
panAMPA
bassoon
merge
biocytin CCK
4 µm
B
biocytin PV bassoon panAMPA STORM LPs
confocal panAMPA STORM panAMPA LPs
biocytin CCK bassoon panAMPA STORM LPs
0.5 µm
0.2 µm
C
Cumulative probability
Normalized number of LPs
Area (µm²)
CCKBC
PV
*
***

Figure 22. ***Excitatory inputs of the two BC types are distinct both in the size of synapses and in their AMPA receptor content.*** *(**A**) Examples of deconvolved confocal images showing bassoon-apposing puncta immunostained for AMPA receptors in a dendritic portion of a PVBC (arrows, upper panels) and a CCKBC (arrows, lower panels). (**B**) Left, the same dendritic fragments shown in (**A**) with the superimposed STORM images obtained for AMPA receptor staining (yellow), aligned and filtered using VividSTORM. Right, higher magnification of representative puncta depicting AMPA receptors along the IN dendrites, showing the deconvolved confocal image aligned with the STORM image. Each yellow sphere corresponds to a LP, while the white lines delineate the 2D convex hull area based on the AMPA LP clusters. (**C**) Cumulative probability distributions of the normalized number of LPs (left) and 2D convex hull area (right) obtained in CCKBCs (n = 30 puncta, blue) and PV-expressing INs (n = 53 puncta, orange). AMPA receptor clusters on CCKBC dendrites are smaller and contain lower number of LPs than those observed on (PV)-immunoreactive dendrites. Each data point in insets represents a cluster, and lines indicate means. Kolmogorov-Smirnov test, *p < 0.05, ***p < 0.001; (Insets) Mann-Whitney U test, *p < 0.05, ***p < 0.001*

4.3 Two parallel BC networks in the BA

4.3.1 The two different BC types avoid innervating each other, but both target AACs

To understand the information processing properties of the microcircuits formed by PNs and PTIs, it is also necessary to reveal the connections between these GABAergic cell types. Therefore, in the final set of experiments, the connectivity among INs expressing PV or CCK was examined. First, using immunocytochemistry, we investigated the anatomical substrate for the connectivity among INs in perfusion-fixed tissue samples. We noticed that boutons expressing CB1, used as a marker of axon terminals of CCKBCs (Katona et al., 2001; Vereczki et al., 2016), often contacted the somata of CCKBCs, while PV-containing boutons often apposed PV-immunolabeled somata. In both cases gephyrin (Sassoe-Pognetto et al., 1999), an anchoring protein of $GABA_A$ receptors was present at the boutons facing the soma,

implying that both PVBCs and CCKBCs formed synaptic contacts with other INs of their own kind (**Fig. 23A**). In sharp contrast, we found that CB1-containing terminals avoided PVBC somata, and vice versa, CCKBCs cell bodies were not contacted by PV-immunolabeled terminals. In some cases, we could notice CB1- and PV-expressing varicosities in close vicinity to PV- and CCK-containing BC somata, respectively. However, gephyrin puncta were characteristically not present between these immunostained profiles, but were instead found on the opposite side of the boutons, implying that the connections were established on unlabeled neighboring structures (**Fig. 23A**). These data suggested that the two BC types might not innervate each other. In contrast, the somata of AACs received synaptic inputs from both CB1- and PV-containing boutons as indicated by the presence of gephyrin labeling (**Fig. 23A**). Quantification showed that CCKBCs and PVBCs did not innervate each other, but they targeted other BCs of the same type as well as AACs (**Fig. 23B**; Number of inputs/100 μm^2: CB1 on PVBC: 0.06 ± 0.03; CB1 on AAC: 0.81 ± 0.21; CB1 on CCKBC: 1.79 ± 0.16; Kruskal-Wallis ANOVA, $p < 0.001$; PVBC versus AAC $p < 0.001$, PVBC versus CCKBC $p < 0.001$, AAC versus CCKBC $p = 0.002$, Mann-Whitney U test; PV on PVBC: 1.25 ± 0.19; PV on AAC: 1.38 ± 0.33; PV on CCKBC: 0.08 ± 0.03, Kruskal-Wallis ANOVA, $p < 0.001$, PVBC versus AAC $p = 0.36$, PVBC versus CCKBC $p < 0.001$, AAC versus CCKBC $p < 0.001$, Mann-Whitney U test).

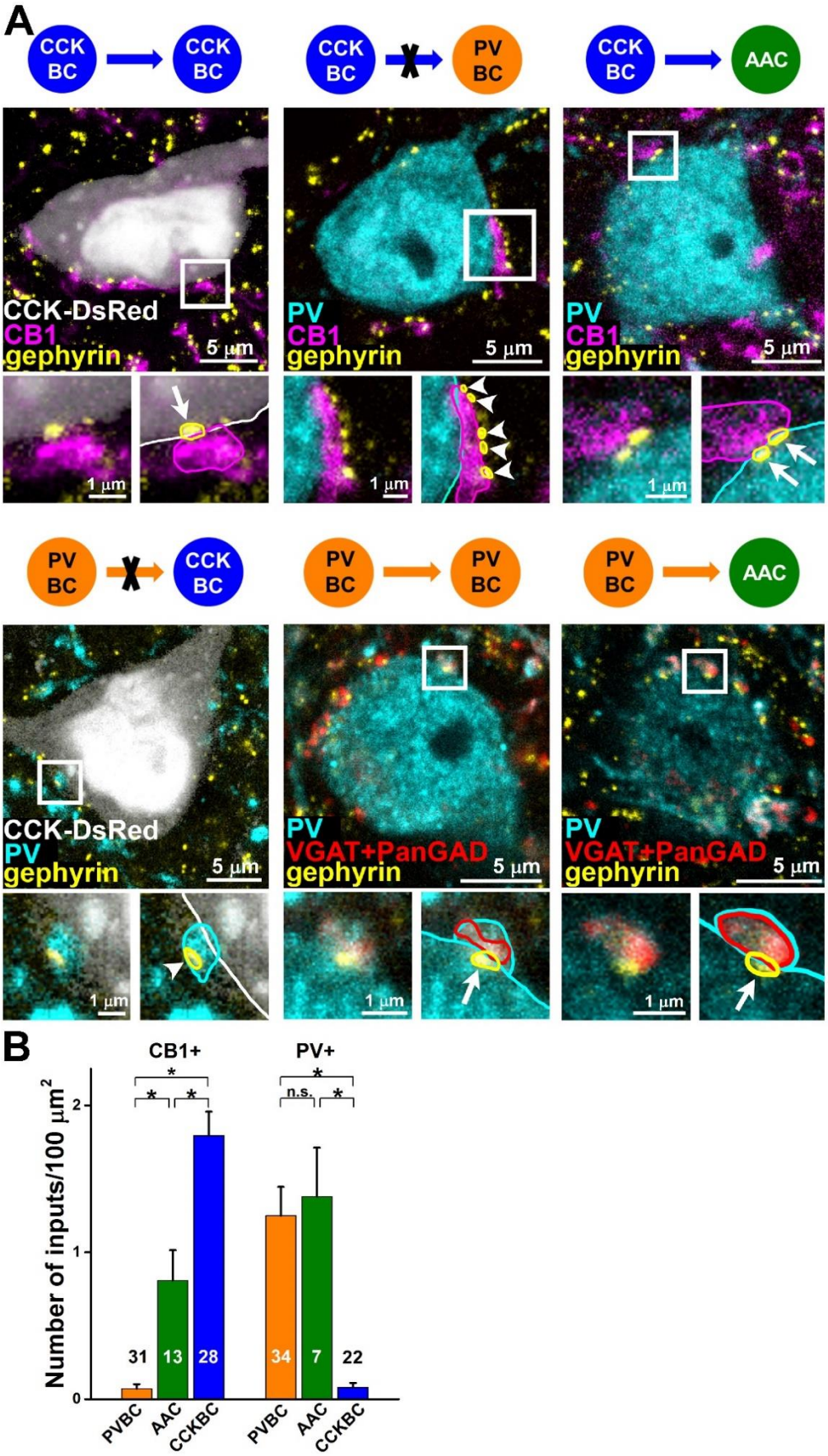
A
CCK BC
CCK BC
CCK BC
PV BC
CCK BC
AAC
CCK-DsRed
CB1
gephyrin
5 µm
1 µm
PV
CB1
gephyrin
5 µm
1 µm
PV
CB1
gephyrin
5 µm
1 µm
PV BC
CCK BC
PV BC
PV BC
PV BC
AAC
CCK-DsRed
PV
gephyrin
5 µm
1 µm
PV
VGAT+PanGAD
gephyrin
5 µm
1 µm
PV
VGAT+PanGAD
gephyrin
5 µm
1 µm
B
CB1+
PV+
Number of inputs/100 µm²
0
1
2
*
*
*
*
n.s.
*
31
13
28
34
7
22
PVBC
AAC
CCKBC
PVBC
AAC
CCKBC

Figure 23. ***CCKBCs and PVBCs avoid innervating each other but establish contacts on AACs.*** *(**A**) Quantification of somatic CB1- and PV-expressing inhibitory inputs (arrows) onto CCKBCs, PVBCs, and AACs using fluorescent immunostainings against gephyrin, CB1, PV, and VGAT/PanGAD. Axon terminals contacting the IN soma and other structures are labeled with arrows and arrowheads, respectively. Delineation of the cell bodies, terminals, and gephyrin puncta are shown for clarity. (**B**) Density of CB1- and PV-immunostained terminals contacting the different types of PTIs, labels on columns show the number of examined somata in each group. Mean ± SEM.*

4.3.2 Functional connectivity among PTIs

To confirm these unexpected results, we performed paired recordings between INs in slice preparations. We found monosynaptic connections between CCKBCs and a unidirectional connectivity from CCKBCs onto AACs. No monosynaptic connection could be detected between CCKBCs and PVBCs, whereas we observed with high likelihood connectivity among PVBCs. In addition, we found that PVBCs innervated AACs, but not CCKBCs (**Fig. 24A-F**). These in vitro results support our morphological data, confirming that PVBCs and CCKBCs do not innervate each other, but form two independent, parallel GABAergic circuits (**Fig. 24A-F**). This active avoidance of cross-connectivity between the two BC types is strengthened by the fact that they both still innervated the intermingled population of AACs expressing PV (**Fig. 24E and F**). Interestingly, the amplitude of uIPSCs in response to the first APs in each train was similar irrespective of the nature of the pre- or postsynaptic INs (**Fig. 24G**; 1st IPSC amplitude: CCKBC-CCKBC: 18.8 ± 5.5 pA, n = 11; CCKBC-AAC: 30.8 ± 18.3 pA, n = 9; PVBC-PVBC: 32.2 ± 9.0 pA, n = 6; PVBC-AAC: 21.1 ± 4.5 pA, n = 6, Kruskal-Wallis ANOVA p = 0.2). A marked difference, however, was seen in the short-term dynamics of synaptic transmission, the output synapses of CCKBCs and PVBCs showed strong facilitation and modest depression, respectively (**Fig. 24H**; *IPSC10/IPSC1: CCKBC-CCKBC: 5.72 ± 1.91, n = 7; CCKBC-AAC: 2.87 ± 0.52, n = 7; PVBC-PVBC: 0.48 ± 0.05, n = 6; PVBC-AAC: 0.53 ± 0.08, n = 4. Kruskal-Wallis ANOVA, p < 0.001*).

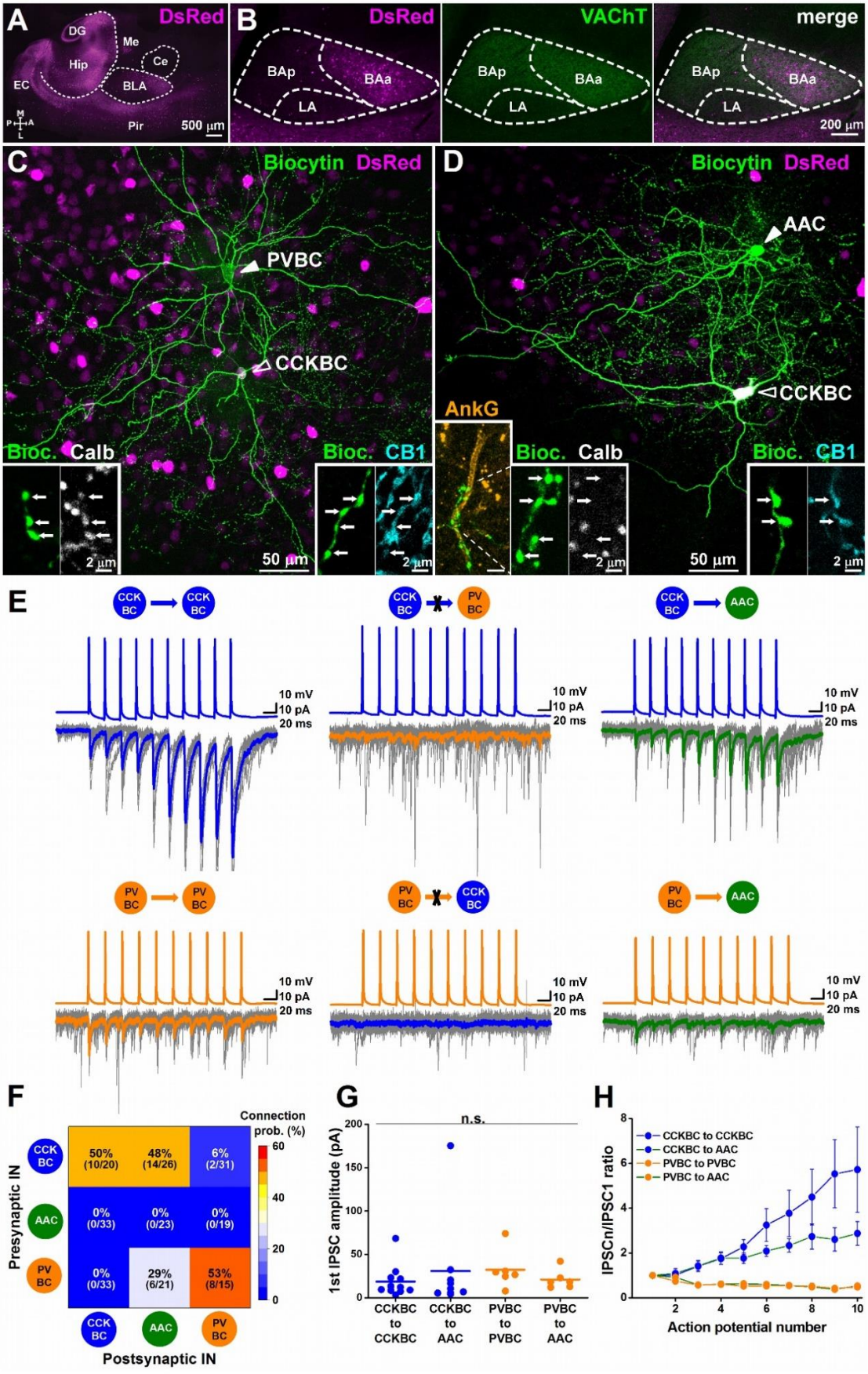
A
DsRed
DG
Me
Hip
Ce
EC
BLA
Pir
500 µm
B
DsRed
BAp
BAa
LA
VAChT
merge
200 µm
C
Biocytin DsRed
PVBC
CCKBC
Bioc. Calb
Bioc. CB1
2 µm
50 µm
D
Biocytin DsRed
AAC
CCKBC
AnkG
E
CCK BC → CCK BC
CCK BC → PV BC
CCK BC → AAC
PV BC → PV BC
PV BC → CCK BC
PV BC → AAC
10 mV
10 pA
20 ms
F
Connection prob. (%)
Presynaptic IN
Postsynaptic IN
50% (10/20)
48% (14/26)
6% (2/31)
0% (0/33)
0% (0/23)
0% (0/19)
0% (0/33)
29% (6/21)
53% (8/15)
G
n.s.
1st IPSC amplitude (pA)
CCKBC to CCKBC
CCKBC to AAC
PVBC to PVBC
PVBC to AAC
H
IPSCn/IPSC1 ratio
Action potential number

Figure 24. ***CCKBCs and PVBCs form two parallel inhibitory circuits, but both innervate AACs.*** *(**A**) Horizontal section taken from the amygdala region of a transgenic mouse expressing CCK-DsRed. BLA, basolateral amygdala complex; EC, entorhinal cortex; Hip, hippocampus; DG, dentate gyrus; Me, medial amygdala; Ce, central amygdala; Pir, piriform cortex. (**B**) DsRed expression and cholinergic fibers visualized by immunostaining against the VAChT parcel out the BLA complex into three parts: the anterior part of the basal amygdala (BAa) contains a pronounced DsRed signal and strong VAChT immunoreactivity, the posterior part of the BA (BAp) is characterized by low and high levels of DsRed and VAChT expression, respectively, and the LA has low levels of both signals. (**C**) Maximum z intensity projection image of a PVBC and a CCKBC recorded in the BAa of a PV-eGFP x CCK-DsRed double transgenic mouse. The soma of the PVBC showed eGFP, but not DsRed signal (solid arrowhead), and its boutons were immunostained for CB (Calb, bottom left panels) that typifies PVBCs. The axon terminals of the CCKBC, which soma contained DsRed but not eGFP signal (open arrowhead), were immunoreactive for CB1 (bottom right panels). (**D**) Maximum z intensity projection image of an AAC and a CCKBC recorded simultaneously in the BAa. The axon collaterals of the AAC, which soma contained eGFP but not DsRed signal (solid arrowhead), formed close apposition with the AISs visualized by immunostaining against ankyrin G (AnkG) and lacked Calb (bottom left panels), typical for AACs. The boutons of the CCKBC (open arrowhead), which soma showed DsRed but not eGFP signal, expressed CB1 (bottom right panels), characteristic for CCKBCs. (**E**) Representative traces from whole-cell paired recordings from post hoc identified different IN-IN pairs. Ten superimposed consecutive traces are in gray, averages are in bold. (**F**) Connection probability matrix of IN-IN synaptic coupling was obtained by paired recordings. (**G**) Comparison of the amplitude of IPSCs. Each data point on the plot is an average obtained from a pair recording, and lines represent mean. (**H**) Comparison of the short-term plasticity of the different types of IN-IN connections. Data are presented as mean ± SEM.*

Finally, we also tested the presence of electrical coupling between the perisomatic inhibitory cell types, a feature that characterizes the IN networks both in

the hippocampus and neocortex (Galarreta and Hestrin, 1999; Tamas et al., 2000). We found that, as in other cortical regions, INs of the same type were often coupled via gap junctions (**Fig. 25A-C**). Notably, a high probability of electrical coupling was observed between AACs that are not coupled via synaptic junctions (**Fig. 25B and C**; Electrical coupling efficacy: 1.05 ± 0.18%, n = 10; Electrical coupling probability: 8/11, 73%).

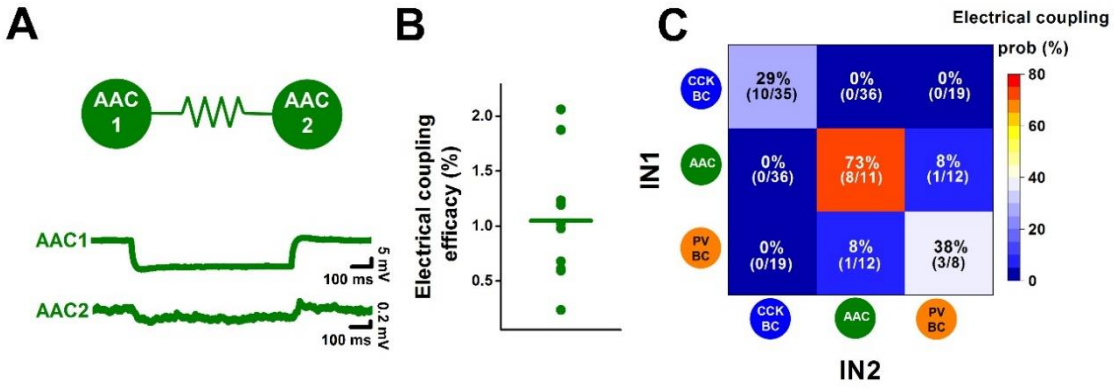

Figure 25. ***Electrical coupling between PTIs in the BA.*** *(**A**) Diagram and representative traces of two electrically coupled AACs. Representative traces showing the voltage response to a -100 pA hyperpolarizing current injected in AAC1, and monitored simultaneously in AAC1 and AAC2. (**B**) Electrical coupling efficacy between AAC-AAC, calculated as the % of voltage change observed in the AAC2 compared to the AAC1 in which the current was injected. Line represents mean. (**C**) Electrical coupling probability matrix of different IN-IN pairs obtained by dual recordings. In parentheses, the number of coupled cells/ the number of dual recordings tested for electrical coupling are shown.*

4.3.3 Circuit model for connectivity matrix formed by PTIs and PNs in the BA

Our data revealed the intricate connectivity among PTIs and PNs in the BA and furthermore allowed us to create a perisomatic inhibitory network model. As in other cortical regions, CCKBCs and PVBCs innervate the soma and proximal dendrites and AACs target the AIS of amygdalar PNs, which was confirmed by neuroanatomical and

electrophysiological approaches (present study, Veres et al., 2014 Vereczki et al., 2016, Veres et al., 2017, Rovira et al., 2017)(**Fig. 26A**). Moreover, additionally to the strategically positioned innervation of PNs, PTIs provide similarly efficient inhibitory input onto PNs that is able to profoundly control their spiking. Besides of the PN innervation, CCKBCs and PVBCs also target their own kind and surprisingly AACs, but extremely rarely each other.

Considering the fact that there are three different types of PTIs in the BA networks with similar inhibitory potential, a question emerges why the BA (and the other cortical) circuit needs to have these cell types? We made an attempt in this study to approximate this question by investigating the local feedback excitatory drive received by the different PTIs. We measured large excitatory events and multiple-terminal innervation that originated from single PNs in both PVBCs and AACs (**Fig. 26B**). By contrast, CCKBCs received only a weak excitation from a smaller number of PNs (**Fig. 26B**). These results together outline the wiring principles of the BA PTI networks, which, regarding the cortical origin of the BA can be a general rule for other cortical structures.

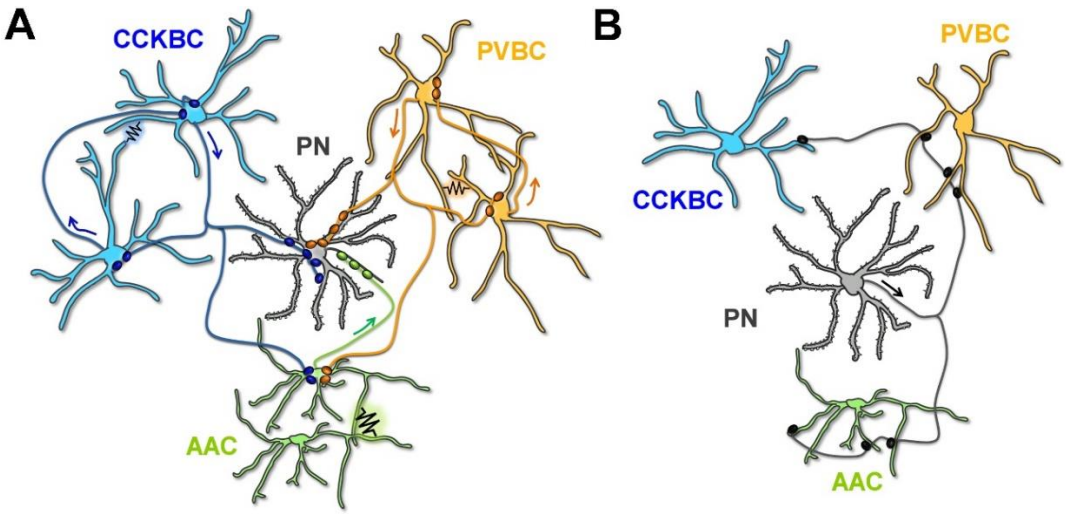

Figure 26. ***The wiring diagram of the three PTIs and PNs in the BA.*** *(**A**) Connectivity among the distinct IN types and from INs to the PNs. Both synaptic connections and gap junctions are indicated. Arrows show the direction of AP spread along the axons. (**B**) Connectivity from the PNs to INs.*

5 DISCUSSION

We examined the intrinsic features of the three different types of the PTIs as well as their output properties in details. Our findings are the followings: the membrane properties of the PTIs, such as input resistance, spike rate, accommodation and AHP are significantly different. Moreover, the kinetic properties of the synaptic transmission from PTIs onto PNs including the peak amplitude, potency, failure rate, rise time 10-90 %, decay tau and latency showed some differences. Furthermore, we found cell-type specific short-term dynamics and degree of asynchronous release in response to AP trains. Analyses of the single-cell properties of PTIs showed that PV-expressing INs display high frequency non-accommodating firing with narrow spikes and fast AHP as well as fast membrane time constant, while CCKBCs have an accommodating regular firing with wide AP half-width and slow AHP and membrane time constant, which data are in line with those reported in the amygdala and other cortical regions (Cea-del Rio et al., 2011; Daw et al., 2009; Galarreta et al., 2008; Galarreta and Hestrin, 1999; Glickfeld and Scanziani, 2006; Jasnow et al., 2009; Rainnie et al., 1993; Rainnie et al., 2006; Szabo et al., 2010; Washburn and Moises, 1992; Woodruff and Sah, 2007a). Comparison of the discharging features of PVBCs and AACs revealed in vivo relevant differences between the two PV-expressing interneurons. It is already known that PV-expressing cells are capable to discharge at high frequencies both in vitro and in vivo, often firing doublets of spikes. Interestingly, however, PVBCs and AACs showed distinct maximum firing rate (Bienvenu et al., 2012; Klausberger et al., 2003; Massi et al., 2012; Varga et al., 2014; Viney et al., 2013), and importantly, the firing rate of AACs can reach even 300-350 Hz, while PVBCs have a maximum discharging rate around 200 Hz, when they fire doublets. Since it is very difficult to distinguish PVBCs and AACs during in vitro and in vivo recordings, the difference in their maximum firing rate can be helpful to identify them during recordings by analyzing the interspike interval between spike doublets.

Although the properties of the synaptic transmission from PV-expressing cells onto PNs have already been studied in the BA, PVBCs and AACs were not separated (Woodruff and Sah, 2007b). Thus, our data presented here are the first to report the cell type specific comparison of PVBCs and AACs in the BA. IPSCs originating from the

three types of PTIs can be characterized by fast kinetics, which is strongly indicative for perisomatic innervation as it was found also in the hippocampus (Szabo et al., 2010). In contrast to the kinetics, the short-term dynamics were substantially different and showed a frequency dependency among PTIs, which may suggest different cell type specific roles in the temporal regulation of PN activity (Klausberger and Somogyi, 2008; Varga et al., 2014). As it has been previously found in other cortical regions, in the BA we also found asynchronous release, which was frequency dependent and was most profound for CCKBC output synapses (Daw et al., 2009; Hefft and Jonas, 2005; Szabo et al., 2010). The mechanisms underlying the asynchronous release is supposed to be in relation with specific voltage gated Ca^{2+} channel composition and/or Ca^{2+} sensors in the terminals. PV-expressing INs express P/Q type channels in their active zones, which are located very close to the Ca^{2+} sensors, thereby facilitating the reliable and temporally precise release. By contrast, CCKBCs use N-type Ca^{2+} channels, which are loosely coupled to the sensors thereby allowing a slower build-up of the intraterminal calcium and consequently leading to a more prolonged release (Bucurenciu et al., 2008; Hefft and Jonas, 2005).

Previous studies investigating the postsynaptic current characteristics generated by the output synapses of BCs in hippocampal slices have suggested that PVBCs and CCKBCs gave rise to synaptic inhibition with different properties (Daw et al., 2009; Glickfeld and Scanziani, 2006; Hefft and Jonas, 2005; Szabo et al., 2010). In contrast, our study in the BA shows that the magnitude of the synaptic events originated from the two BC types is rather similar. The reason for the discrepancy could be twofold. First, in distinct cortical structures the properties of synaptic transmission originating from the two BC types might be different. Second, a technical issue might also contribute to the discrepancy. To study synaptic inhibition, experiments are routinely conducted by an intrapipette solution containing high Cl^- concentration in postsynaptic neurons, while in our study we used a low concentration of Cl^- similar to physiological conditions (Veres et al., 2014). As the intracellular Cl^- concentration may alter some of the parameters of $GABA_A$ receptor-mediated synaptic transmission (Houston et al., 2009), the results obtained with distinct Cl^- concentrations even at the same synaptic junctions can differ, making it hard to compare the synaptic properties, unless the recording circumstances are as identical as possible. Motivated by this potential

concern, we compared the inhibitory efficacy of the three perisomatic inhibitory cells using the same conditions. In spite of the differences observed in some of the features in synaptic transmission (data presented in this thesis and (Veres et al., 2014), the three cell types inhibited PN spiking with equal efficacy. Thus, our results clearly show for the first time that the perisomatic region of PNs in the BA receives three distinct sources of synaptic inhibition and the potency to control the PN spiking by each IN group is similar.

Earlier anatomical studies obtained in the hippocampus (Gulyas et al., 1999; Matyas et al., 2004) showed that the density of excitatory synapses on the dendrites of PV-expressing INs is significantly higher than on the dendrites of CCKBCs. These data implied that these two GABAergic cell types could be distinctly excited by PN activities, a hypothesis that has been strengthened by slice physiology (Glickfeld and Scanziani, 2006). Our data confirmed and substantially extended these results with functional implications in the BA by showing that i) lower activity levels of PNs are sufficient to excite PVBCs and AACs than CCKBCs, ii) the density of VGluT1-expressing glutamatergic inputs is significantly higher on the dendrites of PVBCs than of CCKBCs and, in parallel, the mEPSC frequency in PVBCs is considerably higher than in CCKBCs , iii) uEPSCs originating from single PNs are larger and faster in PVBCs and AACs than in CCKBCs, iv) PVBCs are preferentially innervated by neighboring PNs, while CCKBCs receive excitation from PNs with lower probability but in a distance-independent manner, and v) quantal excitatory events in CCKBCs and AMPA receptor content at individual synapses along their dendrites show a surprisingly uniform distribution, whereas a high variability characterizes both mEPSC amplitude distributions and AMPA receptor content at single clusters in PVBCs. These latter results are specifically interesting, because they suggest that the excitatory inputs onto CCKBCs from PNs may have little potency to undergo plastic changes in comparison to those excitatory inputs received by PVBCs. Indeed, LTP or LTD at the excitatory synapses of hippocampal CCKBCs have not been reported so far (Nissen et al., 2010; Szabo et al., 2012). However, these studies as well as others found long-term changes in excitatory transmission in PVBCs (Lu et al., 2007; Peterfi et al., 2012). Thus, a network of CCKBCs, due to their non-plastic excitatory inputs, may be excited

independently of learning-induced changes, while plastic changes at the excitatory inputs of PVBCs might help memory formation in cortical circuits.

Our results allowed us to construct a detailed wiring diagram of PNs and PTIs in the BA. The uncovered functional organization in this cortical microcircuit indicates that these three types of GABAergic INs control PN spiking with equal efficiency and are wired in a highly cell-type specific manner. Recently, it has been also shown in the hippocampus that PTIs tend to give inhibitory terminals onto other PTIs, mostly targeting their own kind (Kohus et al., 2016). In the hippocampus, it has been also shown that CCK-expressing INs rarely target some PV-expressing cells, although the identity of these PV-expressing INs, i.e. whether they were PVBCs and/or AACs, has not been determined. In line with our data, PV-expressing neurons in the hippocampus did not innervate CCK-expressing INs (Daw et al., 2009). These results from the hippocampus are in line with our findings in the BA, together with the presence of electrical coupling among PTIs from the same group. As found in other cortical structures (Galarreta and Hestrin, 2002; Karnani et al., 2016; Kohus et al., 2016; Pfeffer et al., 2013; Tamas et al., 1998), BCs in the BA are mutually interconnected within their own category. Our novel findings, that the two BC types form independent inhibitory networks whose feedback recruitment is highly dependent on the local PN activity levels, may indicate distinct, largely independent roles for these GABAergic cell types. Furthermore, the unidirectional connectivity between the BCs and AACs may explain the temporal ordering of IN firing during synchronous network activities and sensory processing (Bienvenu et al., 2012; Klausberger et al., 2002; Varga et al., 2014; Zhu et al., 2004).

Our conclusion that CCKBCs and PVBCs form two parallel networks is based on the results obtained by two independent approaches. As CCKBCs and PVBCs receive distinct excitation from PNs (this thesis, (Glickfeld et al., 2009)), differ in subcortical inputs and are endowed with specific sets of receptors (Freund and Katona, 2007), the two GABAergic networks should function largely separately, probably fulfilling distinct roles in neural operation (Freund, 2003). This hypothesis is supported by in vivo data showing that the two BC types fire distinctly during oscillatory activities in the hippocampus (Klausberger et al., 2005), providing temporarily segregated inhibition on the same membrane domain of PNs. Surprisingly, we found that AACs

receive inputs from both BC types with high probability and magnitude. Thus, our wiring diagram suggests that this third perisomatic inhibitory cell type can predominantly, if not exclusively spike when the two BC types are silent. Indeed, hippocampal AACs have been found to be silent during sharp wave-ripple activities when the firing rate of PVBCs is maximal, and in a different phase of theta rhythms in comparison to BCs (Klausberger and Somogyi, 2008; Varga et al., 2014). Interestingly, AAC firing precedes firing of other IN types upon sensory stimuli (Bienvenu et al., 2012; Massi et al., 2012; Zhu et al., 2004). These results imply a critical role for AACs at the first stages of sensory processing (Wang et al., 2016), likely promoting the spiking activity of PNs by de-inactivating the voltage-gated Na^+ channels located at the highest density along the AISs (Debanne et al., 2011; Lorincz and Nusser, 2010; Veres et al., 2014).

The sole communication between AACs can be achieved via electrical coupling, since these GABAergic INs do not form synaptic contacts with each other (present study, (Freund et al., 1983)). This type of network structures is not unique for AACs in the CNS, but has been observed e.g. among cerebellar Golgi cells, whose synchronous activity can be promoted or reduced via gap junctions depending on the input patterns (van Welie et al., 2016; Vervaeke et al., 2010). Thus, synaptic inhibition arriving on the AISs may help the synchronization or de-synchronization of the activity in PN ensembles as a function of the gap junction strength among AACs, which might be a subject of plasticity (Mathy et al., 2014).

6 CONCLUSION

The generality of our present findings is supported by data obtained in the hippocampus, in which the cross-connectivity between the two BC types is low, if any (Kohus et al., 2016), a significantly lower number of excitatory inputs is received by CCKBCs in comparison to PVBCs (Gulyas et al., 1999; Matyas et al., 2004), and PVBCs can be activated more reliably than CCKBCs (Glickfeld and Scanziani, 2006), similarly to those observed in the BA. Although comparable studies have not been performed in neocortical areas, the presence of analogous cell types and the connectivity patterns (Jiang et al., 2015) as well as the documented distance dependence in the connection probability between pyramidal cells and PVBCs (Holmgren et al., 2003; Pala and Petersen, 2015; Perin et al., 2011) imply that microcircuits in the cerebral cortex may be organized along similar principles as in the BA and hippocampus.

In summary, as the same IN types are present in all cortical structures studied to date (Harris and Shepherd, 2015; Markram et al., 2004), the circuit motifs and synaptic organizing principles revealed here in the BA offer a framework for understanding the temporal dynamics of the three IN types providing equally potent perisomatic inhibition during oscillatory activities and sensory processing.

7 SUMMARY

GABAergic basket cells (BCs) and axo-axonic cells (AACs) targeting the perisomatic region of cortical principal neurons (PNs) are in a key position to effectively control the firing of their postsynaptic partners. In this study, we investigated the anatomical and functional connectivity among perisomatic-targeting inhibitory neurons (PTIs) and PNs in the basal nucleus of the amygdala (BA), which is known to be the site of emotional memory formation.

To reveal the wiring principles of PTIs and PNs, we combined optogenetic, electrophysiological and neuroanatomical approaches. Electrophysiological recordings in PTIs showed that the parvalbumin expressing basket cells (PVBCs), AACs and cholecystokinin/type 1 cannabinoid receptor (CCKBC) expressing basket cells are substantially different in many single-cell electrophysiological features as well as in their synaptic output dynamics. Paired recordings of interneuron (IN)-PN pairs indicated that, although the three types of PTI differ in many aspects, they inhibit PNs with almost identical efficiency. These findings raised the question, why the network needs three different types of similarly potent inhibitory cells. To address this question, we sought to reveal the recruitment of the three IN types by the local PNs. Combined optogenetic stimulation and dual intracellular recordings allowed us to compare the activation threshold and determine the basic properties of the excitatory inputs of the three IN types. Our results indicated that PNs in the BA preferentially target PVBCs and AACs. They were innervated with high probability and received large and fast excitatory events compared to CCKBCs. Finally, we determined the connectivity matrix among the PTIs and PNs. Based on the results we were able to create a connectivity map, where we showed that BC types innervate their own kind and AACs, but avoid innervating each other, thereby forming parallel inhibitory circuits in the BA networks.

In summary, as the same IN types are present in all cortical structures, the circuit motifs and synaptic organizing principles revealed here in the BA offer a framework for understanding the temporal dynamics of the three IN types during oscillatory activities and sensory processing.

8 ÖSSZEFOGLALÁS

Az idegsejtek periszomatikus régióját beidegző GABAerg kosár és axo-axonikus sejtek pozíciójuknál fogva rendkívül hatékonyan képesek szabályozni más idegsejtek működését. Jelen értekezésben megvizsgáltuk ezen sejttípusok anatómiai és funkcionális kapcsolatrendszerét a bazális amigdala magban, mely köztudottan fontos szerepet játszik az emocionális tanulási folyamatokban.

Kísérleteink során optogenetikai, elektrofiziológiai és anatómiai módszereket kombináltunk annak érdekében, hogy megfejtsük a periszomatikus régiót innerváló gátlósejt típusok és a principális sejtek kapcsolatrendszerének vezérelveit. A különböző típusú gátlósejtekből történt mérések lényeges fiziológiás eltéréseket mutattak a parvalbumint termelő kosár és axo-axonikus sejtek, valamint a kolecisztokinint és 1-es típusú kannabinoid receptort kifejező kosársejtek között. Az interneuronok és principális sejtek közötti páros elvezetések azt mutatták, hogy a különböző gátlósejt típusok szinaptikus kimeneti tulajdonságai eltérnek, azonban mindhárom csoport közel ugyanolyan hatékonyan képes gátolni a serkentő sejtek tüzelését. Felmerül tehát a kérdés, hogy mi szüksége van a hálózatnak három különböző, de hasonlóan potens gátlósejtre. A kérdést megválaszolandó, megvizsgáltuk a gátlósejtekre érkező serkentést. Méréseink alapján a parvalbumint tartalmazó kosár és axo-axonikus sejtek preferáltan nagy serkentést kapnak, ezzel szemben a kolecisztokinines kosársejteket nagyságrendekkel gyengébben idegzik be és serkentik az amigdaláris fősejtek. Végül feltártuk a dolgozatban szereplő sejttípusok közötti kapcsolatrendszert, mely alapján létrehoztunk egy hálózati modellt. A modell szerint a két különböző típusú kosársejt a fősejteken kívül beidegzi a saját csoportjába tartozó kosársejteket valamint az axo-axonikus sejteket, viszont elkerüli a kapcsolatot a másik fajta kosársejttel, ezáltal létrehozva két egymástól független, párhuzamos gátlókört a bazális amigdalában.

Eredményeinket összegezve elmondhatjuk, hogy az általunk elsőként leírt kapcsolati háló amellett, hogy segíthet megérteni a periszomatikus gátlósejtek szerepét az agy működésében, egy általános érvényű hálózati szerveződés alapjaként is szolgálhat, mivel ugyanezek a sejttípusok a többi kérgi régióban szintén szintén fellelhetők.

9 REFERENCES

Acsady, L., Gorcs, T.J., and Freund, T.F. (1996). Different populations of vasoactive intestinal polypeptide-immunoreactive interneurons are specialized to control pyramidal cells or interneurons in the hippocampus. Neuroscience *73*, 317-334.

Aggleton, J.P. (1993). The contribution of the amygdala to normal and abnormal emotional states. Trends Neurosci *16*, 328-333.

Amano, T., Duvarci, S., Popa, D., and Pare, D. (2011). The fear circuit revisited: contributions of the basal amygdala nuclei to conditioned fear. J Neurosci *31*, 15481-15489.

Amano, T., Unal, C.T., and Pare, D. (2010). Synaptic correlates of fear extinction in the amygdala. Nat Neurosci *13*, 489-494.

Anglada-Figueroa, D., and Quirk, G.J. (2005). Lesions of the basal amygdala block expression of conditioned fear but not extinction. J Neurosci *25*, 9680-9685.

Aponte, Y., Bischofberger, J., and Jonas, P. (2008). Efficient Ca2+ buffering in fast-spiking basket cells of rat hippocampus. J Physiol *586*, 2061-2075.

Armony, J.L., Servan-Schreiber, D., Cohen, J.D., and LeDoux, J.E. (1995). An anatomically constrained neural network model of fear conditioning. Behav Neurosci *109*, 246-257.

Ascoli, G.A., Alonso-Nanclares, L., Anderson, S.A., Barrionuevo, G., Benavides-Piccione, R., Burkhalter, A., Buzsaki, G., Cauli, B., Defelipe, J., Fairen, A., Feldmeyer, D., Fishell, G., Fregnac, Y., Freund, T.F., Gardner, D., Gardner, E.P., Goldberg, J.H., Helmstaedter, M., Hestrin, S., Karube, F., Kisvarday, Z.F., Lambolez, B., Lewis, D.A., Marin, O., Markram, H., Munoz, A., Packer, A., Petersen, C.C., Rockland, K.S., Rossier, J., Rudy, B., Somogyi, P., Staiger, J.F., Tamas, G., Thomson, A.M., Toledo-Rodriguez, M., Wang, Y., West, D.C., and Yuste, R. (2008). Petilla terminology: nomenclature of features of GABAergic interneurons of the cerebral cortex. Nature reviews Neuroscience *9*, 557-568.

Baimbridge, K.G., Celio, M.R., and Rogers, J.H. (1992). Calcium-binding proteins in the nervous system. Trends Neurosci *15*, 303-308.

Barna, L., Dudok, B., Miczan, V., Horvath, A., Laszlo, Z.I., and Katona, I. (2016). Correlated confocal and super-resolution imaging by VividSTORM. Nat Protoc *11*, 163-183.

Bartos, M., and Elgueta, C. (2012). Functional characteristics of parvalbumin- and cholecystokinin-expressing basket cells. J Physiol *590*, 669-681.

Basu, J., Srinivas, K.V., Cheung, S.K., Taniguchi, H., Huang, Z.J., and Siegelbaum, S.A. (2013). A cortico-hippocampal learning rule shapes inhibitory microcircuit activity to enhance hippocampal information flow. Neuron *79*, 1208-1221.

Ben-Ari, Y., Zigmond, R.E., Shute, C.C., and Lewis, P.R. (1977). Regional distribution of choline acetyltransferase and acetylcholinesterase within the amygdaloid complex and stria terminalis system. Brain Res *120*, 435-444.

Beyeler, A. (2016). Parsing reward from aversion. Science *354*, 558.

Bezaire, M.J., and Soltesz, I. (2013). Quantitative assessment of CA1 local circuits: Knowledge base for interneuron-pyramidal cell connectivity. Hippocampus *23*, 751-785.

Bienvenu, T.C., Busti, D., Magill, P.J., Ferraguti, F., and Capogna, M. (2012). Cell-type-specific recruitment of amygdala interneurons to hippocampal theta rhythm and noxious stimuli in vivo. Neuron *74*, 1059-1074.

Bienvenu, T.C., Busti, D., Micklem, B.R., Mansouri, M., Magill, P.J., Ferraguti, F., and Capogna, M. (2015). Large intercalated neurons of amygdala relay noxious sensory information. J Neurosci *35*, 2044-2057.

Biro, A.A., Holderith, N.B., and Nusser, Z. (2006). Release probability-dependent scaling of the postsynaptic responses at single hippocampal GABAergic synapses. J Neurosci *26*, 12487-12496.

Bissiere, S., Humeau, Y., and Luthi, A. (2003). Dopamine gates LTP induction in lateral amygdala by suppressing feedforward inhibition. Nat Neurosci *6*, 587-592.

Bocchio, M., Nabavi, S., and Capogna, M. (2017). Synaptic Plasticity, Engrams, and Network Oscillations in Amygdala Circuits for Storage and Retrieval of Emotional Memories. Neuron *94*, 731-743.

Bodor, A.L., Katona, I., Nyiri, G., Mackie, K., Ledent, C., Hajos, N., and Freund, T.F. (2005). Endocannabinoid signaling in rat somatosensory cortex: laminar differences and involvement of specific interneuron types. The Journal of neuroscience : the official journal of the Society for Neuroscience *25*, 6845-6856.

Bucurenciu, I., Kulik, A., Schwaller, B., Frotscher, M., and Jonas, P. (2008). Nanodomain coupling between Ca2+ channels and Ca2+ sensors promotes fast and efficient transmitter release at a cortical GABAergic synapse. Neuron *57*, 536-545.

Buhl, E.H., and Dann, J.F. (1991). Cytoarchitecture, neuronal composition, and entorhinal afferents of the flying fox hippocampus. Hippocampus *1*, 131-152.

Buhl, E.H., Halasy, K., and Somogyi, P. (1994a). Diverse sources of hippocampal unitary inhibitory postsynaptic potentials and the number of synaptic release sites. Nature *368*, 823-828.

Buhl, E.H., Han, Z.S., Lorinczi, Z., Stezhka, V.V., Karnup, S.V., and Somogyi, P. (1994b). Physiological properties of anatomically identified axo-axonic cells in the rat hippocampus. J Neurophysiol *71*, 1289-1307.

Buzsaki, G., and Chrobak, J.J. (1995). Temporal structure in spatially organized neuronal ensembles: a role for interneuronal networks. Curr Opin Neurobiol *5*, 504-510.

Caillard, O., Moreno, H., Schwaller, B., Llano, I., Celio, M.R., and Marty, A. (2000). Role of the calcium-binding protein parvalbumin in short-term synaptic plasticity. Proc Natl Acad Sci U S A *97*, 13372-13377.

Capogna, M. (2014). GABAergic cell type diversity in the basolateral amygdala. Curr Opin Neurobiol *26*, 110-116.

Carlsen, J., and Heimer, L. (1988). The basolateral amygdaloid complex as a cortical-like structure. Brain Res *441*, 377-380.

Carlsen, J., Zaborszky, L., and Heimer, L. (1985). Cholinergic projections from the basal forebrain to the basolateral amygdaloid complex: a combined retrograde fluorescent and immunohistochemical study. J Comp Neurol *234*, 155-167.

Cassell, M.D., Gray, T.S., and Kiss, J.Z. (1986). Neuronal architecture in the rat central nucleus of the amygdala: a cytological, hodological, and immunocytochemical study. J Comp Neurol *246*, 478-499.

Cea-del Rio, C.A., Lawrence, J.J., Erdelyi, F., Szabo, G., and McBain, C.J. (2011). Cholinergic modulation amplifies the intrinsic oscillatory properties of CA1 hippocampal cholecystokinin-positive interneurons. J Physiol *589*, 609-627.

Cea-del Rio, C.A., Lawrence, J.J., Tricoire, L., Erdelyi, F., Szabo, G., and McBain, C.J. (2010). M3 muscarinic acetylcholine receptor expression confers differential cholinergic modulation to neurochemically distinct hippocampal basket cell subtypes. J Neurosci *30*, 6011-6024.

Chen, J.L., Villa, K.L., Cha, J.W., So, P.T., Kubota, Y., and Nedivi, E. (2012). Clustered dynamics of inhibitory synapses and dendritic spines in the adult neocortex. Neuron *74*, 361-373.

Citri, A., and Malenka, R.C. (2008). Synaptic plasticity: multiple forms, functions, and mechanisms. Neuropsychopharmacology *33*, 18-41.

Cobb, S.R., Buhl, E.H., Halasy, K., Paulsen, O., and Somogyi, P. (1995). Synchronization of neuronal activity in hippocampus by individual GABAergic interneurons. Nature *378*, 75-78.

Coghlan, S., Horder, J., Inkster, B., Mendez, M.A., Murphy, D.G., and Nutt, D.J. (2012). GABA system dysfunction in autism and related disorders: from synapse to symptoms. Neurosci Biobehav Rev *36*, 2044-2055.

Cope, D.W., Maccaferri, G., Marton, L.F., Roberts, J.D., Cobden, P.M., and Somogyi, P. (2002). Cholecystokinin-immunopositive basket and Schaffer collateral-associated interneurones target different domains of pyramidal cells in the CA1 area of the rat hippocampus. Neuroscience *109*, 63-80.

Cossart, R. (2014). Operational hub cells: a morpho-physiologically diverse class of GABAergic neurons united by a common function. Curr Opin Neurobiol *26*, 51-56.

David, C., Schleicher, A., Zuschratter, W., and Staiger, J.F. (2007). The innervation of parvalbumin-containing interneurons by VIP-immunopositive interneurons in the primary somatosensory cortex of the adult rat. Eur J Neurosci *25*, 2329-2340.

Davila, J.C., Olmos, L., Legaz, I., Medina, L., Guirado, S., and Real, M.A. (2008). Dynamic patterns of colocalization of calbindin, parvalbumin and GABA in

subpopulations of mouse basolateral amygdalar cells during development. J Chem Neuroanat *35*, 67-76.

Davis, M., and Shi, C. (2000). The amygdala. Curr Biol *10*, R131.

Daw, M.I., Tricoire, L., Erdelyi, F., Szabo, G., and McBain, C.J. (2009). Asynchronous transmitter release from cholecystokinin-containing inhibitory interneurons is widespread and target-cell independent. J Neurosci *29*, 11112-11122.

Debanne, D., Campanac, E., Bialowas, A., Carlier, E., and Alcaraz, G. (2011). Axon physiology. Physiol Rev *91*, 555-602.

DeFelipe, J., Lopez-Cruz, P.L., Benavides-Piccione, R., Bielza, C., Larranaga, P., Anderson, S., Burkhalter, A., Cauli, B., Fairen, A., Feldmeyer, D., Fishell, G., Fitzpatrick, D., Freund, T.F., Gonzalez-Burgos, G., Hestrin, S., Hill, S., Hof, P.R., Huang, J., Jones, E.G., Kawaguchi, Y., Kisvarday, Z., Kubota, Y., Lewis, D.A., Marin, O., Markram, H., McBain, C.J., Meyer, H.S., Monyer, H., Nelson, S.B., Rockland, K., Rossier, J., Rubenstein, J.L., Rudy, B., Scanziani, M., Shepherd, G.M., Sherwood, C.C., Staiger, J.F., Tamas, G., Thomson, A., Wang, Y., Yuste, R., and Ascoli, G.A. (2013). New insights into the classification and nomenclature of cortical GABAergic interneurons. Nat Rev Neurosci *14*, 202-216.

Doischer, D., Hosp, J.A., Yanagawa, Y., Obata, K., Jonas, P., Vida, I., and Bartos, M. (2008). Postnatal differentiation of basket cells from slow to fast signaling devices. J Neurosci *28*, 12956-12968.

Douglass, A.M., Kucukdereli, H., Ponserre, M., Markovic, M., Grundemann, J., Strobel, C., Alcala Morales, P.L., Conzelmann, K.K., Luthi, A., and Klein, R. (2017). Central amygdala circuits modulate food consumption through a positive-valence mechanism. Nat Neurosci *20*, 1384-1394.

Drake, C.T., and Milner, T.A. (2002). Mu opioid receptors are in discrete hippocampal interneuron subpopulations. Hippocampus *12*, 119-136.

Dudok, B., Barna, L., Ledri, M., Szabo, S.I., Szabadits, E., Pinter, B., Woodhams, S.G., Henstridge, C.M., Balla, G.Y., Nyilas, R., Varga, C., Lee, S.H., Matolcsi, M., Cervenak, J., Kacskovics, I., Watanabe, M., Sagheddu, C., Melis, M., Pistis, M., Soltesz, I., and Katona, I. (2015). Cell-specific STORM super-resolution imaging reveals nanoscale organization of cannabinoid signaling. Nat Neurosci *18*, 75-86.

Eggermann, E., Bucurenciu, I., Goswami, S.P., and Jonas, P. (2011). Nanodomain coupling between Ca(2)(+) channels and sensors of exocytosis at fast mammalian synapses. Nat Rev Neurosci *13*, 7-21.

Ehrlich, I., Humeau, Y., Grenier, F., Ciocchi, S., Herry, C., and Luthi, A. (2009). Amygdala inhibitory circuits and the control of fear memory. Neuron *62*, 757-771.

Evstratova, A., Chamberland, S., and Topolnik, L. (2011). Cell type-specific and activity-dependent dynamics of action potential-evoked Ca2+ signals in dendrites of hippocampal inhibitory interneurons. J Physiol *589*, 1957-1977.

Faber, E.S., Callister, R.J., and Sah, P. (2001). Morphological and electrophysiological properties of principal neurons in the rat lateral amygdala in vitro. J Neurophysiol *85*, 714-723.

Fairen, A., and Valverde, F. (1980). A specialized type of neuron in the visual cortex of cat: a Golgi and electron microscope study of chandelier cells. J Comp Neurol *194*, 761-779.

Fanselow, M.S., and Gale, G.D. (2003). The amygdala, fear, and memory. Ann N Y Acad Sci *985*, 125-134.

Fanselow, M.S., and Poulos, A.M. (2005). The neuroscience of mammalian associative learning. Annu Rev Psychol *56*, 207-234.

Ferraguti, F., Cobden, P., Pollard, M., Cope, D., Shigemoto, R., Watanabe, M., and Somogyi, P. (2004). Immunolocalization of metabotropic glutamate receptor 1alpha (mGluR1alpha) in distinct classes of interneuron in the CA1 region of the rat hippocampus. Hippocampus *14*, 193-215.

Fino, E., and Yuste, R. (2011). Dense inhibitory connectivity in neocortex. Neuron *69*, 1188-1203.

Fishell, G., and Rudy, B. (2011). Mechanisms of inhibition within the telencephalon: "where the wild things are". Annu Rev Neurosci *34*, 535-567.

Foldy, C., Lee, S.Y., Szabadics, J., Neu, A., and Soltesz, I. (2007). Cell type-specific gating of perisomatic inhibition by cholecystokinin. Nat Neurosci *10*, 1128-1130.

Freund, T.F. (2003). Interneuron Diversity series: Rhythm and mood in perisomatic inhibition. Trends Neurosci *26*, 489-495.

Freund, T.F., and Buzsaki, G. (1996). Interneurons of the hippocampus. Hippocampus *6*, 347-470.

Freund, T.F., and Katona, I. (2007). Perisomatic inhibition. Neuron *56*, 33-42.

Freund, T.F., Katona, I., and Piomelli, D. (2003). Role of endogenous cannabinoids in synaptic signaling. Physiol Rev *83*, 1017-1066.

Freund, T.F., Martin, K.A., Smith, A.D., and Somogyi, P. (1983). Glutamate decarboxylase-immunoreactive terminals of Golgi-impregnated axoaxonic cells and of presumed basket cells in synaptic contact with pyramidal neurons of the cat's visual cortex. J Comp Neurol *221*, 263-278.

Fukaya, M., Tsujita, M., Yamazaki, M., Kushiya, E., Abe, M., Akashi, K., Natsume, R., Kano, M., Kamiya, H., Watanabe, M., and Sakimura, K. (2006). Abundant distribution of TARP gamma-8 in synaptic and extrasynaptic surface of hippocampal neurons and its major role in AMPA receptor expression on spines and dendrites. Eur J Neurosci *24*, 2177-2190.

Fukuda, T., and Kosaka, T. (2000). The dual network of GABAergic interneurons linked by both chemical and electrical synapses: a possible infrastructure of the cerebral cortex. Neurosci Res *38*, 123-130.

Galarreta, M., Erdelyi, F., Szabo, G., and Hestrin, S. (2008). Cannabinoid sensitivity and synaptic properties of 2 GABAergic networks in the neocortex. Cereb Cortex *18*, 2296-2305.

Galarreta, M., and Hestrin, S. (1999). A network of fast-spiking cells in the neocortex connected by electrical synapses. Nature *402*, 72-75.

Galarreta, M., and Hestrin, S. (2002). Electrical and chemical synapses among parvalbumin fast-spiking GABAergic interneurons in adult mouse neocortex. Proc Natl Acad Sci U S A *99*, 12438-12443.

Gaudreau, H., and Pare, D. (1996). Projection neurons of the lateral amygdaloid nucleus are virtually silent throughout the sleep--waking cycle. J Neurophysiol *75*, 1301-1305.

Geiger, J.R., Melcher, T., Koh, D.S., Sakmann, B., Seeburg, P.H., Jonas, P., and Monyer, H. (1995). Relative abundance of subunit mRNAs determines gating and Ca2+ permeability of AMPA receptors in principal neurons and interneurons in rat CNS. Neuron *15*, 193-204.

Gidon, A., and Segev, I. (2012). Principles governing the operation of synaptic inhibition in dendrites. Neuron *75*, 330-341.

Glickfeld, L.L., Roberts, J.D., Somogyi, P., and Scanziani, M. (2009). Interneurons hyperpolarize pyramidal cells along their entire somatodendritic axis. Nat Neurosci *12*, 21-23.

Glickfeld, L.L., and Scanziani, M. (2006). Distinct timing in the activity of cannabinoid-sensitive and cannabinoid-insensitive basket cells. Nat Neurosci *9*, 807-815.

Gore, F., Schwartz, E.C., Brangers, B.C., Aladi, S., Stujenske, J.M., Likhtik, E., Russo, M.J., Gordon, J.A., Salzman, C.D., and Axel, R. (2015). Neural Representations of Unconditioned Stimuli in Basolateral Amygdala Mediate Innate and Learned Responses. Cell *162*, 134-145.

Goswami, S.P., Bucurenciu, I., and Jonas, P. (2012). Miniature IPSCs in hippocampal granule cells are triggered by voltage-gated Ca2+ channels via microdomain coupling. J Neurosci *32*, 14294-14304.

Gulyas, A.I., Hajos, N., and Freund, T.F. (1996). Interneurons containing calretinin are specialized to control other interneurons in the rat hippocampus. J Neurosci *16*, 3397-3411.

Gulyas, A.I., Hajos, N., Katona, I., and Freund, T.F. (2003). Interneurons are the local targets of hippocampal inhibitory cells which project to the medial septum. Eur J Neurosci *17*, 1861-1872.

Gulyas, A.I., Megias, M., Emri, Z., and Freund, T.F. (1999). Total number and ratio of excitatory and inhibitory synapses converging onto single interneurons of different types in the CA1 area of the rat hippocampus. J Neurosci *19*, 10082-10097.

Gulyas, A.I., Miles, R., Sik, A., Toth, K., Tamamaki, N., and Freund, T.F. (1993). Hippocampal pyramidal cells excite inhibitory neurons through a single release site. Nature *366*, 683-687.

Gulyas, A.I., Szabo, G.G., Ulbert, I., Holderith, N., Monyer, H., Erdelyi, F., Szabo, G., Freund, T.F., and Hajos, N. (2010). Parvalbumin-containing fast-spiking basket cells generate the field potential oscillations induced by cholinergic receptor activation in the hippocampus. J Neurosci *30*, 15134-15145.

Guzman, S.J., Schlogl, A., Frotscher, M., and Jonas, P. (2016). Synaptic mechanisms of pattern completion in the hippocampal CA3 network. Science *353*, 1117-1123.

Hafting, T., Fyhn, M., Molden, S., Moser, M.B., and Moser, E.I. (2005). Microstructure of a spatial map in the entorhinal cortex. Nature *436*, 801-806.

Hajos, N., Papp, E.C., Acsady, L., Levey, A.I., and Freund, T.F. (1998). Distinct interneuron types express m2 muscarinic receptor immunoreactivity on their dendrites or axon terminals in the hippocampus. Neuroscience *82*, 355-376.

Halasy, K., Buhl, E.H., Lorinczi, Z., Tamas, G., and Somogyi, P. (1996). Synaptic target selectivity and input of GABAergic basket and bistratified interneurons in the CA1 area of the rat hippocampus. Hippocampus *6*, 306-329.

Haller, J. (2018). The role of central and medial amygdala in normal and abnormal aggression: A review of classical approaches. Neurosci Biobehav Rev *85*, 34-43.

Han, Z.S., Buhl, E.H., Lorinczi, Z., and Somogyi, P. (1993). A high degree of spatial selectivity in the axonal and dendritic domains of physiologically identified local-circuit neurons in the dentate gyrus of the rat hippocampus. Eur J Neurosci *5*, 395-410.

Harris, K.D., and Shepherd, G.M. (2015). The neocortical circuit: themes and variations. Nat Neurosci *18*, 170-181.

Hart, S.A., Snyder, M.A., Smejkalova, T., and Woolley, C.S. (2007). Estrogen mobilizes a subset of estrogen receptor-alpha-immunoreactive vesicles in inhibitory presynaptic boutons in hippocampal CA1. J Neurosci *27*, 2102-2111.

Haubensak, W., Kunwar, P.S., Cai, H., Ciocchi, S., Wall, N.R., Ponnusamy, R., Biag, J., Dong, H.W., Deisseroth, K., Callaway, E.M., Fanselow, M.S., Luthi, A., and Anderson, D.J. (2010). Genetic dissection of an amygdala microcircuit that gates conditioned fear. Nature *468*, 270-276.

Hefft, S., and Jonas, P. (2005). Asynchronous GABA release generates long-lasting inhibition at a hippocampal interneuron-principal neuron synapse. Nat Neurosci *8*, 1319-1328.

Hendry, S.H.C., Schwark, H.D., Jones, E.G., and Yan, J. (1987). Numbers and proportions of GABA-immunoreactive neurons in different areas of monkey cerebral cortex. JNeurosci *7*, 1503-1519.

Herry, C., Ciocchi, S., Senn, V., Demmou, L., Muller, C., and Luthi, A. (2008). Switching on and off fear by distinct neuronal circuits. Nature *454*, 600-606.

Herry, C., Ferraguti, F., Singewald, N., Letzkus, J.J., Ehrlich, I., and Luthi, A. (2010). Neuronal circuits of fear extinction. Eur J Neurosci *31*, 599-612.

Holmgren, C., Harkany, T., Svennenfors, B., and Zilberter, Y. (2003). Pyramidal cell communication within local networks in layer 2/3 of rat neocortex. J Physiol *551*, 139-153.

Houston, C.M., Bright, D.P., Sivilotti, L.G., Beato, M., and Smart, T.G. (2009). Intracellular chloride ions regulate the time course of GABA-mediated inhibitory synaptic transmission. J Neurosci *29*, 10416-10423.

Hu, H., Gan, J., and Jonas, P. (2014). Interneurons. Fast-spiking, parvalbumin(+) GABAergic interneurons: from cellular design to microcircuit function. Science *345*, 1255263.

Hu, H., Martina, M., and Jonas, P. (2010). Dendritic mechanisms underlying rapid synaptic activation of fast-spiking hippocampal interneurons. Science *327*, 52-58.

Jasnow, A.M., Ressler, K.J., Hammack, S.E., Chhatwal, J.P., and Rainnie, D.G. (2009). Distinct subtypes of cholecystokinin (CCK)-containing interneurons of the basolateral amygdala identified using a CCK promoter-specific lentivirus. J Neurophysiol *101*, 1494-1506.

Jiang, X., Shen, S., Cadwell, C.R., Berens, P., Sinz, F., Ecker, A.S., Patel, S., and Tolias, A.S. (2015). Principles of connectivity among morphologically defined cell types in adult neocortex. Science *350*, aac9462.

Jinno, S., Klausberger, T., Marton, L.F., Dalezios, Y., Roberts, J.D., Fuentealba, P., Bushong, E.A., Henze, D., Buzsaki, G., and Somogyi, P. (2007). Neuronal diversity in GABAergic long-range projections from the hippocampus. J Neurosci *27*, 8790-8804.

Jolkkonen, E., and Pitkanen, A. (1998). Intrinsic connections of the rat amygdaloid complex: projections originating in the central nucleus. J Comp Neurol *395*, 53-72.

Jonas, P., Racca, C., Sakmann, B., Seeburg, P.H., and Monyer, H. (1994). Differences in Ca2+ permeability of AMPA-type glutamate receptor channels in neocortical neurons caused by differential GluR-B subunit expression. Neuron *12*, 1281-1289.

Jungling, K., Seidenbecher, T., Sosulina, L., Lesting, J., Sangha, S., Clark, S.D., Okamura, N., Duangdao, D.M., Xu, Y.L., Reinscheid, R.K., and Pape, H.C. (2008). Neuropeptide S-mediated control of fear expression and extinction: role of intercalated GABAergic neurons in the amygdala. Neuron *59*, 298-310.

Kano, M., Ohno-Shosaku, T., Hashimotodani, Y., Uchigashima, M., and Watanabe, M. (2009). Endocannabinoid-mediated control of synaptic transmission. Physiol Rev *89*, 309-380.

Karnani, M.M., Jackson, J., Ayzenshtat, I., Tucciarone, J., Manoocheri, K., Snider, W.G., and Yuste, R. (2016). Cooperative Subnetworks of Molecularly Similar Interneurons in Mouse Neocortex. Neuron *90*, 86-100.

Katona, I., Rancz, E.A., Acsady, L., Ledent, C., Mackie, K., Hajos, N., and Freund, T.F. (2001). Distribution of CB1 cannabinoid receptors in the amygdala and their role in the control of GABAergic transmission. J Neurosci *21*, 9506-9518.

Katona, I., Sperlagh, B., Sik, A., Kafalvi, A., Vizi, E.S., Mackie, K., and Freund, T.F. (1999). Presynaptically located CB1 cannabinoid receptors regulate GABA release from axon terminals of specific hippocampal interneurons. J Neurosci *19*, 4544-4558.

Katona, L., Lapray, D., Viney, T.J., Oulhaj, A., Borhegyi, Z., Micklem, B.R., Klausberger, T., and Somogyi, P. (2014). Sleep and movement differentiates actions of two types of somatostatin-expressing GABAergic interneuron in rat hippocampus. Neuron *82*, 872-886.

Kawaguchi, Y., and Kondo, S. (2002). Parvalbumin, somatostatin and cholecystokinin as chemical markers for specific GABAergic interneuron types in the rat frontal cortex. J Neurocytol *31*, 277-287.

Keimpema, E., Straiker, A., Mackie, K., Harkany, T., and Hjerling-Leffler, J. (2012). Sticking out of the crowd: the molecular identity and development of cholecystokinin-containing basket cells. J Physiol *590*, 703-714.

Kemppainen, S., and Pitkanen, A. (2000). Distribution of parvalbumin, calretinin, and calbindin-D(28k) immunoreactivity in the rat amygdaloid complex and colocalization with gamma-aminobutyric acid. J Comp Neurol *426*, 441-467.

Kepecs, A., and Fishell, G. (2014). Interneuron cell types are fit to function. Nature *505*, 318-326.

Khirug, S., Yamada, J., Afzalov, R., Voipio, J., Khiroug, L., and Kaila, K. (2008). GABAergic depolarization of the axon initial segment in cortical principal neurons is caused by the Na-K-2Cl cotransporter NKCC1. J Neurosci *28*, 4635-4639.

Kim, J., Lee, S., Park, K., Hong, I., Song, B., Son, G., Park, H., Kim, W.R., Park, E., Choe, H.K., Kim, H., Lee, C., Sun, W., Kim, K., Shin, K.S., and Choi, S. (2007). Amygdala depotentiation and fear extinction. Proc Natl Acad Sci U S A *104*, 20955-20960.

Kim, J., Pignatelli, M., Xu, S., Itohara, S., and Tonegawa, S. (2016). Antagonistic negative and positive neurons of the basolateral amygdala. Nat Neurosci *19*, 1636-1646.

Kisvarday, Z.F., Martin, K.A., Freund, T.F., Maglóczky, Z., Whitteridge, D., and Somogyi, P. (1986). Synaptic targets of HRP-filled layer III pyramidal cells in the cat striate cortex. ExpBrain Res *64*, 541-552.

Kitamura, T., Ogawa, S.K., Roy, D.S., Okuyama, T., Morrissey, M.D., Smith, L.M., Redondo, R.L., and Tonegawa, S. (2017). Engrams and circuits crucial for systems consolidation of a memory. Science *356*, 73-78.

Klausberger, T., Magill, P.J., Marton, L.F., Roberts, J.D., Cobden, P.M., Buzsaki, G., and Somogyi, P. (2003). Brain-state- and cell-type-specific firing of hippocampal interneurons in vivo. Nature *421*, 844-848.

Klausberger, T., Marton, L.F., Baude, A., Roberts, J.D., Magill, P.J., and Somogyi, P. (2004). Spike timing of dendrite-targeting bistratified cells during hippocampal network oscillations in vivo. Nat Neurosci *7*, 41-47.

Klausberger, T., Marton, L.F., O'Neill, J., Huck, J.H., Dalezios, Y., Fuentealba, P., Suen, W.Y., Papp, E., Kaneko, T., Watanabe, M., Csicsvari, J., and Somogyi, P. (2005). Complementary roles of cholecystokinin- and parvalbumin-expressing GABAergic neurons in hippocampal network oscillations. J Neurosci *25*, 9782-9793.

Klausberger, T., Roberts, J.D., and Somogyi, P. (2002). Cell type- and input-specific differences in the number and subtypes of synaptic GABA(A) receptors in the hippocampus. J Neurosci *22*, 2513-2521.

Klausberger, T., and Somogyi, P. (2008). Neuronal diversity and temporal dynamics: the unity of hippocampal circuit operations. Science *321*, 53-57.

Kohus, Z., Kali, S., Rovira-Esteban, L., Schlingloff, D., Papp, O., Freund, T.F., Hajos, N., and Gulyas, A.I. (2016). Properties and dynamics of inhibitory synaptic communication within the CA3 microcircuits of pyramidal cells and interneurons expressing parvalbumin or cholecystokinin. J Physiol *594*, 3745-3774.

Kole, M.H., and Stuart, G.J. (2012). Signal processing in the axon initial segment. Neuron *73*, 235-247.

Kraushaar, U., and Jonas, P. (2000). Efficacy and stability of quantal GABA release at a hippocampal interneuron-principal neuron synapse. J Neurosci *20*, 5594-5607.

Krook-Magnuson, E., Varga, C., Lee, S.H., and Soltesz, I. (2012). New dimensions of interneuronal specialization unmasked by principal cell heterogeneity. Trends Neurosci *35*, 175-184.

Kubota, Y., Karube, F., Nomura, M., Gulledge, A.T., Mochizuki, A., Schertel, A., and Kawaguchi, Y. (2011). Conserved properties of dendritic trees in four cortical interneuron subtypes. Sci Rep *1*, 89.

Kubota, Y., Kondo, S., Nomura, M., Hatada, S., Yamaguchi, N., Mohamed, A.A., Karube, F., Lubke, J., and Kawaguchi, Y. (2015). Functional effects of distinct innervation styles of pyramidal cells by fast spiking cortical interneurons. Elife *4*.

Kullmann, D.M. (2011). Interneuron networks in the hippocampus. Curr Opin Neurobiol *21*, 709-716.

LaBar, K.S., Gatenby, J.C., Gore, J.C., LeDoux, J.E., and Phelps, E.A. (1998). Human amygdala activation during conditioned fear acquisition and extinction: a mixed-trial fMRI study. Neuron *20*, 937-945.

Lamsa, K.P., Heeroma, J.H., Somogyi, P., Rusakov, D.A., and Kullmann, D.M. (2007). Anti-Hebbian long-term potentiation in the hippocampal feedback inhibitory circuit. Science *315*, 1262-1266.

Lang, E.J., and Pare, D. (1997). Similar inhibitory processes dominate the responses of cat lateral amygdaloid projection neurons to their various afferents. J Neurophysiol *77*, 341-352.

Lasztoczi, B., Tukker, J.J., Somogyi, P., and Klausberger, T. (2011). Terminal field and firing selectivity of cholecystokinin-expressing interneurons in the hippocampal CA3 area. J Neurosci *31*, 18073-18093.

LeDoux, J. (2007). The amygdala. Curr Biol *17*, R868-874.

LeDoux, J.E. (2000). Emotion circuits in the brain. Annu Rev Neurosci *23*, 155-184.

Lee, S., Kim, S.J., Kwon, O.B., Lee, J.H., and Kim, J.H. (2013). Inhibitory networks of the amygdala for emotional memory. Front Neural Circuits *7*, 129.

Lee, S.C., Amir, A., Haufler, D., and Pare, D. (2017). Differential Recruitment of Competing Valence-Related Amygdala Networks during Anxiety. Neuron *96*, 81-88 e85.

Lee, S.H., and Soltesz, I. (2011). Requirement for CB1 but not GABAB receptors in the cholecystokinin mediated inhibition of GABA release from cholecystokinin expressing basket cells. J Physiol *589*, 891-902.

Lee, S.Y., Foldy, C., Szabadics, J., and Soltesz, I. (2011). Cell-type-specific CCK2 receptor signaling underlies the cholecystokinin-mediated selective excitation of hippocampal parvalbumin-positive fast-spiking basket cells. J Neurosci *31*, 10993-11002.

Levy, R.B., and Reyes, A.D. (2012). Spatial profile of excitatory and inhibitory synaptic connectivity in mouse primary auditory cortex. J Neurosci *32*, 5609-5619.

Lewis, D.A., Curley, A.A., Glausier, J.R., and Volk, D.W. (2012). Cortical parvalbumin interneurons and cognitive dysfunction in schizophrenia. Trends Neurosci *35*, 57-67.

Li, X.F., Armony, J.L., and LeDoux, J.E. (1996a). GABAA and GABAB receptors differentially regulate synaptic transmission in the auditory thalamo-amygdala pathway: an in vivo microiontophoretic study and a model. Synapse *24*, 115-124.

Li, X.F., Stutzmann, G.E., and LeDoux, J.E. (1996b). Convergent but temporally separated inputs to lateral amygdala neurons from the auditory thalamus and auditory cortex use different postsynaptic receptors: in vivo intracellular and extracellular recordings in fear conditioning pathways. Learn Mem *3*, 229-242.

Lien, C.C., and Jonas, P. (2003). Kv3 potassium conductance is necessary and kinetically optimized for high-frequency action potential generation in hippocampal interneurons. J Neurosci *23*, 2058-2068.

Likhtik, E., Popa, D., Apergis-Schoute, J., Fidacaro, G.A., and Pare, D. (2008). Amygdala intercalated neurons are required for expression of fear extinction. Nature *454*, 642-645.

Lorincz, A., and Nusser, Z. (2010). Molecular identity of dendritic voltage-gated sodium channels. Science *328*, 906-909.

Losonczy, A., Zemelman, B.V., Vaziri, A., and Magee, J.C. (2010). Network mechanisms of theta related neuronal activity in hippocampal CA1 pyramidal neurons. Nat Neurosci *13*, 967-972.

Lu, J., Tucciarone, J., Padilla-Coreano, N., He, M., Gordon, J.A., and Huang, Z.J. (2017). Selective inhibitory control of pyramidal neuron ensembles and cortical subnetworks by chandelier cells. Nat Neurosci *20*, 1377-1383.

Lu, J.T., Li, C.Y., Zhao, J.P., Poo, M.M., and Zhang, X.H. (2007). Spike-timing-dependent plasticity of neocortical excitatory synapses on inhibitory interneurons depends on target cell type. J Neurosci *27*, 9711-9720.

Ma, Y., Hu, H., Berrebi, A.S., Mathers, P.H., and Agmon, A. (2006). Distinct subtypes of somatostatin-containing neocortical interneurons revealed in transgenic mice. J Neurosci *26*, 5069-5082.

Maccaferri, G., Roberts, J.D., Szucs, P., Cottingham, C.A., and Somogyi, P. (2000). Cell surface domain specific postsynaptic currents evoked by identified GABAergic neurones in rat hippocampus in vitro. J Physiol *524 Pt 1*, 91-116.

Magee, J.C. (2000). Dendritic integration of excitatory synaptic input. Nat Rev Neurosci *1*, 181-190.

Magee, J.C., and Johnston, D. (1995). Synaptic activation of voltage-gated channels in the dendrites of hippocampal pyramidal neurons [see comments]. Science *268*, 301-304.

Malenka, R.C., and Bear, M.F. (2004). LTP and LTD: an embarrassment of riches. Neuron *44*, 5-21.

Manko, M., Bienvenu, T.C., Dalezios, Y., and Capogna, M. (2012). Neurogliaform cells of amygdala: a source of slow phasic inhibition in the basolateral complex. J Physiol *590*, 5611-5627.

Mann, E.O., Suckling, J.M., Hajos, N., Greenfield, S.A., and Paulsen, O. (2005). Perisomatic feedback inhibition underlies cholinergically induced fast network oscillations in the rat hippocampus in vitro. Neuron *45*, 105-117.

Maren, S. (2001). Neurobiology of Pavlovian fear conditioning. Annu Rev Neurosci *24*, 897-931.

Maren, S., and Fanselow, M.S. (1996). The amygdala and fear conditioning: has the nut been cracked? Neuron *16*, 237-240.

Marin, O. (2012). Interneuron dysfunction in psychiatric disorders. Nat Rev Neurosci *13*, 107-120.

Markram, H., Toledo-Rodriguez, M., Wang, Y., Gupta, A., Silberberg, G., and Wu, C. (2004). Interneurons of the neocortical inhibitory system. Nat Rev Neurosci *5*, 793-807.

Marsicano, G., and Lutz, B. (1999). Expression of the cannabinoid receptor CB1 in distinct neuronal subpopulations in the adult mouse forebrain. Eur J Neurosci *11*, 4213-4225.

Marsicano, G., Wotjak, C.T., Azad, S.C., Bisogno, T., Rammes, G., Cascio, M.G., Hermann, H., Tang, J., Hofmann, C., Zieglgansberger, W., Di Marzo, V., and Lutz, B. (2002). The endogenous cannabinoid system controls extinction of aversive memories. Nature *418*, 530-534.

Mascagni, F., and McDonald, A.J. (2003). Immunohistochemical characterization of cholecystokinin containing neurons in the rat basolateral amygdala. Brain Research *976*, 171-184.

Massi, L., Lagler, M., Hartwich, K., Borhegyi, Z., Somogyi, P., and Klausberger, T. (2012). Temporal dynamics of parvalbumin-expressing axo-axonic and basket cells in the rat medial prefrontal cortex in vivo. J Neurosci *32*, 16496-16502.

Mate, Z., Poles, M.Z., Szabo, G., Bagyanszki, M., Talapka, P., Fekete, E., and Bodi, N. (2013). Spatiotemporal expression pattern of DsRedT3/CCK gene construct during postnatal development of myenteric plexus in transgenic mice. Cell Tissue Res *352*, 199-206.

Mathy, A., Clark, B.A., and Hausser, M. (2014). Synaptically induced long-term modulation of electrical coupling in the inferior olive. Neuron *81*, 1290-1296.

Matyas, F., Freund, T.F., and Gulyas, A.I. (2004). Convergence of excitatory and inhibitory inputs onto CCK-containing basket cells in the CA1 area of the rat hippocampus. Eur J Neurosci *19*, 1243-1256.

McBain, C.J., DiChiara, T.J., and Kauer, J.A. (1994). Activation of metabotropic glutamate receptors differentially affects two classes of hippocampal interneurons and potentiates excitatory synaptic transmission. J Neurosci *14*, 4433-4445.

McDonald, A.J. (1982a). Cytoarchitecture of the central amygdaloid nucleus of the rat. J Comp Neurol *208*, 401-418.

McDonald, A.J. (1982b). Neurons of the lateral and basolateral amygdaloid nuclei: a Golgi study in the rat. J Comp Neurol *212*, 293-312.

McDonald, A.J. (1989). Coexistence of somatostatin with neuropeptide Y, but not with cholecystokinin or vasoactive intestinal peptide, in neurons of the rat amygdala. Brain Res *500*, 37-45.

McDonald, A.J. (1992). Projection neurons of the basolateral amygdala: a correlative Golgi and retrograde tract tracing study. Brain Res Bull *28*, 179-185.

McDonald, A.J. (1998). Cortical pathways to the mammalian amygdala. Prog Neurobiol *55*, 257-332.

McDonald, A.J., and Betette, R.L. (2001). Parvalbumin-containing neurons in the rat basolateral amygdala: morphology and co-localization of Calbindin-D(28k). Neuroscience *102*, 413-425.

McDonald, A.J., and Mascagni, F. (2001a). Colocalization of calcium-binding proteins and GABA in neurons of the rat basolateral amygdala. Neuroscience *105*, 681-693.

McDonald, A.J., and Mascagni, F. (2001b). Localization of the CB1 type cannabinoid receptor in the rat basolateral amygdala: high concentrations in a subpopulation of cholecystokinin-containing interneurons. Neuroscience *107*, 641-652.

McDonald, A.J., and Mascagni, F. (2002). Immunohistochemical characterization of somatostatin containing interneurons in the rat basolateral amygdala. Brain Res *943*, 237-244.

McDonald, A.J., Mascagni, F., and Zaric, V. (2012). Subpopulations of somatostatin-immunoreactive non-pyramidal neurons in the amygdala and adjacent external capsule project to the basal forebrain: evidence for the existence of GABAergic projection neurons in the cortical nuclei and basolateral nuclear complex. Front Neural Circuits *6*, 46.

McDonald, A.J., and Zaric, V. (2015). GABAergic somatostatin-immunoreactive neurons in the amygdala project to the entorhinal cortex. Neuroscience *290*, 227-242.

Megias, M., Emri, Z., Freund, T.F., and Gulyas, A.I. (2001). Total number and distribution of inhibitory and excitatory synapses on hippocampal CA1 pyramidal cells. Neuroscience *102*, 527-540.

Melzer, S., Michael, M., Caputi, A., Eliava, M., Fuchs, E.C., Whittington, M.A., and Monyer, H. (2012). Long-range-projecting GABAergic neurons modulate inhibition in hippocampus and entorhinal cortex. Science *335*, 1506-1510.

Meyer, A.H., Katona, I., Blatow, M., Rozov, A., and Monyer, H. (2002). In vivo labeling of parvalbumin-positive interneurons and analysis of electrical coupling in identified neurons. J Neurosci *22*, 7055-7064.

Milad, M.R., and Quirk, G.J. (2002). Neurons in medial prefrontal cortex signal memory for fear extinction. Nature *420*, 70-74.

Miles, R., Toth, K., Gulyas, A.I., Hajos, N., and Freund, T.F. (1996). Differences between somatic and dendritic inhibition in the hippocampus. Neuron *16*, 815-823.

Miles, R., and Wong, R.K. (1986). Excitatory synaptic interactions between CA3 neurones in the guinea-pig hippocampus. JPhysiol *373*, 397-418.

Millhouse, O.E. (1986). The intercalated cells of the amygdala. J Comp Neurol *247*, 246-271.

Mizuseki, K., Diba, K., Pastalkova, E., and Buzsaki, G. (2011). Hippocampal CA1 pyramidal cells form functionally distinct sublayers. Nat Neurosci *14*, 1174-1181.

Molnar, G., Rozsa, M., Baka, J., Holderith, N., Barzo, P., Nusser, Z., and Tamas, G. (2016). Human pyramidal to interneuron synapses are mediated by multi-vesicular release and multiple docked vesicles. Elife *5*.

Morales, M., Hein, K., and Vogel, Z. (2008). Hippocampal interneurons co-express transcripts encoding the alpha7 nicotinic receptor subunit and the cannabinoid receptor 1. Neuroscience *152*, 70-81.

Morozov, A., Sukato, D., and Ito, W. (2011). Selective suppression of plasticity in amygdala inputs from temporal association cortex by the external capsule. J Neurosci *31*, 339-345.

Morris, J.S., Ohman, A., and Dolan, R.J. (1998). Conscious and unconscious emotional learning in the human amygdala. Nature *393*, 467-470.

Muller, J.F., Mascagni, F., and McDonald, A.J. (2006). Pyramidal cells of the rat basolateral amygdala: synaptology and innervation by parvalbumin-immunoreactive interneurons. J Comp Neurol *494*, 635-650.

Muller, J.F., Mascagni, F., and McDonald, A.J. (2007). Postsynaptic targets of somatostatin-containing interneurons in the rat basolateral amygdala. J Comp Neurol *500*, 513-529.

Mullner, F.E., Wierenga, C.J., and Bonhoeffer, T. (2015). Precision of Inhibition: Dendritic Inhibition by Individual GABAergic Synapses on Hippocampal Pyramidal Cells Is Confined in Space and Time. Neuron *87*, 576-589.

Namburi, P., Beyeler, A., Yorozu, S., Calhoon, G.G., Halbert, S.A., Wichmann, R., Holden, S.S., Mertens, K.L., Anahtar, M., Felix-Ortiz, A.C., Wickersham, I.R., Gray, J.M., and Tye, K.M. (2015). A circuit mechanism for differentiating positive and negative associations. Nature *520*, 675-678.

Neu, A., Foldy, C., and Soltesz, I. (2007). Postsynaptic origin of CB1-dependent tonic inhibition of GABA release at cholecystokinin-positive basket cell to pyramidal cell synapses in the CA1 region of the rat hippocampus. J Physiol *578*, 233-247.

Nissen, W., Szabo, A., Somogyi, J., Somogyi, P., and Lamsa, K.P. (2010). Cell type-specific long-term plasticity at glutamatergic synapses onto hippocampal interneurons expressing either parvalbumin or CB1 cannabinoid receptor. J Neurosci *30*, 1337-1347.

Norenberg, A., Hu, H., Vida, I., Bartos, M., and Jonas, P. (2010). Distinct nonuniform cable properties optimize rapid and efficient activation of fast-spiking GABAergic interneurons. Proc Natl Acad Sci U S A *107*, 894-899.

Nuss, P. (2015). Anxiety disorders and GABA neurotransmission: a disturbance of modulation. Neuropsychiatr Dis Treat *11*, 165-175.

Olah, S., Fule, M., Komlosi, G., Varga, C., Baldi, R., Barzo, P., and Tamas, G. (2009). Regulation of cortical microcircuits by unitary GABA-mediated volume transmission. Nature *461*, 1278-1281.

Olmos-Serrano, J.L., Paluszkiewicz, S.M., Martin, B.S., Kaufmann, W.E., Corbin, J.G., and Huntsman, M.M. (2010). Defective GABAergic neurotransmission and pharmacological rescue of neuronal hyperexcitability in the amygdala in a mouse model of fragile X syndrome. J Neurosci *30*, 9929-9938.

Oren, I., Hajos, N., and Paulsen, O. (2010). Identification of the current generator underlying cholinergically induced gamma frequency field potential oscillations in the hippocampal CA3 region. J Physiol *588*, 785-797.

Packer, A.M., and Yuste, R. (2011). Dense, unspecific connectivity of neocortical parvalbumin-positive interneurons: a canonical microcircuit for inhibition? J Neurosci *31*, 13260-13271.

Pala, A., and Petersen, C.C. (2015). In vivo measurement of cell-type-specific synaptic connectivity and synaptic transmission in layer 2/3 mouse barrel cortex. Neuron *85*, 68-75.

Palay, S.L., Sotelo, C., Peters, A., and Orkand, P.M. (1968). The axon hillock and the initial segment. J Cell Biol *38*, 193-201.

Pape, H.C., and Pare, D. (2010). Plastic synaptic networks of the amygdala for the acquisition, expression, and extinction of conditioned fear. Physiol Rev *90*, 419-463.

Papp, O.I., Karlocai, M.R., Toth, I.E., Freund, T.F., and Hajos, N. (2013). Different input and output properties characterize parvalbumin-positive basket and Axo-axonic cells in the hippocampal CA3 subfield. Hippocampus *23*, 903-918.

Paulsen, O., and Moser, E.I. (1998). A model of hippocampal memory encoding and retrieval: GABAergic control of synaptic plasticity. Trends Neurosci *21*, 273-278.

Pawelzik, H., Hughes, D.I., and Thomson, A.M. (2002). Physiological and morphological diversity of immunocytochemically defined parvalbumin- and cholecystokinin-positive interneurones in CA1 of the adult rat hippocampus. J Comp Neurol *443*, 346-367.

Pelkey, K.A., Chittajallu, R., Craig, M.T., Tricoire, L., Wester, J.C., and McBain, C.J. (2017). Hippocampal GABAergic Inhibitory Interneurons. Physiol Rev *97*, 1619-1747.

Perin, R., Berger, T.K., and Markram, H. (2011). A synaptic organizing principle for cortical neuronal groups. Proc Natl Acad Sci U S A *108*, 5419-5424.

Peterfi, Z., Urban, G.M., Papp, O.I., Nemeth, B., Monyer, H., Szabo, G., Erdelyi, F., Mackie, K., Freund, T.F., Hajos, N., and Katona, I. (2012). Endocannabinoid-mediated long-term depression of afferent excitatory synapses in hippocampal pyramidal cells and GABAergic interneurons. J Neurosci *32*, 14448-14463.

Peters, A., Proskauer, C.C., and Kaiserman-Abramof, I.R. (1968). The small pyramidal neuron of the rat cerebral cortex. The axon hillock and initial segment. J Cell Biol *39*, 604-619.

Petkova-Kirova, P., Giovannini, M.G., Kalfin, R., and Rakovska, A. (2012). Modulation of acetylcholine release by cholecystokinin in striatum: receptor specificity; role of dopaminergic neuronal activity. Brain Res Bull *89*, 177-184.

Pfeffer, C.K., Xue, M., He, M., Huang, Z.J., and Scanziani, M. (2013). Inhibition of inhibition in visual cortex: the logic of connections between molecularly distinct interneurons. Nat Neurosci *16*, 1068-1076.

Phelps, E.A., Delgado, M.R., Nearing, K.I., and LeDoux, J.E. (2004). Extinction learning in humans: role of the amygdala and vmPFC. Neuron *43*, 897-905.

Phelps, E.A., and LeDoux, J.E. (2005). Contributions of the amygdala to emotion processing: from animal models to human behavior. Neuron *48*, 175-187.

Pi, H.J., Hangya, B., Kvitsiani, D., Sanders, J.I., Huang, Z.J., and Kepecs, A. (2013). Cortical interneurons that specialize in disinhibitory control. Nature *503*, 521-524.

Pitkanen, A., Jolkkonen, E., and Kemppainen, S. (2000). Anatomic heterogeneity of the rat amygdaloid complex. Folia Morphol (Warsz) *59*, 1-23.

Pouille, F., Marin-Burgin, A., Adesnik, H., Atallah, B.V., and Scanziani, M. (2009). Input normalization by global feedforward inhibition expands cortical dynamic range. Nat Neurosci *12*, 1577-1585.

Pouille, F., and Scanziani, M. (2001). Enforcement of temporal fidelity in pyramidal cells by somatic feed-forward inhibition. Science *293*, 1159-1163.

Povysheva, N.V., Zaitsev, A.V., Gonzalez-Burgos, G., and Lewis, D.A. (2013). Electrophysiological heterogeneity of fast-spiking interneurons: chandelier versus basket cells. PLoS One *8*, e70553.

Prager, E.M., Bergstrom, H.C., Wynn, G.H., and Braga, M.F. (2016). The basolateral amygdala gamma-aminobutyric acidergic system in health and disease. J Neurosci Res *94*, 548-567.

Prager, G., Hadamitzky, M., Engler, A., Doenlen, R., Wirth, T., Pacheco-Lopez, G., Krugel, U., Schedlowski, M., and Engler, H. (2013). Amygdaloid signature of peripheral immune activation by bacterial lipopolysaccharide or staphylococcal enterotoxin B. J Neuroimmune Pharmacol *8*, 42-50.

Price, C.J., Cauli, B., Kovacs, E.R., Kulik, A., Lambolez, B., Shigemoto, R., and Capogna, M. (2005). Neurogliaform neurons form a novel inhibitory network in the hippocampal CA1 area. J Neurosci *25*, 6775-6786.

Quirk, G.J., Armony, J.L., and LeDoux, J.E. (1997). Fear conditioning enhances different temporal components of tone-evoked spike trains in auditory cortex and lateral amygdala. Neuron *19*, 613-624.

Quirk, G.J., Repa, C., and LeDoux, J.E. (1995). Fear conditioning enhances short-latency auditory responses of lateral amygdala neurons: parallel recordings in the freely behaving rat. Neuron *15*, 1029-1039.

Rainnie, D.G., Asprodini, E.K., and Shinnick-Gallagher, P. (1993). Intracellular recordings from morphologically identified neurons of the basolateral amygdala. J Neurophysiol *69*, 1350-1362.

Rainnie, D.G., Mania, I., Mascagni, F., and McDonald, A.J. (2006). Physiological and morphological characterization of parvalbumin-containing interneurons of the rat basolateral amygdala. J Comp Neurol *498*, 142-161.

Ramirez, S., Liu, X., Lin, P.A., Suh, J., Pignatelli, M., Redondo, R.L., Ryan, T.J., and Tonegawa, S. (2013). Creating a false memory in the hippocampus. Science *341*, 387-391.

Ramirez, S., Liu, X., MacDonald, C.J., Moffa, A., Zhou, J., Redondo, R.L., and Tonegawa, S. (2015). Activating positive memory engrams suppresses depression-like behaviour. Nature *522*, 335-339.

Rasband, M.N. (2010). The axon initial segment and the maintenance of neuronal polarity. Nat Rev Neurosci *11*, 552-562.

Rescorla, R.A. (2004). Spontaneous recovery. Learn Mem *11*, 501-509.

Rescorla, R.A., and Heth, C.D. (1975). Reinstatement of fear to an extinguished conditioned stimulus. J Exp Psychol Anim Behav Process *1*, 88-96.

Rogan, M.T., Staubli, U.V., and LeDoux, J.E. (1997). Fear conditioning induces associative long-term potentiation in the amygdala. Nature *390*, 604-607.

Romanski, L.M., and LeDoux, J.E. (1992). Equipotentiality of thalamo-amygdala and thalamo-cortico-amygdala circuits in auditory fear conditioning. J Neurosci *12*, 4501-4509.

Rovira-Esteban, L., Peterfi, Z., Vikor, A., Mate, Z., Szabo, G., and Hajos, N. (2017). Morphological and physiological properties of CCK/CB1R-expressing interneurons in the basal amygdala. Brain Struct Funct *222*, 3543-3565.

Rudy, B., and McBain, C.J. (2001). Kv3 channels: voltage-gated K+ channels designed for high-frequency repetitive firing. Trends Neurosci *24*, 517-526.

Ruehle, S., Remmers, F., Romo-Parra, H., Massa, F., Wickert, M., Wortge, S., Haring, M., Kaiser, N., Marsicano, G., Pape, H.C., and Lutz, B. (2013). Cannabinoid CB1 receptor in dorsal telencephalic glutamatergic neurons: distinctive sufficiency for hippocampus-dependent and amygdala-dependent synaptic and behavioral functions. J Neurosci *33*, 10264-10277.

Sah, P., Faber, E.S., Lopez De Armentia, M., and Power, J. (2003). The amygdaloid complex: anatomy and physiology. Physiol Rev *83*, 803-834.

Sahara, S., Yanagawa, Y., O'Leary, D.D., and Stevens, C.F. (2012). The fraction of cortical GABAergic neurons is constant from near the start of cortical neurogenesis to adulthood. J Neurosci *32*, 4755-4761.

Sassoe-Pognetto, M., Giustetto, M., Panzanelli, P., Cantino, D., Kirsch, J., and Fritschy, J.M. (1999). Postsynaptic colocalization of gephyrin and GABAA receptors. Ann N Y Acad Sci *868*, 693-696.

Schlingloff, D., Kali, S., Freund, T.F., Hajos, N., and Gulyas, A.I. (2014). Mechanisms of sharp wave initiation and ripple generation. J Neurosci *34*, 11385-11398.

Schumann, C.M., Bauman, M.D., and Amaral, D.G. (2011). Abnormal structure or function of the amygdala is a common component of neurodevelopmental disorders. Neuropsychologia *49*, 745-759.

Sik, A., Penttonen, M., Ylinen, A., and Buzsaki, G. (1995). Hippocampal CA1 interneurons: an in vivo intracellular labeling study. J Neurosci *15*, 6651-6665.

Smith, Y., Pare, J.F., and Pare, D. (2000). Differential innervation of parvalbumin-immunoreactive interneurons of the basolateral amygdaloid complex by cortical and intrinsic inputs. J Comp Neurol *416*, 496-508.

Sohal, V.S., Zhang, F., Yizhar, O., and Deisseroth, K. (2009). Parvalbumin neurons and gamma rhythms enhance cortical circuit performance. Nature *459*, 698-702.

Solstad, T., Boccara, C.N., Kropff, E., Moser, M.B., and Moser, E.I. (2008). Representation of geometric borders in the entorhinal cortex. Science *322*, 1865-1868.

Somogyi, P. (1977). A specific 'axo-axonal' interneuron in the visual cortex of the rat. Brain Res *136*, 345-350.

Somogyi, P., Kisvarday, Z.F., Martin, K.A., and Whitteridge, D. (1983). Synaptic connections of morphologically identified and physiologically characterized large basket cells in the striate cortex of cat. Neuroscience *10*, 261-294.

Somogyi, P., Tamas, G., Lujan, R., and Buhl, E.H. (1998). Salient features of synaptic organisation in the cerebral cortex. Brain Res Brain Res Rev *26*, 113-135.

Soriano, E., Nitsch, R., and Frotscher, M. (1990). Axo-axonic chandelier cells in the rat fascia dentata: Golgi-electron microscopy and immunocytochemical studies. J Comp Neurol *293*, 1-25.

Spampanato, J., Polepalli, J., and Sah, P. (2011). Interneurons in the basolateral amygdala. Neuropharmacology *60*, 765-773.

Stuart, G.J., and Sakmann, B. (1994). Active propagation of somatic action potentials into neocortical pyramidal cell dendrites. Nature *367*, 69-72.

Szabadics, J., Varga, C., Molnar, G., Olah, S., Barzo, P., and Tamas, G. (2006). Excitatory effect of GABAergic axo-axonic cells in cortical microcircuits. Science *311*, 233-235.

Szabo, A., Somogyi, J., Cauli, B., Lambolez, B., Somogyi, P., and Lamsa, K.P. (2012). Calcium-permeable AMPA receptors provide a common mechanism for LTP in glutamatergic synapses of distinct hippocampal interneuron types. J Neurosci *32*, 6511-6516.

Szabo, G.G., Holderith, N., Gulyas, A.I., Freund, T.F., and Hajos, N. (2010). Distinct synaptic properties of perisomatic inhibitory cell types and their different modulation by cholinergic receptor activation in the CA3 region of the mouse hippocampus. Eur J Neurosci *31*, 2234-2246.

Szabo, G.G., Lenkey, N., Holderith, N., Andrasi, T., Nusser, Z., and Hajos, N. (2014). Presynaptic calcium channel inhibition underlies CB(1) cannabinoid receptor-mediated suppression of GABA release. J Neurosci *34*, 7958-7963.

Szentagothai, J. (1975). The 'module-concept' in cerebral cortex architecture. Brain Res *95*, 475-496.

Szinyei, C., Heinbockel, T., Montagne, J., and Pape, H.C. (2000). Putative cortical and thalamic inputs elicit convergent excitation in a population of GABAergic interneurons of the lateral amygdala. J Neurosci *20*, 8909-8915.

Tamas, G., Buhl, E.H., Lorincz, A., and Somogyi, P. (2000). Proximally targeted GABAergic synapses and gap junctions synchronize cortical interneurons. Nat Neurosci *3*, 366-371.

Tamas, G., Lorincz, A., Simon, A., and Szabadics, J. (2003). Identified sources and targets of slow inhibition in the neocortex. Science *299*, 1902-1905.

Tamas, G., Somogyi, P., and Buhl, E.H. (1998). Differentially interconnected networks of GABAergic interneurons in the visual cortex of the cat. J Neurosci *18*, 4255-4270.

Taniguchi, H., He, M., Wu, P., Kim, S., Paik, R., Sugino, K., Kvitsiani, D., Fu, Y., Lu, J., Lin, Y., Miyoshi, G., Shima, Y., Fishell, G., Nelson, S.B., and Huang, Z.J. (2011). A resource of Cre driver lines for genetic targeting of GABAergic neurons in cerebral cortex. Neuron *71*, 995-1013.

Taube, J.S., Muller, R.U., and Ranck, J.B., Jr. (1990). Head-direction cells recorded from the postsubiculum in freely moving rats. II. Effects of environmental manipulations. J Neurosci *10*, 436-447.

Terburg, D., Morgan, B.E., Montoya, E.R., Hooge, I.T., Thornton, H.B., Hariri, A.R., Panksepp, J., Stein, D.J., and van Honk, J. (2012). Hypervigilance for fear after basolateral amygdala damage in humans. Transl Psychiatry *2*, e115.

Thome, C., Kelly, T., Yanez, A., Schultz, C., Engelhardt, M., Cambridge, S.B., Both, M., Draguhn, A., Beck, H., and Egorov, A.V. (2014). Axon-carrying dendrites convey privileged synaptic input in hippocampal neurons. Neuron *83*, 1418-1430.

Tovote, P., Fadok, J.P., and Luthi, A. (2015). Neuronal circuits for fear and anxiety. Nat Rev Neurosci *16*, 317-331.

Truitt, W.A., Johnson, P.L., Dietrich, A.D., Fitz, S.D., and Shekhar, A. (2009). Anxiety-like behavior is modulated by a discrete subpopulation of interneurons in the basolateral amygdala. Neuroscience *160*, 284-294.

Tsou, K., Mackie, K., Sanudo-Pena, M.C., and Walker, J.M. (1999). Cannabinoid CB1 receptors are localized primarily on cholecystokinin-containing GABAergic interneurons in the rat hippocampal formation. Neuroscience *93*, 969-975.

Tukker, J.J., Lasztoczi, B., Katona, L., Roberts, J.D., Pissadaki, E.K., Dalezios, Y., Marton, L., Zhang, L., Klausberger, T., and Somogyi, P. (2013). Distinct dendritic arborization and in vivo firing patterns of parvalbumin-expressing basket cells in the hippocampal area CA3. J Neurosci *33*, 6809-6825.

Tully, K., Li, Y., Tsvetkov, E., and Bolshakov, V.Y. (2007). Norepinephrine enables the induction of associative long-term potentiation at thalamo-amygdala synapses. Proc Natl Acad Sci U S A *104*, 14146-14150.

Turner, B.H., and Herkenham, M. (1991). Thalamoamygdaloid projections in the rat: a test of the amygdala's role in sensory processing. J Comp Neurol *313*, 295-325.

Tye, K.M., and Janak, P.H. (2007). Amygdala neurons differentially encode motivation and reinforcement. J Neurosci *27*, 3937-3945.

Tye, K.M., Prakash, R., Kim, S.Y., Fenno, L.E., Grosenick, L., Zarabi, H., Thompson, K.R., Gradinaru, V., Ramakrishnan, C., and Deisseroth, K. (2011). Amygdala circuitry mediating reversible and bidirectional control of anxiety. Nature *471*, 358-362.

Tye, K.M., Stuber, G.D., de Ridder, B., Bonci, A., and Janak, P.H. (2008). Rapid strengthening of thalamo-amygdala synapses mediates cue-reward learning. Nature *453*, 1253-1257.

van Welie, I., Roth, A., Ho, S.S., Komai, S., and Hausser, M. (2016). Conditional Spike Transmission Mediated by Electrical Coupling Ensures Millisecond Precision-Correlated Activity among Interneurons In Vivo. Neuron *90*, 810-823.

Varga, C., Lee, S.Y., and Soltesz, I. (2010). Target-selective GABAergic control of entorhinal cortex output. Nat Neurosci *13*, 822-824.

Varga, C., Oijala, M., Lish, J., Szabo, G.G., Bezaire, M., Marchionni, I., Golshani, P., and Soltesz, I. (2014). Functional fission of parvalbumin interneuron classes during fast network events. Elife *3*.

Vereczki, V.K., Veres, J.M., Muller, K., Nagy, G.A., Racz, B., Barsy, B., and Hajos, N. (2016). Synaptic Organization of Perisomatic GABAergic Inputs onto the Principal Cells of the Mouse Basolateral Amygdala. Front Neuroanat *10*, 20.

Vereecken, T.H., Vogels, O.J., and Nieuwenhuys, R. (1994). Neuron loss and shrinkage in the amygdala in Alzheimer's disease. Neurobiology of aging *15*, 45-54.

Veres, J.M., Nagy, G.A., and Hajos, N. (2017). Perisomatic GABAergic synapses of basket cells effectively control principal neuron activity in amygdala networks. Elife *6*.

Veres, J.M., Nagy, G.A., Vereczki, V.K., Andrasi, T., and Hajos, N. (2014). Strategically positioned inhibitory synapses of axo-axonic cells potently control principal neuron spiking in the basolateral amygdala. J Neurosci *34*, 16194-16206.

Vervaeke, K., Lorincz, A., Gleeson, P., Farinella, M., Nusser, Z., and Silver, R.A. (2010). Rapid desynchronization of an electrically coupled interneuron network with sparse excitatory synaptic input. Neuron *67*, 435-451.

Viney, T.J., Lasztoczi, B., Katona, L., Crump, M.G., Tukker, J.J., Klausberger, T., and Somogyi, P. (2013). Network state-dependent inhibition of identified hippocampal CA3 axo-axonic cells in vivo. Nat Neurosci *16*, 1802-1811.

Vogel, E., Krabbe, S., Grundemann, J., Wamsteeker Cusulin, J.I., and Luthi, A. (2016). Projection-Specific Dynamic Regulation of Inhibition in Amygdala Micro-Circuits. Neuron *91*, 644-651.

Wang, Y., Zhang, P., and Wyskiel, D.R. (2016). Chandelier Cells in Functional and Dysfunctional Neural Circuits. Front Neural Circuits *10*, 33.

Washburn, M.S., and Moises, H.C. (1992). Electrophysiological and morphological properties of rat basolateral amygdaloid neurons in vitro. J Neurosci *12*, 4066-4079.

Willadt, S., Nenniger, M., and Vogt, K.E. (2013). Hippocampal feedforward inhibition focuses excitatory synaptic signals into distinct dendritic compartments. PLoS One *8*, e80984.

Wilson, R.I., and Nicoll, R.A. (2001). Endogenous cannabinoids mediate retrograde signalling at hippocampal synapses. Nature *410*, 588-592.

Wilson, R.I., and Nicoll, R.A. (2002). Endocannabinoid signaling in the brain. Science *296*, 678-682.

Wolff, S.B., Grundemann, J., Tovote, P., Krabbe, S., Jacobson, G.A., Muller, C., Herry, C., Ehrlich, I., Friedrich, R.W., Letzkus, J.J., and Luthi, A. (2014). Amygdala interneuron subtypes control fear learning through disinhibition. Nature *509*, 453-458.

Woodruff, A.R., Anderson, S.A., and Yuste, R. (2010). The enigmatic function of chandelier cells. Front Neurosci *4*, 201.

Woodruff, A.R., McGarry, L.M., Vogels, T.P., Inan, M., Anderson, S.A., and Yuste, R. (2011). State-dependent function of neocortical chandelier cells. J Neurosci *31*, 17872-17886.

Woodruff, A.R., Monyer, H., and Sah, P. (2006). GABAergic excitation in the basolateral amygdala. J Neurosci *26*, 11881-11887.

Woodruff, A.R., and Sah, P. (2007a). Inhibition and synchronization of basal amygdala principal neuron spiking by parvalbumin-positive interneurons. J Neurophysiol *98*, 2956-2961.

Woodruff, A.R., and Sah, P. (2007b). Networks of parvalbumin-positive interneurons in the basolateral amygdala. J Neurosci *27*, 553-563.

Xu, H., Jeong, H.Y., Tremblay, R., and Rudy, B. (2013). Neocortical somatostatin-expressing GABAergic interneurons disinhibit the thalamorecipient layer 4. Neuron *77*, 155-167.

Yamamoto, T. (2007). Brain regions responsible for the expression of conditioned taste aversion in rats. Chem Senses *32*, 105-109.

Yi, F., Ball, J., Stoll, K.E., Satpute, V.C., Mitchell, S.M., Pauli, J.L., Holloway, B.B., Johnston, A.D., Nathanson, N.M., Deisseroth, K., Gerber, D.J., Tonegawa, S., and Lawrence, J.J. (2014). Direct excitation of parvalbumin-positive interneurons by M1 muscarinic acetylcholine receptors: roles in cellular excitability, inhibitory transmission and cognition. J Physiol *592*, 3463-3494.

Zemankovics, R., Kali, S., Paulsen, O., Freund, T.F., and Hajos, N. (2010). Differences in subthreshold resonance of hippocampal pyramidal cells and interneurons: the role of h-current and passive membrane characteristics. J Physiol *588*, 2109-2132.

Zhu, Y., Stornetta, R.L., and Zhu, J.J. (2004). Chandelier cells control excessive cortical excitation: characteristics of whisker-evoked synaptic responses of layer 2/3 nonpyramidal and pyramidal neurons. J Neurosci *24*, 5101-5108.

10 LIST OF PUBLICATIONS

Publications related to the dissertation:

Andrási, T., Veres, J.M., Rovira-Esteban, L., Kozma, R., Vikór, A., Gregori, E., and Hájos, N. (2017). Differential Excitatory Control of 2 Parallel Basket Cell Networks in Amygdala Microcircuits. PLoS Biol *15*, e2001421.

Barsy, B., Szabo, G.G., Andrasi, T., Vikor, A., and Hajos, N. (2017). Different output properties of perisomatic region-targeting interneurons in the basal amygdala. Eur J Neurosci *45*, 548-558.

Veres, J.M., Nagy, G.A., Vereczki, V.K., Andrasi, T., and Hajos, N. (2014). Strategically positioned inhibitory synapses of axo-axonic cells potently control principal neuron spiking in the basolateral amygdala. J Neurosci *34*, 16194-16206.

Other publications:

Kohidi, T., Jady, A.G., Marko, K., Papp, N., Andrasi, T., Kornyei, Z., and Madarasz, E. (2017). Differentiation-Dependent Motility-Responses of Developing Neural Progenitors to Optogenetic Stimulation. Front Cell Neurosci *11*, 401.

Brunner, J., Neubrandt, M., Van-Weert, S., Andrasi, T., Kleine Borgmann, F.B., Jessberger, S., and Szabadics, J. (2014). Adult-born granule cells mature through two functionally distinct states. Elife *3*, e03104.

Szabo, G.G., Lenkey, N., Holderith, N., Andrasi, T., Nusser, Z., and Hajos, N. (2014). Presynaptic calcium channel inhibition underlies CB(1) cannabinoid receptor-mediated suppression of GABA release. J Neurosci *34*, 7958-7963.

Brunner, J., Ster, J., Van-Weert, S., Andrasi, T., Neubrandt, M., Corti, C., Corsi, M., Ferraguti, F., Gerber, U., and Szabadics, J. (2013). Selective silencing of individual dendritic branches by an mGlu2-activated potassium conductance in dentate gyrus granule cells. J Neurosci *33*, 7285-7298.

11 ACKNOWLEDGEMENTS

First, I would like to say thanks to my supervisor, Norbert Hájos, who gave me the chance to accomplish the present work. His knowledge, patience and support pushed me up to the peaks and over the troughs during the oscillation of the research work. I would like to say special thanks to János Szabadics, who introduced me into the neuroscience and electrophysiology. Thanks to János Brunner, Máté Neubrandt, Viktor Oláh, Judit Veres, Orsolya Papp, Laura Rovira, Erzsébet Gregori and Éva Krizsán for the inspiring discussions, for their essential help and contribution to my successes. Thanks to my recent and former colleauges and thanks to the KOKI for the supporting environment. Last, but not least thanks to Dóri, my family and my friends for their patience and support.